SOME PROPERTIES OF THE DYNAMIC INTERMEDIATE STATE IN TYPE I SUPERCONDUCTORS

Richard A. Lerski

A Thesis Submitted for the Degree of PhD
at the
University of St Andrews

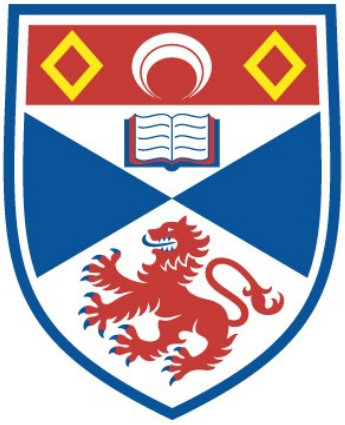

1974

SOME PROPERTIES OF THE DYNAMIC INTERMEDIATE STATE IN TYPE I SUPERCONDUCTORS

A Thesis

presented by

Richard A. Lerski, B.Sc.,

to the

University of St. Andrews

in application for the Degree

of Doctor of Philosophy.

ProQuest LLC.
789 East Eisenhower Parkway
P.O. Box 1346
Ann Arbor, MI 48106 – 1346

Th

8059

DECLARATION

I hereby certify that this thesis has been composed by me, and is a record of work done by me, and has not previously been presented for a Higher Degree.

The research was carried out in the School of Physical Sciences in the University of St. Andrews, under the supervision of Professor J.F. Allen, F.R.S.

Richard A. Lerski

CERTIFICATE

I certify that Richard A. Lerski, B.Sc., has spent nine terms at research work in the School of Physical Sciences in the University of St. Andrews under my direction, that he has fulfilled the conditions of the Resolution of the University Court, 1967, No. 1, and that he is qualified to submit the accompanying thesis in application for the Degree of Doctor of Philosophy.

Research Supervisor

CAREER

I matriculated in the University of Edinburgh in October, 1966, and obtained Upper Second Class Honours in Physics in 1970.

In October, 1970, following the award of an S.R.C. Research Studentship, I was enrolled as a research student under Resolution of the University Court, 1967, No. 1, as a candidate for the degree of Ph.D.

ACKNOWLEDGEMENTS

The author wishes to express his gratitude to Professor J.F. Allen, F.R.S. for his helpful supervision, to Mr. J.G.M. Armitage for many useful suggestions, and to Dr. H. Kirchner for his invaluable advice on the application of the magneto-optic method and for the gift of a quantity of europium sulphide.

He thanks Mr. R.H. Mitchell for a plentiful supply of liquid helium, and the workshop staff of the School of Physical Sciences for skilful technical assistance.

He especially wishes to thank his wife, Janice, for her careful typing of all of this thesis.

ABSTRACT

The high resolution magneto-optic method using the Faraday effect in thin films of EuS:EuF_2 has been used to observe the dynamic intermediate state induced by the passage of an electric current or a heat current through thin slabs of the superconductors Pb, In and Sn.

The ease with which the various intermediate state topologies could be made to move has been studied and several features of the interaction of moving flux with pinning sites have been noted.

In the case of the current induced motion the measured characteristics of flux flow velocity versus current have been found to exhibit two distinct regions. Firstly, a linear region where the observed velocity was found to agree reasonably well with the predictions of the recent general theory of Andreev and Dzhikaev when allowance was made for the effects of pinning by the introduction of a velocity independent pinning force. Secondly, a curved region was found for currents close to the critical current J_o in agreement with earlier work using other methods of observation. Possible reasons for the existence of this curvature were examined in detail, and it was found that a phenomenological model based on the presence of a Gaussian distribution of critical current values throughout the sample could account satisfactorily for the observations. The presence of such a Gaussian distribution was confirmed by observing the variations in distance travelled by a domain subjected to a pulsed driving current. The curvature was found in disagreement with the theory of thermal activation and no evidence could be found for the presence of a velocity dependent pinning force.

In the case of the thermally induced motion which was investigated only in Pb, it was found, in agreement with the very recent work of Laeng and Rinderer, that there exist two competing mechanisms driving the flux. The first of these, that treated by

Andreev and Dzhikaev in their general theory, which acts in a direction parallel to the heat flow, was found to be effective at low temperatures ($T \leqslant 4.2K$) but to be negligible at high temperatures. The magnitude of the velocity produced by this mechanism agreed reasonably well with the theory at low temperatures but was in complete disagreement at high temperatures when the theory predicts that it should still be observable. The second mechanism which acts perpendicularly to the heat flow dominated the motion at high temperatures but its magnitude did not agree with the predictions of the recent theory of Rothen, which ascribes the effect to the thermoelectric power of the normal state. It should be noted that to overcome the pinning all of the low temperature observations ($T \lesssim 4.2K$) were performed in the presence of an electric current. Clearly, much more work requires to be done to clarify these observations.

CONTENTS

LIST OF SYMBOLS

B	magnetic flux density.
B_e	flux density outside specimen.
B_i	flux density inside specimen.
D	demagnetization constant.
E	electric field strength.
E_J	domain energy due to influence of Lorentz force.
E_o	pinning energy.
H_a	applied magnetic field strength.
H_c	critical magnetic field strength.
H_i	field strength inside specimen.
H_o	critical magnetic field strength at 0 K.
h	reduced applied field ($h = H_a/H_c$).
J	electric current density.
J_s	surface current density.
J_o	critical current density.
$\overline{J}_o$	average critical current density.
L	latent heat of the transition normal to superconducting.
M	magnetization (magnetic moment per unit volume).
Q	heat current density.
Q_o	critical heat current density.
R	flux creep rate.
S	standard deviation of the critical current distribution.
T	temperature.
T_c	superconducting transition temperature.
V	domain velocity or Verdet constant.
V_J	domain velocity due to influence of current J.
V_o	critical domain velocity.
V_p	domain velocity when $E_J = E_o$.

V_{th} domain velocity due to influence of normal state thermoelectric power.

$V_{\varkappa}$ domain velocity due to influence of the mechanism of Andreev and Dzhikaev.

x_n fraction of metal in normal state.

x_s fraction of metal in superconducting state.

α surface energy per unit area.

α_N numerical value of the thermoelectric power of the normal state.

σ electrical conductivity.

λ penetration depth, or wavelength.

ξ coherence length.

ω order parameter.

ψ order parameter.

μ permeability.

Δ surface energy parameter ($\alpha = \Delta \frac{H_c^2}{8\pi}$).

$\varkappa_n$ thermal conductivity of normal state.

$\varkappa_s$ thermal conductivity of superconducting state.

ρ_{ik} resistivity tensor.

α_{ik} thermoelectric tensor.

$\delta(J)$ deviation of the effective average critical current value from the real average.

NOTE

In all the diagrams and photographs of the intermediate state in this thesis the superconducting regions are dark and the normal regions light.

Never seen the like since I been born, the people keep a-coming, and the train's done gone.

Traditional.

CHAPTER 1 - INTRODUCTION

1.1 Discovery and basic theory of superconductors

Superconductivity was first discovered and so named by Kamerlingh Onnes in 1911. Soon after his successful liquefaction of helium he became engaged in investigating the behaviour of the electrical resistance of various metals. During measurements on a sample of mercury he observed that its resistance dropped from 0.08 Ω at about 4K to less than 3×10^{-6}Ω at 3K, and that this drop occurred over a temperature interval of 0.01K.

The most recent measurements of the resistance of the superconducting state by Quinn and Ittner (1962) indicate an upper limit to the resistivity of 3.6×10^{-23}Ω.cm. Thus we arrive at the first characteristic property of a superconductor: its electrical resistance, for all practical purposes, is zero below a well defined transition temperature T_c.

The second and perhaps the more interesting characteristic property of a superconductor is that at any temperature T below T_c the application of a critical magnetic field H_c destroys the superconductivity and causes the resistance to revert to that of the normal state (Kamerlingh Onnes (1913)). This critical field is found experimentally to obey, to within a few percent, the relation

$$H_c = H_o \left(1 - (T/T_c)^2\right), \qquad (1.1)$$

where H_o is the value of the critical field appropriate to T = 0K.

For twenty years after their discovery it was assumed that the magnetic properties of superconductors were solely those to be expected for a perfect conductor, i.e. the magnetic field inside a superconductor should remain constant with time ($\dot{\underline{B}} = 0$). This follows from Ohm's law $\underline{J} = \sigma\underline{E}$ and the Maxwell equation $\nabla \times \underline{E} = -\dot{\underline{B}}/c$ when $\sigma \to \infty$

Indeed it was not until 1933 that Meissner and Ochsenfeld (1933) discovered that superconductors have the additional property in equilibrium of never possessing an internal flux, regardless of the path by which the

superconducting state is reached. That is to say, not only does a superconductor not allow any variation of flux with time to occur within it ($\dot{\underline{B}} = 0$), as would be expected for a perfect conductor, but there is also no flux within it ($\underline{B} = 0$). This is known as the Meissner effect.

The discovery of the Meissner effect dispelled the doubts which had existed up to that time about whether the superconducting transition was a reversible one, and led to the development of a thermodynamic treatment by Gorter and Casimir (1934 a, b). They regarded the superconductor as a system of two fluids - (a) the superelectrons which flow with no resistance, and (b) the normal electrons, and imagined that it possessed an order characterised by a parameter ω which could be thought of as the fraction of electrons which had become superelectrons.

About the same time, the brothers Fritz and Heinz London (1935 a, b) developed a model which described the Meissner effect by assuming that a magnetic field (less than critical) applied to a superconductor decays exponentially inwards from its surface, with a characteristic distance λ (where $H_\lambda = \frac{1}{e} H_{surface}$) called the penetration depth. Experimentally λ ($T = 0K$) is around 10^{-5}cm rising to $\lambda = \infty$ at T_c.

These two theories have been very successful in simple problems where size or surface effects are unimportant and, in particular, they provide a good description of what is called the intermediate state.

An important point noted by H. London (1935) is that the exclusion of an external field does not lead to the lowest energy state unless there is a positive surface energy on the boundary between normal and superconducting phases. This is because the energy of a superconductor increases by $\frac{H_a^2}{8\pi}$ (per unit volume) in the presence of an excluded magnetic field H_a, and a lowering of this energy increase could easily be achieved by a splitting of the superconductor into normal and superconducting laminae of widths $\ll \lambda$ and $< \lambda$ respectively. The free energy of the superconducting laminae would be lowered since being thinner than the penetration depth the magnetic field

would penetrate their entire width, while the free energy of the normal regions would be negligible because of their extreme narrowness. However, such a fine splitting is not observed experimentally so a positive surface energy must exist on the phase boundaries to preclude it.

The existence of this high surface energy and problems in the London model concerning the entropy density at the surface of the superconductor led Pippard (1950, 1951, 1953) to propose a modification of the London model in which the order parameter ω did not change abruptly at a phase boundary but rather gradually over a characteristic distance ξ which he called the coherence length. He found ξ to be about 20 times the penetration depth, or of the order of 10^{-4}cm. This difference between the penetration depth and the coherence length explained the existence of the surface energy since at a boundary the condensation energy of the superconducting state falls off with a characteristic length ξ while the magnetic energy of the normal state falls off with characteristic length λ, thus leading to an energy surplus.

A phenomenological quantum mechanical theory compatible with Pippard's approach was developed by Ginzburg and Landau (1950) by expressing the free energy of the superconductor in terms of an order parameter ψ and minimising it with respect to this parameter.

Finally, in 1957 a complete microscopic theory of superconductivity was given by Bardeen, Cooper and Schrieffer (1957) based on the pairing of electrons of opposite spin and momentum which condensed into a lower energy state than unpaired electrons (Fröhlich (1950), Cooper (1956)). Although the BCS theory correctly predicts most, if not all, of the electromagnetic and thermal properties of superconductors, it is not important for the results of this work and will not be discussed further.

1.2 Surface energy - Type I and Type II superconductors

As previously discussed, H. London (1935) pointed out the necessity

of the existence of a positive surface energy at a boundary between superconducting and normal regions and since this idea was supported by the Pippard and Ginzburg-Landau theories, for many years all superconductors were assumed to exhibit this property. This was despite the fact that deviations from the 'ideal' Meissner behaviour had been observed in superconducting alloys (Mendelssohn and Moore (1935)). These deviations were at this time generally considered to be impurity effects and of little fundamental interest, and consequently it was not until 1957 upon the publication of Abrikosov's paper on the possibility of the existence of a new class of 'Type II' superconductors, that it was realised that these deviations were in fact fundamental properties of this new type. It is implicit in Abrikosov's theory that these Type II materials should exhibit a negative surface energy due to their coherence length being less than their penetration depth.

The reason why this behaviour is observed in alloys is that the electron mean free path and hence the coherence length is reduced by the addition of impurities. The BCS theory shows that it is also possible for the coherence length to be shorter than the penetration depth in pure materials with a high T_c. This is found to be the case in niobium (Stromberg and Swenson (1962)) and vanadium (Radebaugh and Keesom (1966 a, b)). These are the only two known elemental Type II superconductors.

The existence of this negative surface energy in Type II superconductors means, as one would expect, that the Meissner effect does not occur, but rather it is energetically more favourable for an applied magnetic field to penetrate in the form of a large number of normal filaments. This is called the MIXED state. It is a fundamental property of a Type II superconductor which occurs because of the negative surface energy and is not, as is the case for the intermediate state of Type I superconductors, dependent on the shape of the sample.

1.3 Magnetic properties of Type I superconductors

The Meissner effect in a bulk Type I superconductor, that is the condition of zero magnetic flux inside a superconductor placed in a magnetic field $\underline{H}_a$, may be considered as arising from induced surface currents whose magnitude and direction are such that they create an internal field that just cancels out the applied field inside the specimen.

Formally we may write

$$\text{Interior:} \quad \underline{B}_i = \underline{H}_i = \underline{M} = 0,$$

$$\text{Surface:} \quad \underline{J}_s \neq 0,$$

$$\text{Outside:} \quad \underline{B}_e = \underline{H}_a + \underline{H}_s,$$

where $\underline{H}_s$ is the field due to the surface currents.

However, since from outside the specimen it is impossible to distinguish between effects due to surface currents and those due to bulk magnetization (see for example Panofsky and Philips (1962) ch. 8), we may also write

$$\text{Interior:} \quad \underline{B}_i = 0, \ \underline{H}_i \neq 0, \ \underline{M} \neq 0,$$

$$\text{Surface:} \quad \underline{J}_s = 0,$$

$$\text{Outside:} \quad \underline{B}_e = \underline{H}_a + \underline{H}_s,$$

where $\underline{H}_s$ is now the field due to the magnetization of the sample.

$$\text{Now} \quad \underline{B} = \underline{H} + 4\pi \underline{M},$$

$$\text{And hence} \quad \underline{B}_i = \underline{H}_i + 4\pi \underline{M} = 0,$$

$$\therefore \quad \underline{M} = -\frac{1}{4\pi} \underline{H}_i. \qquad (1.2)$$

Thus this approach attributes to the superconductor an ideal diamagnetic susceptibility of $-\frac{1}{4\pi}$. Both of these descriptions are of course equally valid but it is the second which will be used throughout this work.

1.4 The intermediate state - static and dynamic properties

The treatment of the previous section dealt with a long superconducting needle in a parallel field where no complications arise due to demagnetisation effects. Let us now consider the situation for a uniform ellipsoid of demagnetisation coefficient D situated in an applied field $\underline{H}_a$ parallel to its major axis.

Standard electrodynamic treatments (Brailsford (1966)), which are independent of susceptibility and therefore applicable to superconductors yield

$$\underline{H}_i = \underline{H}_a - 4\pi D\underline{M}. \tag{1.3}$$

Now using equation (1.2) from the previous section, we obtain

$$\underline{M} = -\frac{\underline{H}_a}{(1-D)}, \tag{1.4a}$$

and

$$\underline{H}_i = \frac{\underline{H}_a}{(1-D)}. \tag{1.4b}$$

Let us now consider the special case of a sphere for which $D = \frac{1}{3}$. Then,

$$\underline{M} = -\frac{3}{2}\underline{H}_a,$$

and

$$\underline{H}_i = \frac{3}{2}\underline{H}_a.$$

Hence we see that the induced magnetisation of the superconductor distorts the external field and the above calculations indicate that the field at the equator of the sphere will reach the critical value before the external field does. One is then led to the question of what happens when this occurs. To assume that a portion of the specimen near the equator becomes normal would lead to a contradiction. The boundary between superconducting and normal regions occurs when $H = H_c$, but in the now normal region the field would equal $H_a < H_c$. There is, in fact, no simple large scale division which will satisfy these conditions and instead one must postulate, as was first done by Peierls (1936) and F. London (1936), that once $\underline{H}_a \geqslant (1 - D)\, H_c$, the entire specimen is subdivided into a small scale

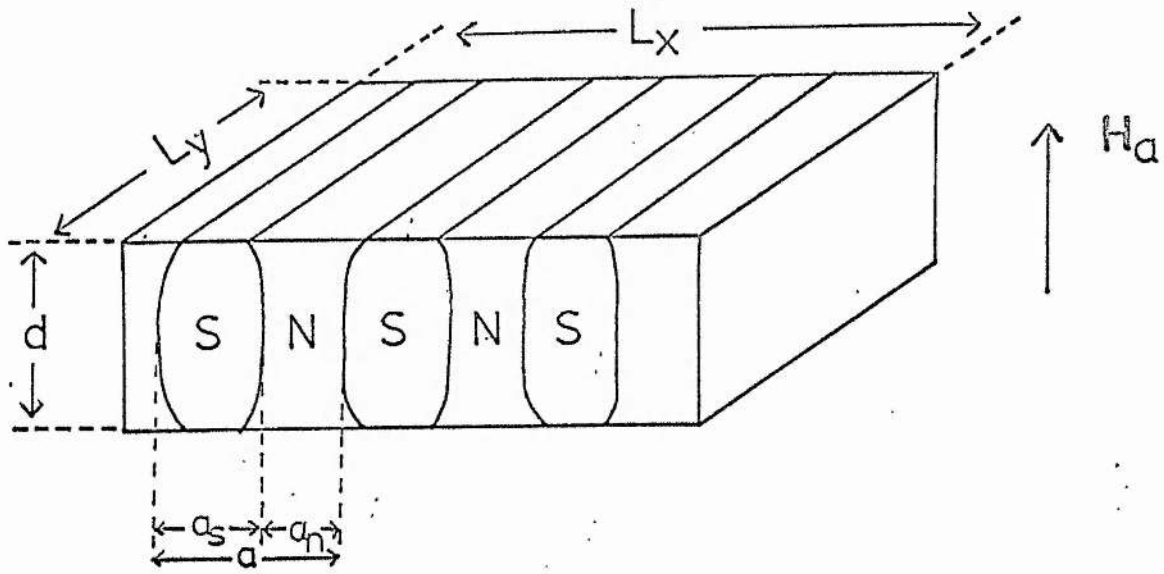

Fig. 1.1 Landau's Model of the Intermediate State.

arrangement of alternating normal and superconducting regions, with $B = H_c$ in the normal regions, and $B = 0$ in the superconducting ones.

This mixture of the two states - normal and superconducting - in the one specimen at the same time has become known as the INTERMEDIATE STATE. It exists, in some field interval, for all geometries other than that of a long needle situated in a field parallel to its axis.

In general, the problem of the determination of the shape of the intermediate state structure is not a simple one, and can only be attempted if some assumptions about the shape are made. The first and still the most successful theory is that due to Landau (1937).

Landau considered an infinite plate in a perpendicular field H_a and assumed that it would split up into alternate superconducting and normal regions as shown in Fig. 1.1. He then found the laminar period a by minimizing the free energy with respect to the size of the domains. There are five terms in the expression for the total free energy:

(i) the condensation energy in the superconducting domains is given by

$$F_1 = - \frac{H_c^2}{8\pi} L_x L_y d . a_s/a ,$$

(ii) the magnetic field energy in the normal regions is given by

$$F_2 = \frac{H_a^2}{8\pi} L_x L_y d . a/a_n ,$$

(iii) the energy per unit area of boundary between the superconducting and normal regions is usually denoted by α, and in this case we can simplify the analysis by expressing the surface energy in terms of a characteristic length Δ such that

$$\alpha = \frac{1}{8\pi} \Delta H_c^2 .$$

The contribution of the surface energy is thus

$$F_3 = \alpha d L_y . (\text{number of walls}) = \frac{H_c^2}{8\pi} L_x L_y d . \frac{2\Delta}{a}$$

(iv) as shown in the figure the lines of force 'open up' near the sample surface and hence the superconducting domains become thinner at their ends and some condensation energy is lost. This loss will be of the form

$$F_4 = \frac{H_c^2}{8\pi} \; a_s^2/a \; L_x L_y U_o \; (a_s/a) \; ,$$

where U_o is a dimensionless function that can be computed when the exact shape of the superconducting regions is known,

(v) the spreading of the normal domains also modifies the magnetic field energy, and this gives a term

$$F_5 = \frac{H_a^2}{8\pi} \; a_s^2/a \; L_x L_y V_o \; (a_s/a) \; ,$$

where V_o is another dimensionless function. The calculation of U_o and V_o is described by Landau and Lifshitz (1960).

We can choose as independent variables a and a_s/a. First minimizing the total free energy with respect to a_s/a, we find

$$1 - a_s/a = \frac{H_a}{H_c} \qquad (1.5)$$

This just expresses the fact that the field in the normal regions is equal to H_c. Then, minimizing the free energy with respect to a we find

$$a^2 = \frac{\Delta d}{\frac{1}{2}\left(\frac{a_s^2}{a^2} \; U_o + \frac{a_s^2}{a^2} \; \left(1 - \frac{a_s}{a}\right)^2 \; V_o\right)}$$

$$\text{i.e.,} \quad a^2 = \frac{\Delta d}{\phi\left(\frac{a_s}{a}\right)} \qquad (1.6)$$

and from equation (1.5),

$$a^2 = \frac{\Delta d}{\phi \; (1 + h)} \qquad (1.7)$$

where $h = \frac{H_a}{H_c}$, the reduced applied field, and ϕ is a numerical function which has been tabulated by Lifshitz and Sharvin (1951).

A typical value of ϕ is 10^{-2} for $h \sim 0.7$, so for a sample 1 mm thick

with surface energy parameter $\Delta \sim 10^{-4}$ mm the laminar period should be

$$a = \frac{10^{-4}.\ 1}{10^{-2}} = 0.1 \text{ mm.}$$

This, as will be seen later, is similar to that found experimentally.

The spreading of the normal laminae as they reach the surface means that since the local field is equal to H_c on the interface, the field in the middle of a normal laminae must drop below H_c when it spreads out. This difficulty led Landau (1943) to the development of a branching model in which a normal lamina was supposed to split first into two, then four laminae, etc., becoming finely divided as it approached the surface of the superconductor.

Early experiments did not show a branching type of structure although more recent experiments have done so, (Allen and Lerski (1972 a), Solomon (1971), Kirchner (private communication)). This has been shown (Allen and Lerski (1972 b)) to be in agreement with the theory of Lifshitz and Sharvin (1951). The latter, using Landau's geometry, on minimizing the free energy of a branching structure with respect to the number of branches, showed that this number would be small in typical experimental situations. This is because the reduction in magnetic free energy achieved through the branching is outweighed by the increase in surface energy.

It will be shown in a later chapter that significant branching did not occur in the geometry used in this work.

Various attempts to improve on Landau's model have been made. Of these, mention should be made of Andrew (1948), who proposed a branching model where the branches were threads rather than laminae, and Kuper (1951) who developed a slightly different unbranched model. As has been stated, however, Landau's simple unbranched model has proved the most successful of these and is still the most widely used.

The free energy of an unbranched laminar structure can be lowered by the development of corrugations in the laminae near the surface (Faber (1958); Balashova and Sharvin (1957)). Like the branching model, this lowered the field energy at the expense of increasing the surface energy, and Faber (1958) has presented arguments to explain why corrugations rather than branching should be observed in practice.

It should finally be stated that the differences in total free energy between the various morphologies are so small that the structure actually observed in practice often depends on how the state was achieved, on details of the specimen shape and on specimen inhomogeneities.

The first suggestion that an intermediate state structure would move under the influence of a transport current flowing through a superconductor was made by Gorter (1957, 1958). He predicted that the motion would occur at right angles to the direction of the current J with a velocity

$$V = \frac{\sigma J}{\sigma H_c} , \qquad (1.8)$$

where σ is the conductivity in the normal state.

The first attempts to observe this particular phenomenon produced conflicting results. Sharvin (1965), using a point contact to the superconductor, claimed observation of the domain motion but this experimental method was later called into question by Chandrasekhar et al (1967). A repetition of the Sharvin experiment using a superconducting microbridge magnetometer by Brandt and Parks (1967) revealed no motion of the intermediate state structure.

More recently, however, motion has been observed (Solomon (1969), Van Gurp (1969)). In fact, Solomon and Harris (1971) have shown that any intermediate state topology is unstable with respect to transverse motion in the presence of a transport current.

In his original paper, Sharvin (1965) pointed out that the motion

of normal regions in a dynamic intermediate state involves a transport in entropy, and should produce a temperature difference. Conversely, temperature gradients cause a force on flux bundles and should produce a motion just like a transport current. Equivalent effects in the mixed state of Type II superconductors have been observed (Fiory and Serin (1966), Otter and Solomon (1966)) but until this work and the very recent publications of Gupta and Farell (1973) and Laeng and Rinderer (1973) no experiments had been reported in the intermediate state of Type I superconductors.

1.5 Methods of observation of the intermediate state

The problem of observing the structure of the intermediate state is one of resolving the change in magnetic field (typically ~400 Oersteds) between normal and superconducting regions whose dimensions are typically of the order of 100 μm. Basically this has been accomplished experimentally through three different methods, (a) magneto-resistance in small bismuth probes, (b) Bitter patterns using ferromagnetic or superconducting powders, and (c) Faraday rotation.

The first of these was utilised by Meshkovsky and Shalnikov (1947) in the first successful observation of the structure of the intermediate state. Convinced by Landau's branching theory that the flux structure would be very fine at the external surface of a superconductor, they measured the field distribution between two halves of a tin sphere. The disadvantage of this method is that the spatial resolution is limited by the size of the Bismuth probe used, and cannot reasonably be reduced below about 20 μm. Consequently, it has not been used in more recent experiments.

The second of these methods was used for the first observation of intermediate state patterns on the outside of a superconductor by Balashova and Sharvin (1956). They spread 1 μm ferromagnetic

nickel powder onto the sample; this powder was, of course, attracted by the magnetic field onto the normal regions when the sample went into the intermediate state. A series of rich and complex patterns was revealed as the external field was varied. Many subsequent experiments have been reported using superconducting (e.g. Schawlow et al (1958, 1959)) as well as ferromagnetic powders. The disadvantage of this simple powder method is that, as was shown by Olafsson (1971), the use of a powder which does not move very easily makes it difficult to obtain more than one flux distribution picture per run. On the other hand if one uses a powder which is fairly mobile (small and superconducting) then care must be taken in the interpretation of the pattern obtained since it may represent the paths of the penetrating or escaping flux. The resolution of this powder technique has not been established, but certainly it cannot be less than several times the particle diameter (~ 5 μm).

The resolution has recently been considerably improved through the method of forming an extremely fine powder (~ 50 Å) by means of an evaporation inside the cryostat itself, letting it drop onto the sample under the influence of the magnetic field in the normal regions. When the particles of powder fall onto the surface they become immobile and the sample can be warmed up and the pattern examined under an optical or electron microscope. In this way, Träuble and Essmann (1966 a, b) and Sarma and Moon (1967) have obtained pictures of the intermediate state with the highest resolution yet obtained (< 0.1 μm).

The third of these methods is based upon the fact that if a thin sheet of paramagnetic material is placed over a specimen in the intermediate state it will be magnetized only over the normal regions. Polarized light passing through this material and reflected from its bottom surface will experience Faraday rotation in these regions, the rotations experienced on the two passages through the material being additive. Thus light reflected over normal areas will have a different

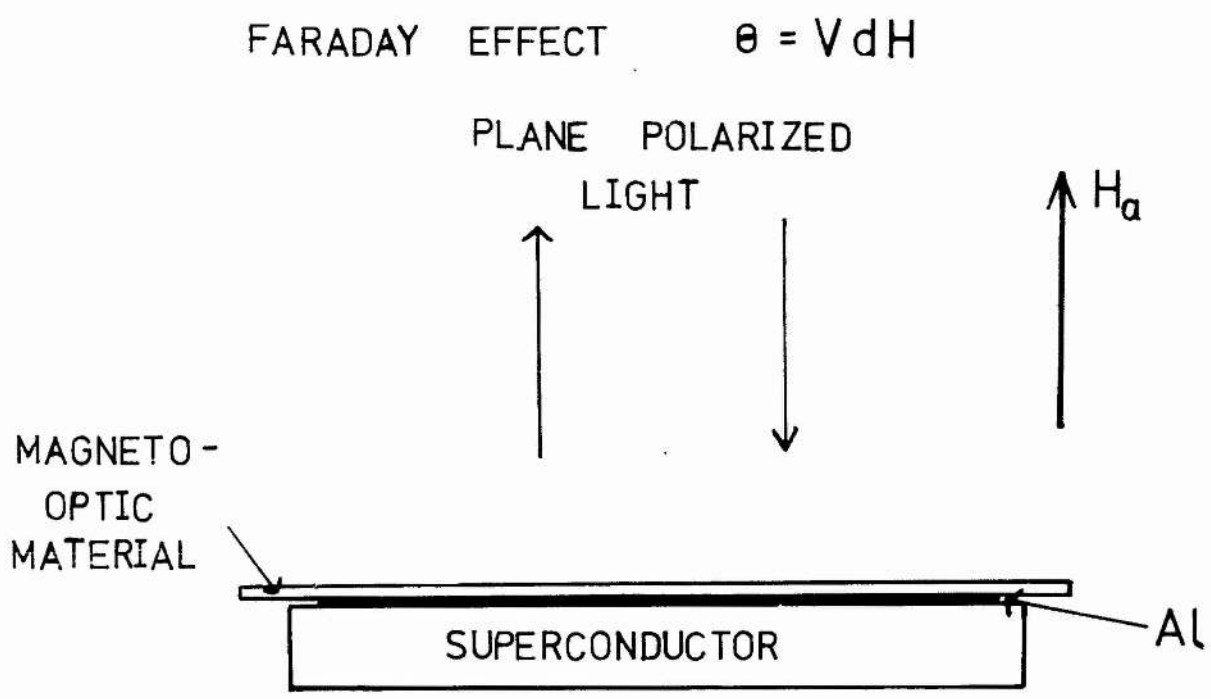

Fig. 1.2 BASIC MAGNETO-OPTIC SET-UP

plane of polarization from that reflected over superconducting areas, and this difference may be seen with an analyser. The rotation of the plane of polarization experienced upon passing through a thickness d of paramagnetic material in a field H is given by Faraday's law

$$\theta = V.H.d, \qquad (1.9)$$

V is called the Verdet constant of the material.

This use of the Faraday effect to observe the field distribution in a superconductor was introduced by Alers (1956, 1959) and subsequently used extensively by Desorbo et al (1960, 1962, 1964, 1965) and by Baird (1964, 1965). The paramagnetic material used in all these experiments was Cerium Metaphosphate (CMP) glass from 0.2 to 0.5 mm thick. Figure (1.2) shows a typical magneto-optic set-up. Due to the spreading of the magnetic field from the normal regions upon leaving the specimen, the resolution of the method is of the order of the thickness of the CMP (Kirchner 1968 (a)) and hence in these experiments was at best 200 μm.

An improvement of this resolution cannot simply be achieved by further thinning of the CMP glass since, from equation (1.9), we see that the magnitude of the rotation of the plane of polarization depends linearly on the thickness and hence would quickly drop below the limit of detectability. Hence, to use a thin Faraday rotator one must find a material with a very high Verdet constant. Such a material is the ferromagnetic semiconductor europium sulphide EuS, which can be evaporated into thin films possessing enough specific Faraday rotation to render the intermediate state visible.

The use of EuS films was pioneered by H. Kirchner (1968 a, 1968 b, 1969, 1972) and used with varying success by other workers (Solomon and Harris (1970), Huebener et al (1970 a, 1970 b, 1971, 1972 a, 1972 b)). The resolution achieved by Kirchner was 0.5 μm which is quite adequate for most intermediate state studies.

The great advantage of this high resolution magneto-optic method is that dynamic processes can be studied and indeed cine film or videotape recordings of the flux motion can be obtained. None of the other methods is capable of providing a record of dynamic processes except the magneto-resistance method and this with a much poorer resolution.

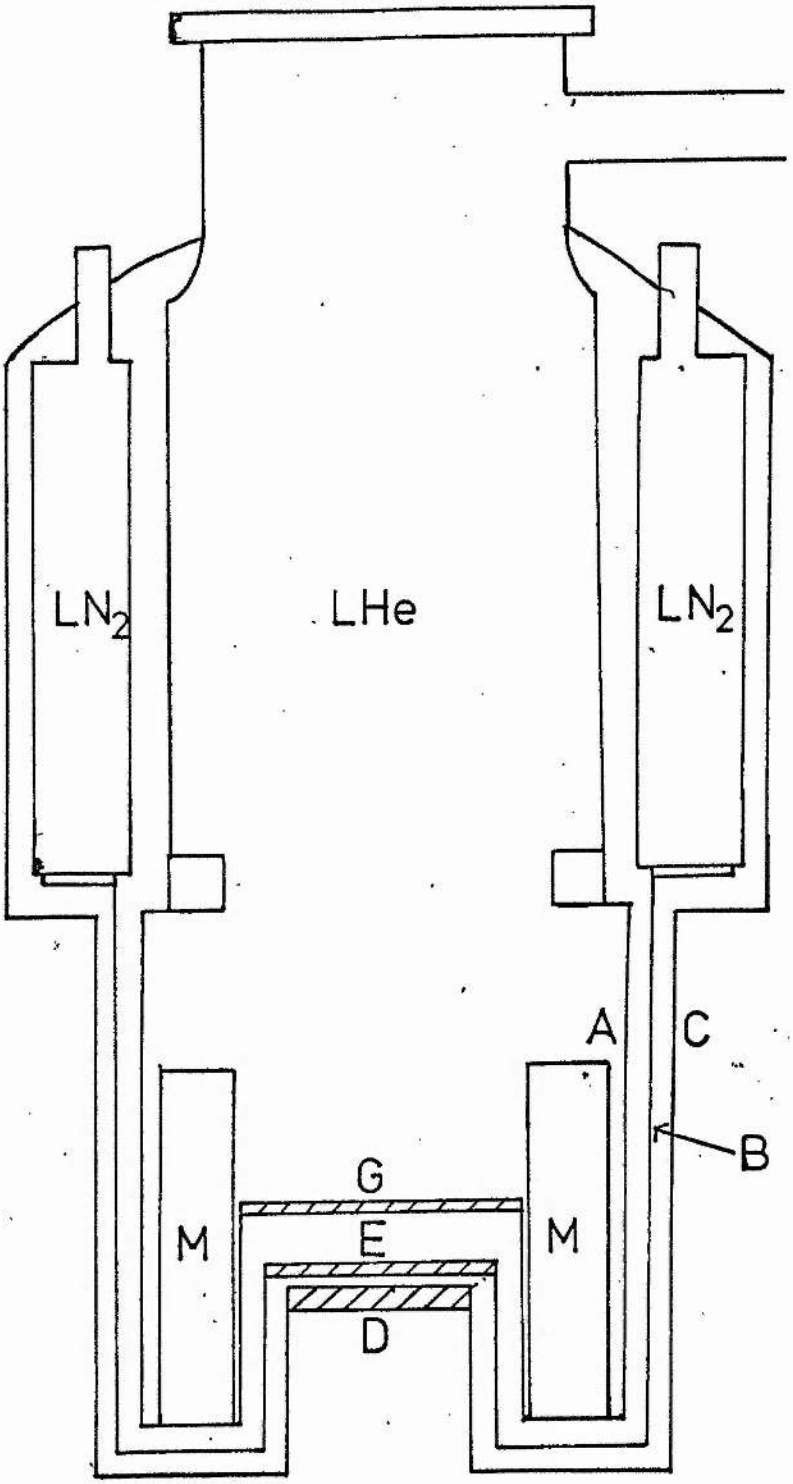

Fig. 2.1. The stainless steel dewar.

CHAPTER II - APPARATUS and EXPERIMENTAL DETAILS

2.1 Introduction

The resolution of intermediate state structure attainable with the magneto-optic method using europium films is limited only by the optical system used. For the optical set-up in this work to be capable of resolving the finest details of the intermediate state in Type I superconductors it has to have a resolution of the order of 5 μm. Such an optical resolution can only reasonably be achieved using a microscope, hence, in the manner of Kirchner (1968 b), it was decided to design a stainless steel helium dewar with optical access for a polarized light microscope.

2.2 The Cryostat

The dewar which was used (Fig. 2.1) was a modular series 100 type obtained from Thor Cryogenics Ltd. Although the main section was their standard design in stainless steel, the tail was specially designed for this experiment. It consisted of a stainless steel inner liquid helium can A shaped to accommodate a superconducting magnet M described below, a copper shield attached to the liquid nitrogen reservoir in the main section B, and an outer stainless steel can C.

The optical access was through three glass windows. The outer of these D was made of Schott SF57 glass (for reasons to be discussed later) and was simply glued into place using Araldite. The middle one E was made of Chance heat absorbing glass and was kept in thermal contact with the nitrogen-cooled shield using GE 7031 varnish. The inner window F, again made of Schott SF57 glass, formed the bottom of the liquid helium space and was sealed to a stainless steel mount using an indium O ring carefully made from 0.5 mm indium wire by soldering the ends together. It was found that such a seal if made with care would remain leak tight for up

to five cycles from room to helium temperatures. An important feature of the design was that the distance from the outside of D to the sample position G was kept below 15 mm to allow microscope objectives of fairly high numerical aperture to be used.

The length of the tail was chosen so that the liquid helium capacity of the whole dewar was ~ 5 litres, sufficient to allow for a run time between transfers of up to 48 hours when three radiation baffles were fitted up the dewar neck.

The magnetic field used in these experiments was applied perpendicularly to the sample and was supplied by a magnet made previously in this laboratory for another purpose. It was 150 mm long with a bore of 45 mm and consisted of 2000 turns of NbZr copper sheathed superconducting wire wound in 16 layers. Its calculated field/current coefficient was 426 Oe/Amp at its centre.

The current for the magnet was provided by a British Oxygen Cryoproducts power supply which maintained the current constant to 0.1% and had safety provisions built in in the event of the magnet going normal. The magnet current was found by measuring the voltage across a standard one ohm resistor through which it passed with a Dynamco DM 2022S digital voltmeter. The magnetic field was then determined from the calculated field/current coefficient.

Bath temperatures between 4.2K and 1.2K were achieved by pumping on the helium. The temperature was obtained by measuring the vapour pressure above the bath using a mercury manometer and cathetometer or a McLeod gauge. Two carbon resistors mounted in the helium space served to indicate the helium level and temperature, their resistance being measured with an Oxford Instruments AC resistance bridge which dissipates less than 10^{-9}W in the resistor.

A combination of 2" oil diffusion pump and rotary pump was used to

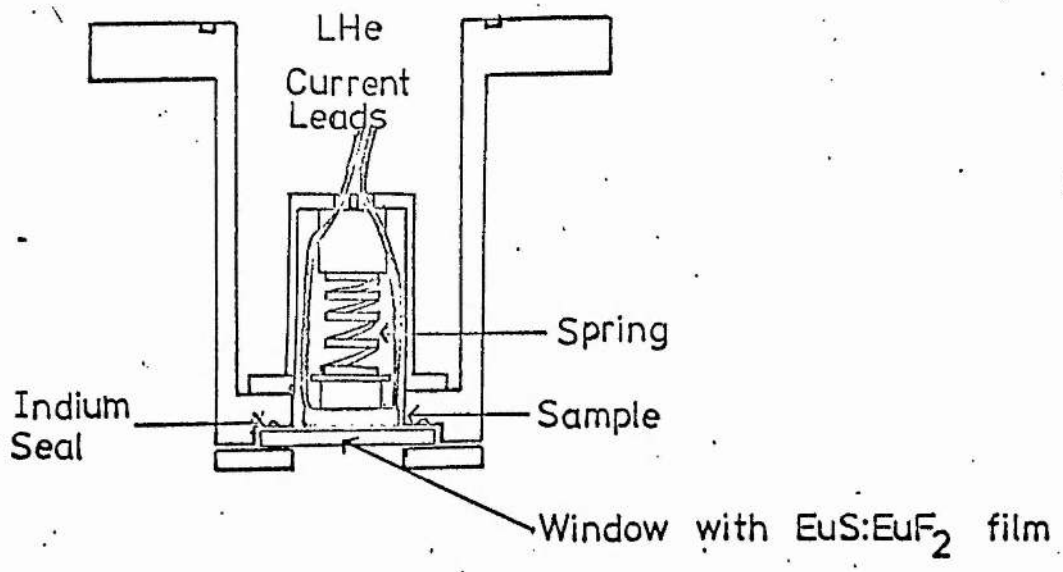

Fig. 2.2. Sample mount for the observation of current-induced flow.

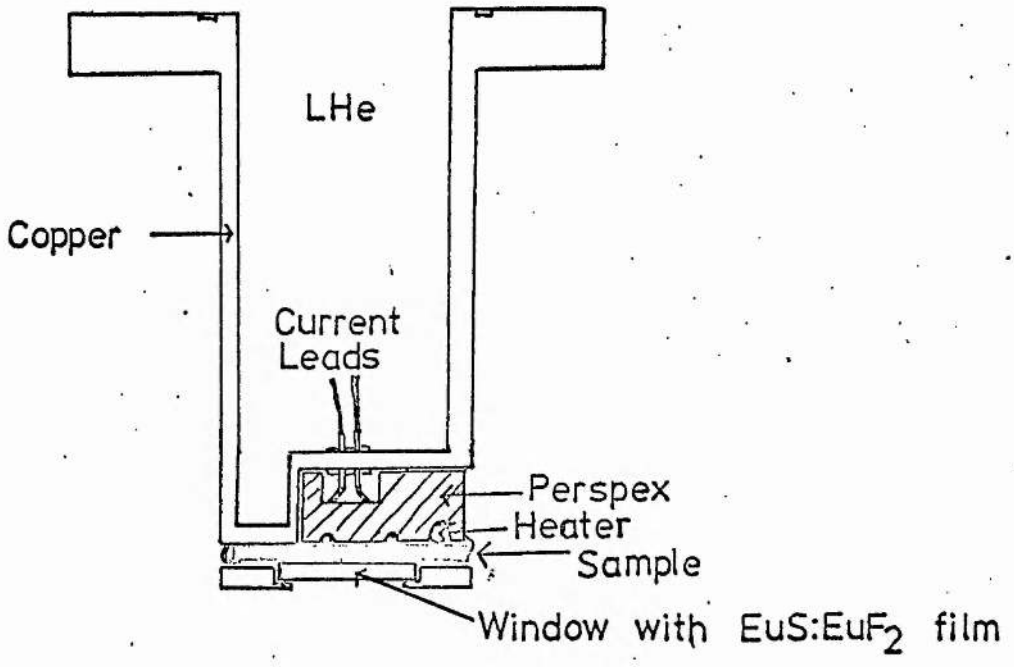

Fig. 2.3. Sample mount for the observation of thermally-induced flow.

pump the vacuum insulation space of the dewar to a pressure of less than 10^{-5} torr before helium transfer when the dewar was sealed off. The avoidance of diffusion pump oil coating the dewar windows was ensured by the use of a stainless steel liquid nitrogen-cooled trap on the diffusion pump.

2.3 Construction of the sample mount

(i) For the observation of current-induced flow

As will be shown later, to obtain meaningful results for current-induced flow it was necessary to ensure that the superconducting sample was in good thermal contact with its surroundings. The samples were consequently pressed against the EuS:EuF_2-coated inner window from inside the liquid helium space and hence were immersed in liquid helium.

Fig. 2.2 shows the details of the sample mount. All samples were thin slabs of approximate dimensions 10 mm x 5 mm x 2 mm thick. Good contact between the sample and the magneto-optic mirror was ensured by the use of a non-magnetic stainless steel spring (made from 18 gauge wire) which pressed them together. The leads for passing a current through the sample were soldered to its ends with indium and were made from copper coated NbTi filamentary superconducting wire. After a length of about 10 cm these wires were soldered to 20 swg copper wires which led up to the cryostat top.

Currents up to 10 amp could be passed through these leads using a Farnell L30F power supply which held the current constant to better than 1%.

(ii) For the observation of thermally-induced flow

It was necessary in this case to mount the sample so that a known temperature gradient could be established along it and a current passed through it. Fig. 2.3 shows how this was accomplished.

All of the samples were thin slabs of dimensions 15 mm x 5 mm x 2 mm thick. One end of the sample was screwed to a copper post mounted at the bottom of the liquid helium bath. The other end was supported by a similar

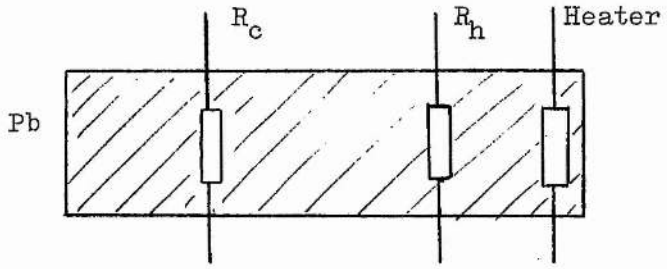

Fig. 2.4 Arrangement of the thermometers and heater on the sample for the observation of thermally induced flow.

perspex post, which had a heater resistor inserted in it. Good thermal contact between the copper post and the sample was ensured by soldering them together with Woods metal. Good thermal contact with the heater was accomplished using GE 7031 varnish. The heater used was a 1KΩ carbon film resistor, this type being chosen because the resistance changes very little in the liquid helium temperature range.

The disc of SF 57 glass bearing the europium film was located in a perspex mount which was then firmly screwed down against the sample. A copper heatshield with a small hole to allow observation was attached to the copper post and surrounded the sample mount.

As in the last case the leads supplying a current to the ends of the sample were of NbTi superconducting wire. These were soldered with indium to the sample and were passed through a glass/metal seal in the copper mount up into the liquid helium bath.

Temperatures at two points on the sample (Fig. 2.4) were measured using 100 Ω Allen-Bradley resistors of dimensions 4 mm long x 1 mm diameter; these being the smallest available. The resistors were varnished to the underside of the sample using GE 7031 varnish. Their resistance was measured with the Oxford Instruments AC bridge. The leads from these two resistors were of thin (38 swg) silk-covered constantan wire. These were thermally anchored to the copper post with GE 7031 varnish after a long coil to ensure good thermal isolation from the bath. The leads to the heater were of 36 swg enamelled copper wire and were similarly treated. All these leads were taken to the outside at the base of the cryostat, being thermally anchored to the nitrogen shield with GE 7031 varnish on the way.

The power for the heater came from a Farnell L30A power supply, 500 mW being the maximum power required.

2.4 Requirements of the magneto-optic experiment

The main disadvantage of EuS:EuF_2 films is their large absorption coefficient of $2 \times 10^{+5} cm^{-1}$ (Suits and Argyle (1965)); this limits the thickness that can be used and hence the rotation attainable. In the present work all the films used were about 2000 Å thick and transmitted about 25% of the light incident upon them.

Suppose in a particular situation a rotation θ_R of the plane of polarization of the incident light is obtained. On analysis the intensity of transmitted light is reduced by a factor $\cos^2\theta_R$, and since θ_R is typically 30', the intensity loss through absorption in the film and analysis of the light is 99.8%. Consequently, if sufficient light is to be left for examination, a light source of high intensity must be used and the illumination of the sample must be as efficient as possible.

Obviously the resolution attainable by this method is limited by the film thickness, the contact to the sample, and the optical system. The film thickness is 0.2 μm and the sample surfaces can be pressed or polished flat to 0.5 μm so that in practice the largest limitation on the resolution is that of the optical system.

Martin (1966) has given the resolution limit of a microscope objective as

$$R_\lambda = \frac{\lambda}{A_o + A_c} ,$$

where λ is the wavelength of the light in use,

A_o is the numerical aperture of the objective, and

A_c is the numerical aperture of the condenser.

Hence the objective must be chosen to have the highest numerical aperture given that the limitation of the working distance is a minimum of 15 mm. Care must also be taken with the condenser system.

The contrast between normal and superconducting regions depends on the angle of rotation θ_R produced by the field H_c and in fact the condition

for a contrast to appear is that the intensity of rotated light must exceed the overall intensity of light passed at the extinction I_E , i.e.,

$$I_o \sin^2\theta_R \geqslant I_E \ .$$

The magnitude of I_E depends on two factors: (a) the practical limit to performance of the polarizer and analyser, and (b) any ellipticity in the state of polarization due to strain in the cryostat windows or microscope objective. King and Talim (1970) have measured the extinction ratio $\frac{I_E}{I_0}$, of various polarizers and analysers. They found values of $\sim 10^{-6}$ for the best available dichroic polaroid sheet, Käsemann MIK. Substituting in the above equation we see that the smallest θ_R discernible, ignoring strain ellipticity, $\frac{t}{\lambda}$, is about four minutes of angle. However, the presence of strain can easily increase the extinction ratio to as high as 10^{-3} and this dramatically raises the smallest θ_R discernible to almost 2^o. Hence, clearly the best quality polaroid must be used and extreme care must be taken to minimise strain in the system.

King and Talim also showed that the avoidance of dust and extreme cleanliness are important if a high extinction ratio is to be maintained.

Now the window into the helium space and the outer window both form vacuum seals and hence are unavoidably under strain. To minimise the effect this strain would have on the state of polarization of the light passing through them, a glass with a low photoelastic constant was chosen for their construction. The photoelastic constant of a glass relates the birefringence produced in the glass to the applied stress (Hendry (1966)).

This glass was obtained from JENAer Glaswerk Schott and Gen. under the Code No. SF57. Its maximum birefringence is 2 nm/cm and its refractive index is 1.85. Both windows were made from discs 1.5 mm thick, the inner window being 15 mm in diameter and the outer 25 mm in diameter.

2.5 Preparation of the EuS:EuF_2 films

Kirchner (1968 a) found in the course of his development of the use of europium films that a pure EuS film, since it is ferromagnetic below 16K (Enz et al (1962)), perturbs the intermediate state structure of the superconductor. He showed, however, that a mixed film of EuS and the paramagnetic material EuF_2 did not have a ferromagnetic transition in the temperature range of interest although it still exhibited a high Faraday rotation. Laeng and Rinderer (1972) have shown that the proportions of EuS and EuF_2 in the mixture is vitally important if alterations to the intermediate state structure are to be avoided. They found that EuS:EuF_2 in the proportion 2:3 was most suitable and this was the proportion used in the present work.

The evaporation technique used was similar to that of Kirchner (private communication). The films were evaporated onto the SF57 glass inner window against which the superconducting samples would be pressed. EuS obtained from Dr. Kirchner and EuF_2 obtained from K & K Labs., New York, were mixed together in the proportions indicated above. They were then placed on a tantalum boat 0.01 mm thick in a standard high vacuum coating unit. A shutter between the boat and the substrate was used during degassing at a boat temperature of about 750°C. The evaporation was then performed at a boat temperature of about 2300°C. The process was essentially a 'flash' one; the evaporation was over in a few seconds, with the pressure being always held below 2×10^{-5} torr. Four or five such evaporations were needed to achieve a film of the required thickness, the vacuum being broken to replenish the boat each time.

It was found vitally important to use stainless steel fittings in the coating unit since the high boat temperature produced contamination due to zinc sublimation when brass fittings were used. An EuS:EuF_2 film contaminated with zinc had an increased optical density and produced no measurable rotation under typical experimental conditions. This almost complete

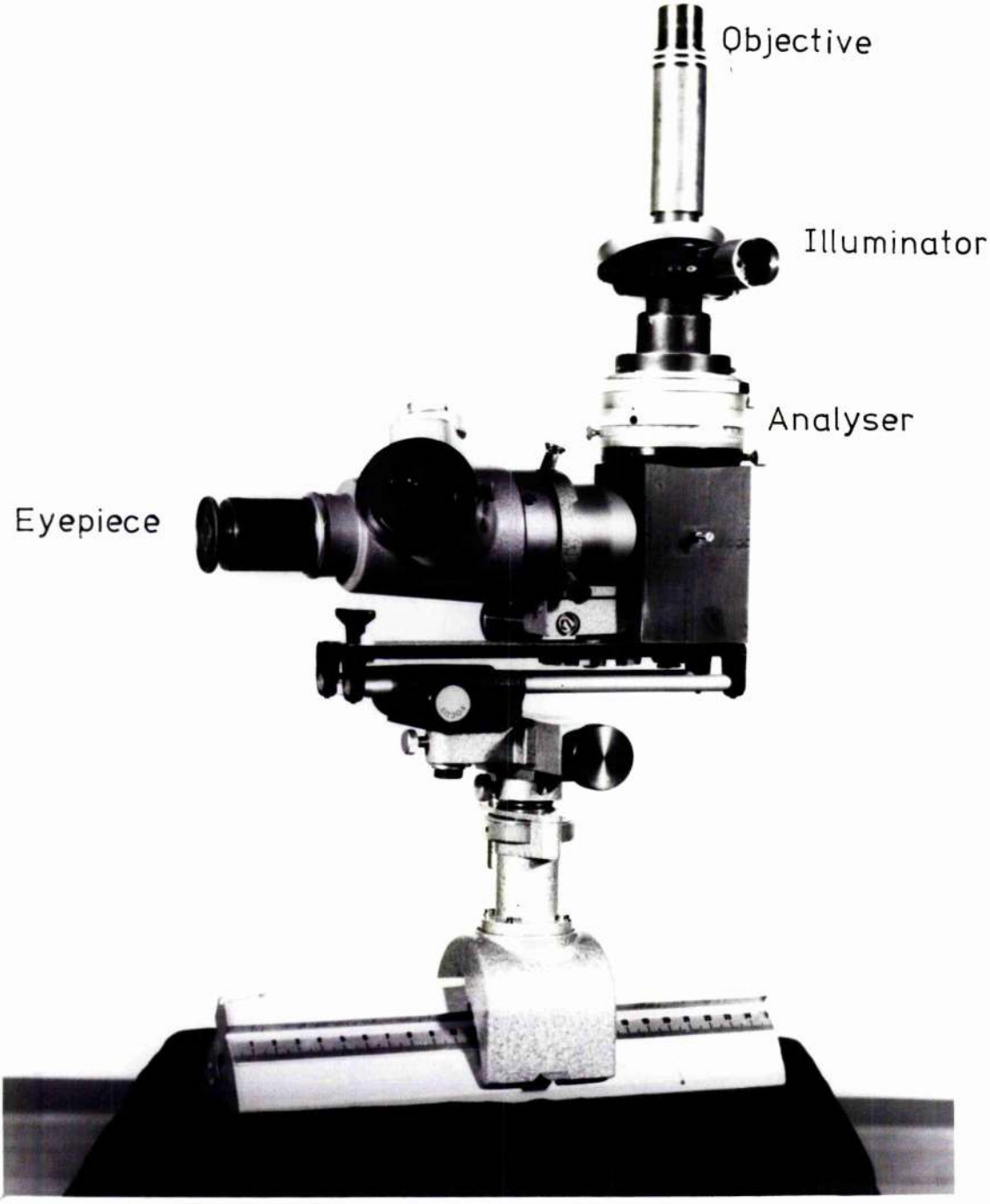

Fig. 2.5 The microscope

absence of rotation would not be expected if the only effect of the zinc were to increase the absorption of the film. Hence, the presence of the zinc must, in some manner, have destroyed the magnetic properties of the film. This phenomenon was not investigated further.

The film thickness was controlled by measuring the film absorption with a Pye spectrophotometer and using the data of Suits and Argyle (1965). An aluminium film of 1000 Å thickness was then evaporated on top of the EuS:EuF_2 film to complete the magneto-optic mirror.

2.6 Optical equipment

The requirements of the magneto-optic experiment were not met by a single commercially available microscope; in consequence a microscope had to be assembled from various component parts as shown in Fig. 2.5.

The restriction of the cryostat design (i.e. the insert tube) meant that the illumination of the sample had to be accomplished through the microscope objective; an incident illuminator was obtained from Vickers Ltd. for this purpose. This was specially designed to minimize the introduction of ellipticity into the polarized light by using two acute angle reflections to deviate the light.

The analyser was also obtained from Vickers. It contained a sheet of Käsemann MIK polaroid mounted between two strain-free pieces of glass. As stated in a previous section this was the best available dichroic polaroid sheet according to the data of King and Talim (1970). The orientation of the analyser could be read to 0.1° by means of a vernier scale.

After reflection from a mirror mounted in a machined brass jointing piece the light entered a double eyepiece holder also obtained from Vickers. One eyepiece was used for visual observation, the other for photographic work. The eyepiece used for visual observation was obtained from E. Leitz GmbH and had a magnification of 6.3x. The eyepiece used for photographic work was obtained from Reichert Wein GmbH and had a magnification of 5x.

Table 2.1 Microscope Objectives.

Manufacturer	Nominal Magnification	Numerical Aperture	Resolution Limit (μm)	Working Distance (mm)
(i) Ealing Beck	2	0.08	3.1	45
(ii) Vickers	3	0.1	2.5	35
(iii) Leitz	6.3	0.2	1.3	21

The four objectives used in the course of this work are listed in Table 2.1 together with their specifications. The resolution limits are calculated for light of wavelength 5481 Å. All the objectives were types designed for use with polarized light, their mountings being strain-free. Most of the observations were made with the x3 objective (No. ii), and hence the magnification usually employed was about 30. A graticule obtained from Leitz, which divided the field of view into sixteen squares, served to provide a quantitative measurement of the observed structure sizes, the calibration standard used being a stage micrometer of one hundred 10 μm divisions obtained from J. Swift Ltd.

The whole microscope was mounted on an optical bench stand made by Ealing Beck Ltd., which incorporated provision for vertical motion for focussing purposes, and for horizontal motion along and perpendicular to the optical bench for alignment on the correct part of the sample. The construction of this stand was made as rigid as possible to reduce shaking of the microscope whilst in use.

As previously stated the light source used in these experiments had to be of high intensity and the illumination of the sample as efficient as possible. Since the highest rotation of the plane of polarization by europium films occurs at short wavelengths (Suits and Argyle (1965)) a blue or green light source was required.

An attempt was made to use a HeCd laser which emits at 4800 Å, but this proved unsuccessful due to interference effects obscuring the required picture.

A high pressure mercury discharge lamp (Osram HBO 200) was then successfully used. This was obtained from Leitz mounted in a housing with provision for focussing and collimating the beam to give the maximum possible intensity input to the microscope system. The main wavelength emitted is 5481 Å but filters must be employed to remove the large quantities of

(b)

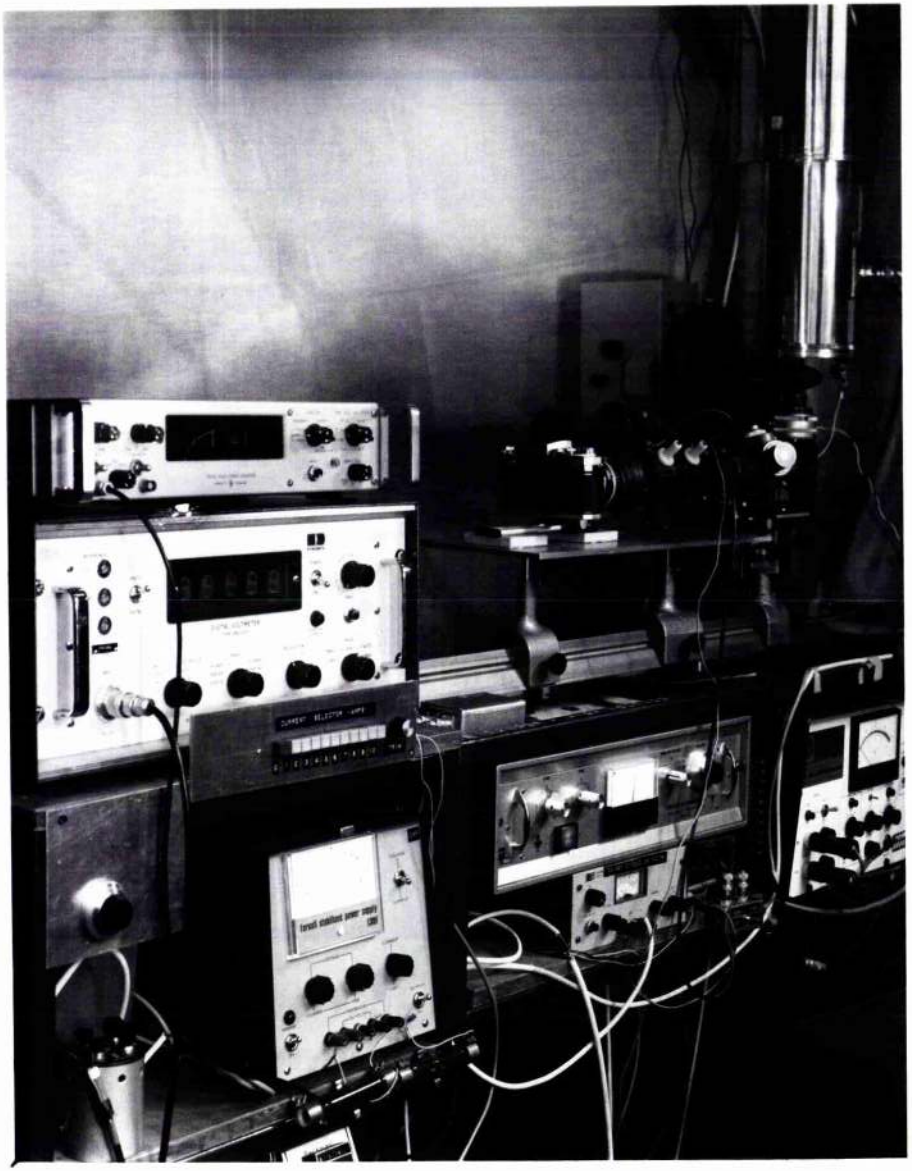

(a)

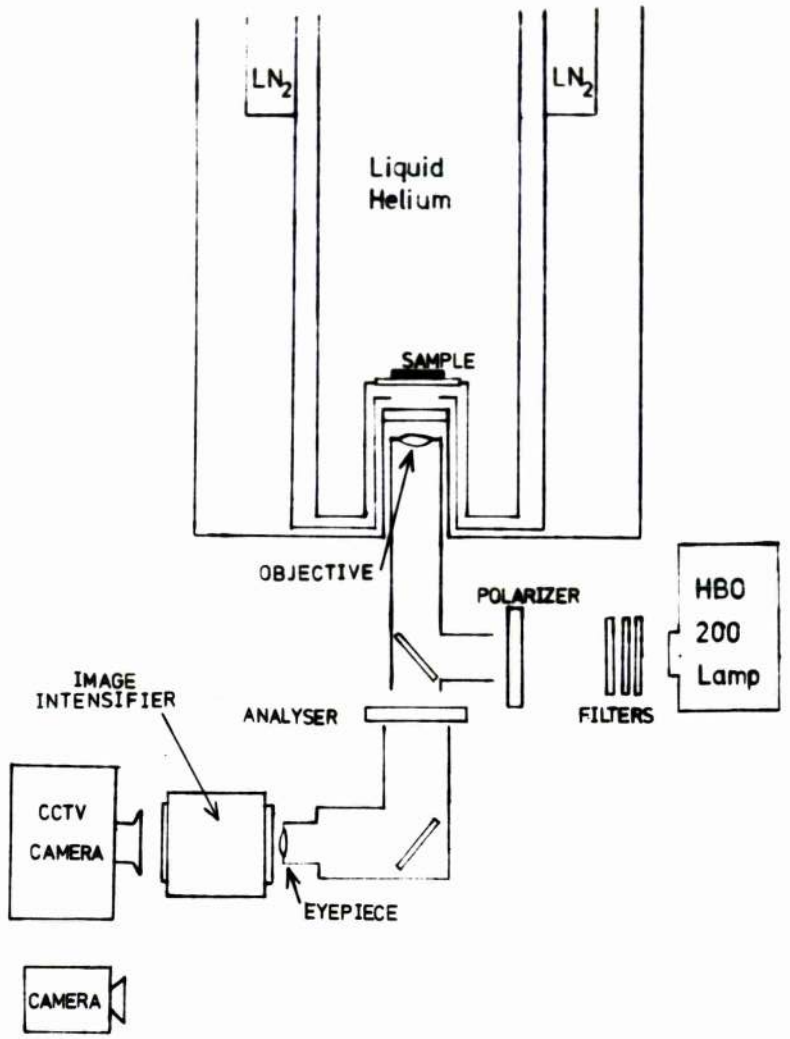

Fig. 2.7 The optical and cryostat set-up

ultra-violet which are also emitted. The estimated luminous flux entering the polarizer was ~ 3000 lumens.

To preserve this high intensity input to the microscope as much as possible a nicol prism was used to polarize the beam. This has a low loss (10%) compared to high quality dichroic polaroid which absorbs ~ 70% of the incident light. This nicol prism was made by Bellingham & Stanley Ltd. and was incorporated in a mounting which enabled its orientation to be adjusted and measured to 0.1°. This mounting also served to improve the collimation of the beam before it entered the microscope.

As previously mentioned, the small rotation and high absorption of the europium films lead to very little of the light incident from the lamp emerging from the eyepiece for observation. For photographic purposes the emergent light is in fact insufficient to produce a high contrast fine grain record of the flux distribution. Consequently, an image intensifier (Mullard Type XX1050) was used to amplify the light level to improve the photographic results. This had a gain of ~ 95 at 5481 Å and was mounted in a specially designed casing. Fig. 2.6 shows its construction. The outer brass casing connected to the cathode served as a screen to minimize the background illumination. The resolution of the intensifier device at 60 line pairs/mm was such that it introduced no image degradation. A high voltage (15 kV) was required for the image intensifier and this was supplied by a Brandenburg 776A encapsulated power supply driven by a Hewlett Packard 6284 variable DC power supply.

All still photographs were taken with a Nikon F 35 mm single lens reflex camera. When used with the image intensifier, bellows and a Nikon 50 mm f/2 lens were used to give a reproduction ratio of about $^{1}/_{2}$. When the image intensifier was not in use the microscope eyepiece was used to project the image directly into the camera with lens removed.

Some 16 mm cine film was taken using a Bolex H16 camera. This was usually used without the image intensifier.

h = 0.4

100μm

h = 0.6

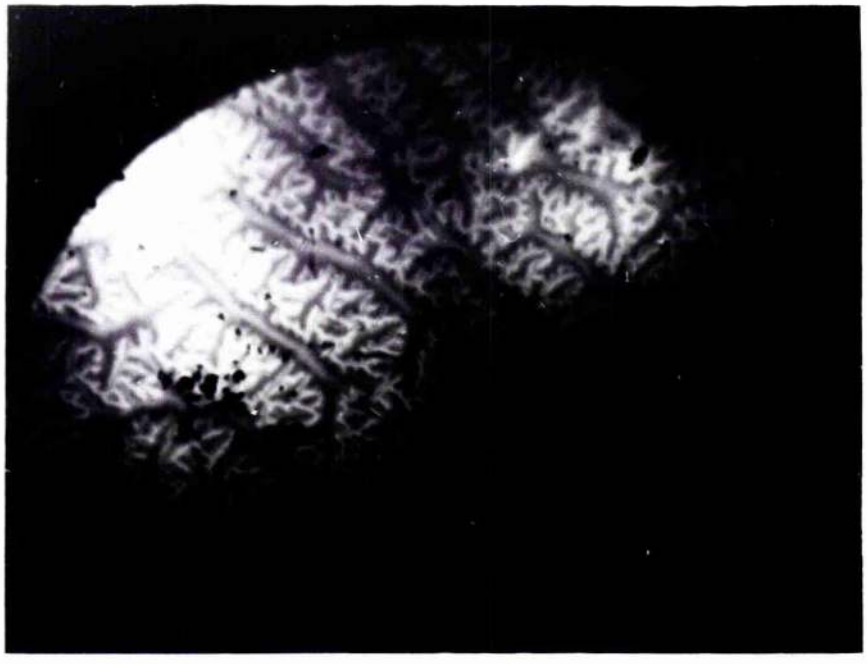

Fig. 2.8 Intermediate state in Pure Pb, T = 1.3K

The complete optical and cryostat set-up is shown in the diagram of Fig. 2.7(a) and the photograph of Fig. 2.7(b). As can be seen in the photograph the dewar was mounted on a frame welded together from 1" box steel section with two steel optical benches being bolted to the frame beneath the dewar to carry the optical equipment. The whole structure was bolted to the floor and wall of the Laboratory to increase its rigidity. Another small frame by the side of this frame carried the electronic equipment whilst the vacuum equipment was mounted on a 'Unistrut' frame behind the main frame.

2.7 Performance of the apparatus

The optical apparatus performed in general very well and the resolution achieved was certainly of the same order as the theoretical prediction. The photographs of Fig. 2.8 illustrate the quality of intermediate state pictures obtained. The magneto-optic contrast was such that observations could be made with critical field values as low as 90 oersted. This is quite sufficient to allow the study of the superconductors Pb (H_o = 803 Oe), Sn (H_o = 309 Oe), and In (H_o = 293 Oe). Greater field sensitivity could have been achieved by increasing the film thickness slightly, but this was not found to be necessary for this work.

The long run-time possible with the stainless steel dewar was advantageous when the experiment was functioning correctly but the consequently long time necessary to precool before helium transfer led to long turn round times for simple adjustments to the experimental structure. Recent advances have, however, given continuous flow systems which have turn round times of ~ 1 hour and these would perhaps be more convenient in this experiment.

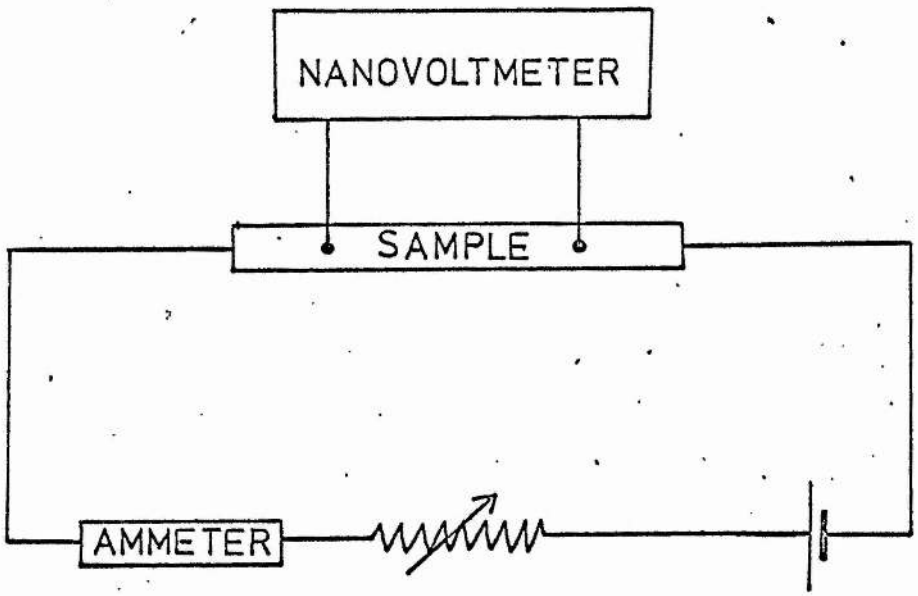

Fig. 2.9. The circuit for four terminal measurements of sample conductivity.

2.8 Measurement of the sample conductivity

The normal state conductivity of the materials used in the magneto-optic experiment were measured using a conventional four terminal technique (Fig. 2.9).

The voltage across the sample was measured using a Keithley 149 nanovoltmeter, the current through the sample being provided by a 2V accumulator and measured with an Avo multimeter. The experiment was performed in a large glass helium dewar previously built in this laboratory. A small superconducting magnet of computed field/current coefficient 320 Oe/amp was used to supply a magnetic field large enough to quench the superconductivity when measurements were being taken, the field being applied transversely to the wire.

As in the other experiments the current for the superconducting magnet was supplied by the British Oxygen Cryoproducts power supply, its magnitude being measured in the same manner as before.

Temperatures between 4.2K and 1.2K could be obtained by reducing the pressure above the helium bath. The pressure above the helium bath was measured with a simple manometer for pressures not much below atmospheric or with a McLeod gauge for low pressures.

Due to the high purity, 6-9's, of all the metals used it was found impossible to produce a measurable voltage across the same samples that were used for the magneto-optic experiments. Consequently, wires of ~ 1 mm diameter were used in the conductivity measurements, the leads being attached to them using indium as a solder. In the case of Pb and In these wires were extruded from the same batch of metal as was used to make the slab samples, whereas in the case of Sn the slab samples were made from commercially produced wire, initially used for the conductivity measurement.

In all these measurements it was found to be very important to apply the correct magnetic field to just quench the superconductivity and not a bigger one since all these metals exhibit appreciable magneto-resistance at the temperatures used (Olsen (1962)).

The calculation of the conductivity from the measured resistance requires a knowledge of the ratio of the wires length to its average area. This was calculated by measuring their resistance at room temperature (with a small current to avoid Joule heating) and using values obtained in the literature for the room temperature resistivity. The ratio obtained in this manner agreed with that directly measured using a micrometer and caliper gauge to within about 10%. The value obtained from electrical measurements was, however, used since it was considered that it represented a more reliable average value that that based on mechanical measurement.

	T_c(K)	H_o(Oe)
Indium	3.40	293
Lanthanum	6.0	1600
Lead	7.18	803
Mercury α	4.15	411
" β	3.95	340
Tantalum	4.48	830
Thallium	2.39	171
Tin	3.72	309

Table 3.1

CHAPTER III - SAMPLES

3.1 Introduction

There exist seven Type I superconducting metals whose transition temperatures are in the range 1.2K to 4.2K as shown in Table 3.1.

Lanthanum and mercury are difficult to handle, the first because of rapid oxidation in air and the second because it is, of course, liquid at room temperature. Tantalum has a high melting point (2832°C) and is very hard, making the production of samples difficult. This leaves indium, lead, thallium and tin; all are soft with low melting points and hence are easily pressed or cast to any desired shape.

In the present work all were used except thallium which was excluded because it could only have been used in the restricted temperature range 1.2K → 2.2K.

The importance of the recognition of the existence of magneto-resistance in these materials during the conductivity measurements has already been mentioned in Chapter II. The competing nature of this magneto-resistance and the intrinsic temperature dependence of the resistivity means that the effective conductivity important in the present work (i.e. that in a field H_c) has a different temperature dependence from the zero field conductivity. Indeed, after the resistivity has reached the residual value the magneto-resistance effect can produce a slightly increasing resistivity as the temperature falls.

The conductivity values were corrected to give those appropriate to the slab samples instead of the thin wires (Newhouse (1964)). This necessitated the assumption of values for the bulk electron mean free path at 4.2K. For Pb this was taken to be 4×10^{-4}cm (Cody and Miller (1968a)), for Sn 8×10^{-3}cm (Cody and Miller (1968b)), and for In 1.6×10^{-2}cm (Blatt et al (1967)). These assumptions were considered justified since

	EXPERIMENT	DIMENSIONS (mm)	σ MEAS. ($mhos.cm^{-1}$) T = 4.2K
Pb 1	Current-induced motion	6 x 5 x 1.4 thick	
Pb 2	Thermally-induced motion	15 x 3.9 x 1.1 thick	
Pb 3	Thermally-induced motion	15 x 6.5 x 1.8 thick	$(4.1 \pm 0.3) \times 10^8$
Pb 4	Thermally-induced motion	15 x 5.6 x 1.5 thick	
Pb 5	Current-induced motion	6 x 5 x 1.4 thick	

Table 3.2. The Pb samples.

the samples used in these other studies yielded very similar values for the bulk resistivity at 4.2K. The calculated corrections amounted to 1% for Pb, 9% for Sn and 5% for In.

3.2 Lead

The magneto-optic contrast is, as was shown in Chapter II, best for high fields and hence the observation of the intermediate state was most easily performed using lead which has a high critical field in the available temperature range. This was, consequently, the material used most throughout the present work.

The metal which was used to make all of the samples was obtained from Koch-Light Laboratories in the form of small shot of 99.9999% purity. The slab samples were produced by pouring the molten lead from a porcelain crucible into a stainless steel mould. The inside of the mould was coated with 'Acheson' colloidal graphite to inhibit sticking of the lead and to avoid it making contact with the stainless steel. Careful preheating of the mould to a temperature above the melting point of lead ($326^{\circ}C$) and slow cooling of the mould from its bottom after insertion of the lead ensured that the resultant slab contained fairly large crystallites.

After removal from the mould the slab of lead was chemically polished in a mixture of four parts glacial acetic acid to one part of hydrogen peroxide (100 vol.). Its faces were then pressed flat by squeezing them against quartz flats in a hydraulic press. The quartz flats were obtained from Jencons Limited and were guaranteed flat to $\lambda/8$ across their diameter (15 mm).

Table 3.2 gives the characteristics of the five lead samples used. The resistance ratio of the metal used ($\frac{R_{300}}{R_{4.2}}$) was 9300 ± 100. Samples Pb4 and Pb5 were annealed at $260^{\circ}C$ under a vacuum of $<10^{-5}$ torr for 48 hours after pressing to shape, to remove strain.

	EXPERIMENT	DIMENSIONS (mm)	σ MEAS. ($mhos.cm^{-1}$) T = 4.2K
Sn 1	Current-induced motion	6 x 5 x 1.5 thick	$(6.6 \pm 0.5) \times 10^8$
In 1	Current-induced motion	6 x 5 x 1.3 thick	$(2.5 \pm 0.2) \times 10^9$

Table 3.3. The Sn and In samples.

The intrinsic temperature dependence appeared to just dominate the behaviour of the effective conductivity below 4.2K since a slight increase of 5% occurred between this temperature and 1.3K.

3.3 Tin

The tin was obtained from Metals Research Ltd. in the form of 0.5 mm wire of 99.999% purity. The slab samples were produced by melting this wire in the stainless steel mould as with the lead.

Chemical polishing was done with dilute hydrochloric acid and the faces of the sample were again pressed flat against quartz flats in a hydraulic press. After pressing, the samples were sealed in Pyrex tubes pumped to a pressure of less than 10^{-5} torr and annealed at a temperature of 160°C for 48 hours to remove strains.

Table 3.3 gives the characteristics of the one tin sample used. The resistance ratio ($R_{300}/R_{4.2}$) of the metal was 7200 $\pm$ 150.

In agreement with the conclusions of Laeng et al (1971), the effective conductivity of the tin was found to decrease slightly as the temperature fell below its transition temperature due to the effect of transverse magneto-resistance. The value at the lowest temperature (1.3K) was 12.5% lower than that just above T_c.

3.4 Indium

The indium was obtained from Johnson Matthey Ltd. in the form of a polycrystalline rod of 99.9995% purity. The slab samples required were produced by squeezing sections of this rod (cut with a sharp stainless steel blade) in the hydraulic press.

The polishing and surface preparation was identical to that described above for Sn. No annealing was considered necessary since indium re-crystallises readily at room temperature.

Table 3.3 gives the characteristics of the one indium sample. The

resistance ratio of the metal was found to be 20,000 ± 200.

Again, the effective conductivity was found to be influenced by transverse magneto-resistance but the exact behaviour was slightly different. The conductivity fell as T was reduced below T_c until about 2.2K when it rose again to attain at 1.3K the same value as measured at T_c. The magnitude of this change was 18%.

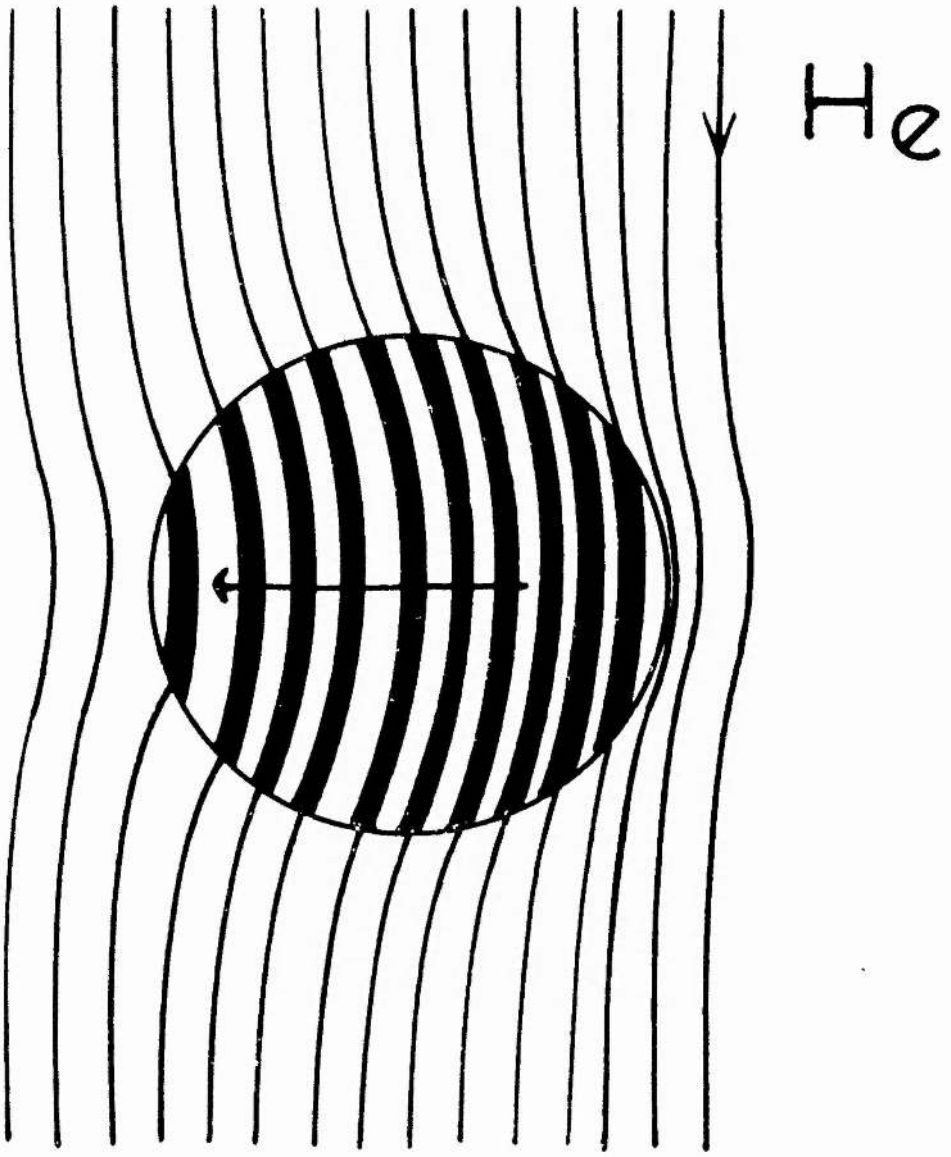

Fig. 4.1 The motion of laminar domains across a wire carrying a current situated in a transverse field H_e.

CHAPTER IV - THEORY of the DYNAMIC INTERMEDIATE STATE

4.1 Introduction

As mentioned in Chapter I, the first suggestion that a dynamic type of intermediate state could be produced by the passage of an electric current through a superconductor was made by Gorter in 1957. The first section of this chapter enlarges on Gorter's arguments and discusses their validity.

A complete theory describing the related electrodynamic and thermal effects that exist in the intermediate state was not given until fairly recently by Andreev and Dzhikaev (1971). This theory is discussed in detail in the following section.

4.2 Early theories

Gorter considered a current flowing through a wire situated in a transverse magnetic field large enough to induce a laminar intermediate state in the wire (Fig. 4.1). De Haas et al (1934) and Andrew (1948) had observed a voltage across a wire subject to these conditions. It is apparent that such a voltage cannot have a simple Ohmic origin and Gorter suggested that it was, in fact, due to induction voltages produced by motion of the boundaries between the normal and superconducting regions. He reasoned that these boundaries would move because of the Lorentz forces that would exist with such a non-homogeneous current distribution. Using a power balance equation he showed that the velocity of motion of the boundaries would be given by

$$V = \frac{cJ}{\sigma H_c} \quad , \qquad (4.1)$$

where J is the current flowing and σ is the conductivity of normal state. The mechanism which limits the motion is a viscous damping due to eddy currents induced in the normal regions.

The above result was obtained for any intermediate state topology by Solomon and Harris (1971) using a similar method.

Now the motion of the phase boundaries is accompanied by the transition of the metal from the normal phase into the superconducting phase and vice versa, and consequently by a release or absorption of the latent heat of the phase transition. It is clear that the electromagnetic phenomena are closely related to thermal effects and therefore that a complete theory must treat the two together. An exception is the case of low temperatures ($\ll T_c$), when the latent heat of the phase transition is small and its influence on the electrodynamics can be neglected. One would imagine, then, that equation (4.1) is only strictly valid for low temperatures since its derivation does not consider thermal effects. However, the complete theory to be described in the next section shows that it is also valid for pure metals.

4.3 General theory of Andreev and Dzhikaev

We consider a superconductor in the intermediate state with a fraction x_n being in the normal state. Initially, we suppose that the arrangement of the normal and superconducting regions is in the form of alternate layers.

The first assumption of this theory is that all quantities to be considered (electromagnetic field, temperature, etc.) change little over distances of the order of the period of the intermediate state structure. The magnetic field $\underline{h}_n$ and the electric field $\underline{e}_n$ in the normal regions are both assumed to obey Maxwell's equations and to be connected to the macroscopic fields $\underline{H}$ and $\underline{E}$ through the relations

$$\underline{H} = \underline{h}_n , \quad \underline{E} = x_n \underline{e}_n , \tag{4.2}$$

where $\underline{H} = H_c$.

Due to the boundary conditions applying on the phase boundaries between

normal and superconducting regions the macroscopic fields $\underline{H}$, $\underline{E}$ also obey Maxwell's equations. Now the location of the boundaries between the phases can be characterized by specifying, at each point of the volume occupied by the intermediate state, a unit vector $\underline{n}$ directed normal to the boundary. Hence, solving Maxwell's equations in a system of co-ordinates attached to the moving boundaries, we show that

$$\underline{e}_n + V\,(\underline{n} \times \underline{h}_n).\underline{n} = 0\ , \tag{4.3}$$

and

$$\underline{n}.\underline{h}_n = 0\ , \tag{4.4}$$

where V is the velocity of the normal regions (V being positive in the direction of $\underline{n}$). Hence, using the equations (4.2) we obtain

$$V = \frac{c}{H_c^2 x_n}\ \underline{n}.(\underline{E} \times \underline{H}). \tag{4.5}$$

Similar considerations apply to a system of filaments (either superconducting or normal) where the result is

$$\underline{V} = \frac{c}{H_c^2 x_n}\ (\underline{E} \times \underline{H})\ . \tag{4.6}$$

Hence the velocity of motion of an intermediate state structure can be calculated if one knows the field $\underline{E}$ in terms of the driving electric current $\underline{J}$ or driving temperature gradient ∇T. Using tensor notation one can write the electric field as follows:-

$$E_i = \rho_{ik} J_k + \alpha_{ik} \frac{\partial T}{\partial x_k}\ , \tag{4.7}$$

where ρ_{ik} is a resistivity tensor and α_{ik} is a thermoelectric tensor which may be calculated for the three simple types of structure mentioned (layered, normal filaments, or superconducting filaments), using the electrodynamic equations, the conservation of energy and the principle of the increase of entropy. The results obtained by Andreev and Dzhikaev for pure metals, neglecting the Hall effect are as follows:-

(i) Layered Structure

$$\left.\begin{aligned} \rho_{ik} &= \frac{x_n}{\sigma}\left(\delta_{ik} - \frac{H_i H_k}{H_c^2}\right), \\ \alpha_{ik} &= \frac{x_n}{\sigma}\cdot\frac{cL}{TH_c^2}\left(1 - \frac{\kappa_\perp}{\kappa_n}\right)\cdot(\underline{n}\times\underline{H})_i\cdot n_k, \end{aligned}\right\} \qquad (4.8)$$

where σ is the normal state conductivity,

δ_{ik} is the Kronecker Delta (Jaeger (1966)),

L is the latent heat of the phase transition,

$\kappa_\perp$ is a function of the thermal conductivity of the normal and superconducting states,

and κ_n is the thermal conductivity of the normal state,

the other symbols having the same meaning as before.

Hence, substituting these results in equation (4.7) and using equation (4.5) one can find the velocity of such a layered structure under the influence of an electric current or a heat current.

(ii) Structure of Normal Filaments in a Superconducting Medium

$$\left.\begin{aligned} \rho_{ik} &= \frac{x_n}{\sigma}\left(\delta_{ik} - \frac{H_i H_k}{H_c^2}\right), \\ \alpha_{ik} &= \frac{x_n}{\sigma}\cdot\frac{cL}{TH_c^2}\left(\frac{\kappa_n - \kappa_s}{\kappa_n + \kappa_s}\right)\varepsilon_{ikl}H_l, \end{aligned}\right\} \qquad (4.9)$$

where κ_s is the thermal conductivity of the superconducting phase.

(iii) Structure of Superconducting Filaments in a Normal Medium

$$\left.\begin{aligned} \rho_{ik} &= \frac{1}{\sigma}\left(1 - x_s\left(1 + \frac{c^2L^2}{\sigma TH_c^2(\kappa_n + \kappa_s)}\right)\right)\cdot\left(\delta_{ik} - \frac{H_i H_k}{H_c^2}\right), \\ \alpha_{ik} &= \frac{x_s}{\sigma}\cdot\frac{cL}{TH_c^2}\left(\frac{\kappa_n - \kappa_s}{\kappa_n + \kappa_s}\right)\varepsilon_{ikl}H_l, \end{aligned}\right\} \qquad (4.10)$$

where x_s is the fraction of metal in the superconducting phase, and ε_{ikl} is the Levi-Civita density (Jaeger (1966)).

The neglect of the Hall effect is justified since no flux precession effects (Haenssler and Rinderer (1965)) were observed during the flux motion experiments.

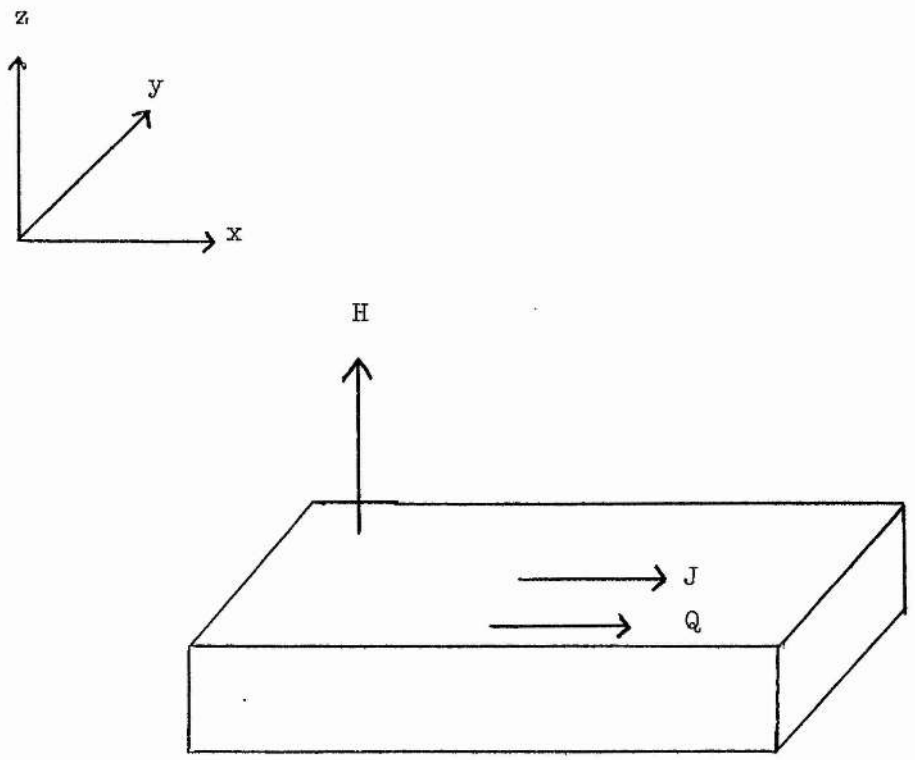

Fig. 4.2 The Experimental Geometry.

Now the geometry used in all the experiments in this work was that of a thin slab in a perpendicular field as shown in Fig. (4.2). Using the axes shown, the electric current ($\underline{J}$) or heat current ($\underline{Q}$) was always applied in the x direction and the field H was in the Z direction, that is,

$$\underline{J} = (J_x, 0, 0) ,$$

$$\underline{Q} = (Q_x, 0, 0) ,$$

$$\underline{H} = (0, 0, H_z) , \quad \text{where } H_z = H_c(T) .$$

The equations (4.8), (4.9) and (4.10) thus give for this geometry the following results for the three structure types.

(i) Layered Structure

For the current induced flow

$$V_x = 0 ,$$

$$\text{and} \quad V_y = \frac{c}{H_c^2} \quad \frac{J_x H_z}{\sigma} \quad n_y ,$$

$$\text{i.e.} \quad V_y = \frac{c n_y}{\sigma H_c} \quad J_x . \qquad (4.11)$$

We see that the velocity of motion of the layered structure is in a direction perpendicular to the driving current, as was stated by Gorter. We also notice that through n_y the magnitude of the velocity depends on the orientation of the layers.

Similarly for the thermally driven flow,

$$\left.\begin{aligned} V_x &= - \frac{c^2 L}{\sigma T H_c^2} \left(1 - \frac{\kappa_\perp}{\kappa_n}\right) n_x \cdot \frac{\partial T}{\partial x} , \\ V_y &= 0 \end{aligned}\right\} \qquad (4.12)$$

We see that the motion occurs along the direction of the thermal gradient (from hot to cold) and that the magnitude of the velocity again depends (through n_x) on the orientation of the layers.

It should be noted that the formulae (4.11) and (4.12) were obtained

for a perfect layered structure in which the vector $\underline{n}$ is constant everywhere. It will be shown later that only under rather special circumstances is such an arrangement attainable in practice, it being more usual to observe a random layered structure in which the vector $\underline{n}$ assumes all possible values. In this case the velocity is more appropriately calculated using equation (4.6) giving the results

$$\text{current induced flow } V_y = \frac{c}{\sigma H_c} \quad J_x \tag{4.13}$$

$$\text{and thermally induced flow } V_x = -\frac{c^2 L}{\sigma T H_c^2} \left(1 - \frac{\kappa_\perp}{\kappa_n}\right) \frac{\partial T}{\partial x}. \tag{4.14}$$

(ii) Structure of Normal Filaments in a Superconducting Medium

For the current induced flow

$$V_y = \frac{c x_n}{\sigma H_c^2 x_n} \quad H_z J_x ,$$

$$\text{i.e.} \quad V_y = \frac{c}{\sigma H_c} \quad J_x , \tag{4.15}$$

and for the thermally induced flow

$$V_x = -\frac{c^2 L}{\sigma T H_c^4} \cdot \frac{\kappa_n - \kappa_s}{\kappa_n + \kappa_s} \cdot \frac{\partial T}{\partial x} \quad H_z^2 ,$$

$$\text{i.e.} \quad V_x = -\frac{c^2 L}{\sigma T H_c^2} \cdot \frac{\kappa_n - \kappa_s}{\kappa_n + \kappa_s} \cdot \frac{\partial T}{\partial x} . \tag{4.16}$$

(iii) Structure of Superconducting Filaments in a Normal Medium

For the current induced flow

$$V_y = \frac{c}{\sigma H_c^2 x_n} \left(1 - x_s \left(1 + \frac{c^2 L^2}{\sigma T H_c^2 (\kappa_n + \kappa_s)}\right)\right). H_z J_x .$$

In the case of pure metals the last term in the bracket is very small and may be neglected,

$$\text{i.e.} \quad V_y = \frac{c}{\sigma H_c^2 x_n} \left(1 - x_s\right) H_z J_x .$$

Clearly $1 - x_s = x_n$ and hence

$$V_y = \frac{c}{\sigma H_c} J_x \,, \tag{4.17}$$

and for the thermally induced motion

$$V_x = - \frac{c^2 L}{\sigma T H_c^4} \cdot \frac{x_s}{x_n} \cdot \frac{\kappa_n - \kappa_s}{\kappa_n + \kappa_s} \cdot \frac{\partial T}{\partial x} H_z^2 \,,$$

$$\text{i.e.} \quad V_x = - \frac{c^2 L}{\sigma T H_c^2} \cdot \frac{x_s}{x_n} \cdot \frac{\kappa_n - \kappa_s}{\kappa_n + \kappa_s} \cdot \frac{\partial T}{\partial x} \,. \tag{4.18}$$

One should notice that the thermally induced motion is caused essentially by the difference in thermal conductivities of the normal and superconducting states.

The purpose of the present work was to attempt the verification of these equations for a number of pure Type I superconductors for a range of reduced applied fields h and temperatures T. It should be pointed out that, due to the coupled nature of the electrodynamic and thermal effects as expressed by equation (4.7), the observation of pure current induced motion requires that no thermal gradient be allowed to develop across the sample. The design of the sample mount ensured this, as mentioned in Chapter II.

4.4 An addition to the theory of Andreev and Dzhikaev

Following some experiments on thermally induced motion by Laeng and Rinderer (1973) a modification to the theory of Andreev and Dzhikaev was proposed by Rothen (1972).

In the calculation of the thermo-electric tensor α_{ik}, Andreev and Dzhikaev did not consider the effect of the thermoelectric power of the normal metal (Wilson (1953)). Steele (1951) has shown that the thermoelectric power of lead at its critical field is particularly large and Rothen has proposed that at high temperatures (near T_c) where the thermal

conductivities of normal and superconducting lead are almost equal, the size of the electric field across the sample is dominated by the thermoelectric power of the normal metal.

For the same geometry as before, the electric field produced by this thermoelectric effect when a heat current Q_x flows in the x direction is then

$$E_x = - \frac{\alpha_N}{\kappa_n} Q_x , \qquad (4.19)$$

where α_N is the thermoelectric power and κ_n is the thermal conductivity of the normal state. Hence the velocity of motion is

$$V_y = - \frac{c\alpha_N}{H_c^2 \kappa_n} Q_x H_z ,$$

$$\text{i.e.} \qquad V_y = - \frac{c\alpha_N}{\kappa_n H_c} Q_x . \qquad (4.20)$$

We see that the motion produced by this effect should be in a direction transverse to the heat current. We also expect that as the temperature falls the direction of motion will vary as a consequence of the competing nature of this thermoelectric effect and the mechanism of Andreev and Dzhikaev. Both of these effects have been observed by Laeng and Rinderer.

CHAPTER V - THE ROLE OF PINNING IN LIMITING FLUX MOTION

5.1 Introduction

The theory of flux motion outlined in the previous chapter includes no dissipation mechanism apart from eddy current damping in the normal regions - the equations predict that motion will occur no matter how small the driving force. As will be seen, this behaviour is not observed experimentally, the current-induced motion being describable by

$$\left.\begin{aligned} V &= 0 \qquad\qquad J < J_o \,, \\ V &= k\,(J - J_o) \quad J \geqslant J_o \,, \end{aligned}\right\} \tag{5.1}$$

where J_o is called the critical current, defined as the current below which motion cannot be observed.

It is possible to account for this behaviour by considering an additional force which acts on the flux apart from the viscous drag force caused by eddy current damping and the driving Lorentz force. This is the pinning force F_p which occurs because flux interacts with the microstructural features of imperfect metals. Pinning can be due to lattice defects, such as dislocations or impurities. Strong pinning materials are metallurgically dirty. The critical current J_o, unlike the critical field, is not a property of a particular superconductor, but of a particular sample of the superconductor, and is strongly influenced by the sample's metallurgical history. For this reason, the calculation or prediction of critical currents cannot be performed with any accuracy.

5.2 The effect of pinning on experimental data

The details of flux flow and the effects of pinning have been most extensively examined in Type II materials where these effects are of interest in the production of stable superconducting solenoids (Williams (1972)). However, the general features observed apply also to Type I

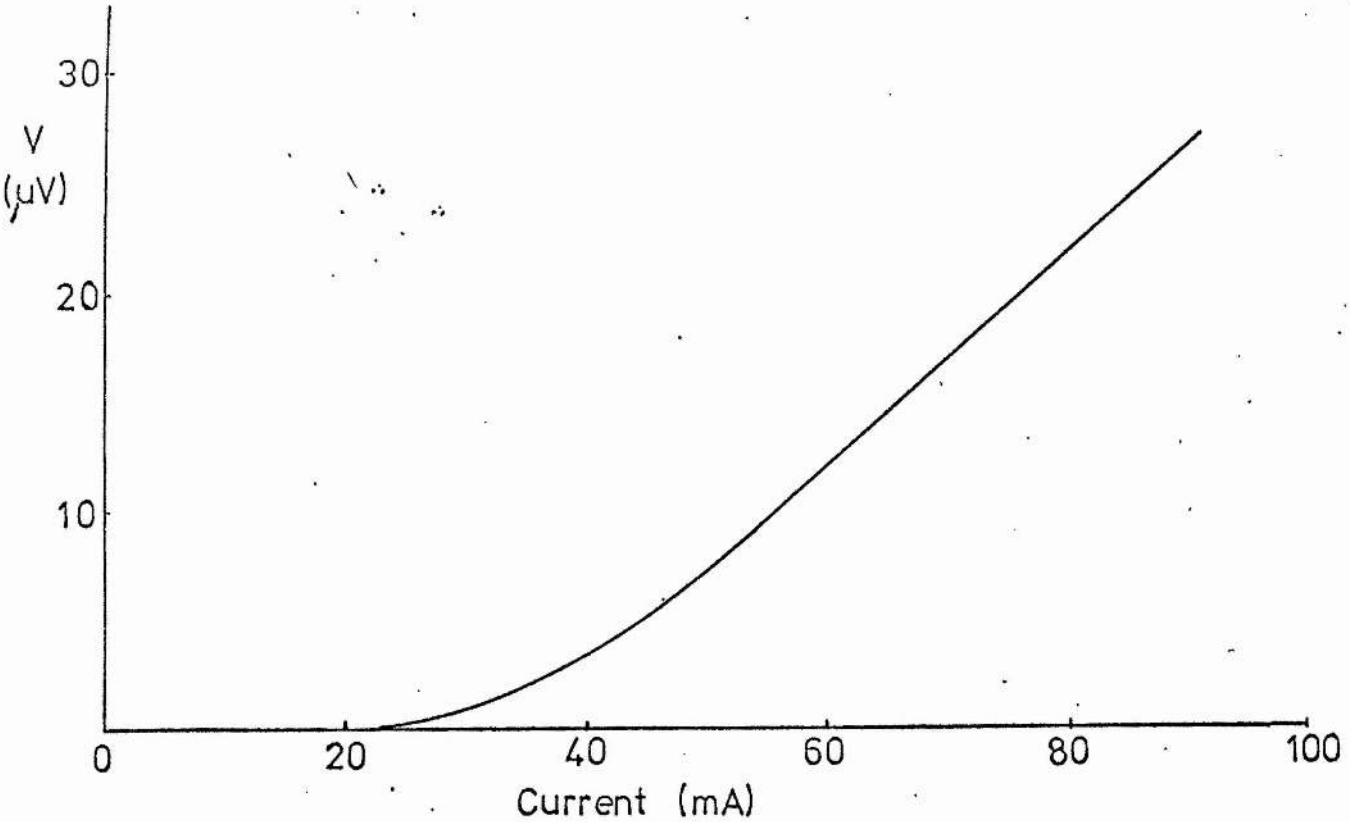

Fig 5.1 A typical flux flow characteristic for a Type II superconductor (after Osborne and Rose-Innes (1972)).

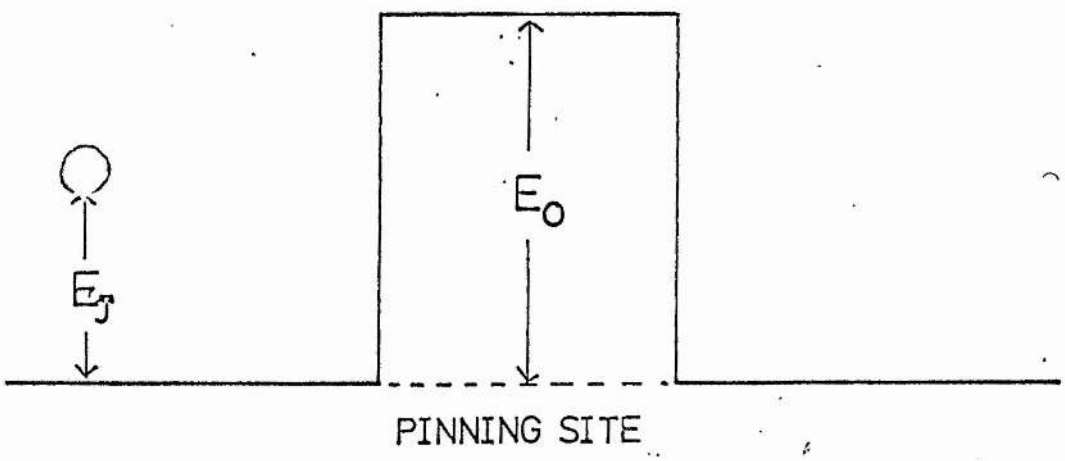

Fig 5.2 A simple model of flux pinning. E_J is the energy of the domain due to the influence of the Lorentz force.

materials and these will now be described.

The direct observation of the motion of flux lines in the mixed state of Type II superconductors has not yet been accomplished and hence all measurements must be of the electric field E existing across the superconductor while the flux lines are in motion. A typical plot of E versus J is shown in Fig. 5.1 (Osborne and Rose-Innes (1972)).

It will be seen that for a short distance above the critical current J_o the characteristic is curved before it enters the expected linear region. This curvature has been variously attributed to a thermally activated flux creep mechanism (Anderson and Kim (1964)), a velocity-dependent frictional force (Farrell, Dinewitz and Chandrasekhar (1966), Lowell (1970)), inhomogeneities (Jones, Rhoderick and Rose-Innes (1967)), (Baixeras and Fournet (1967)) and motion of fluxon lattice dislocation dipoles (Kramer (1970)). The last of these is inapplicable to Type I materials and hence will not be discussed further.

Thermally activated flux creep was proposed by Anderson and Kim to explain the experimentally observed strong linear temperature dependence of the critical current J_o (Anderson (1962)). A simple model of flux pinning is to imagine an energy barrier of height E_o situated at each pinning site as shown in Fig. 5.2. At finite temperatures Anderson and Kim reasoned that flux could not be completely pinned for $E_J < E_o$ since thermal activation would assist the flux over the pinning barrier. They proposed that the resulting flux 'creep' could be described by a rate equation

$$R = R_o \exp\left((E_J - E_o)/kT\right), \qquad (5.2)$$

where R is the rate at which flux jumps from one pinning site to the next and R_o is a constant. This notion invalidates the idea of there being a precise critical current but one may still define a critical current as

being that current below which the experiment cannot detect any flux motion. There will be a corresponding lowest rate detectable R_o and hence from (5.2)

$$(E_{J_o} - E_o)/kT = C, \text{ a constant},$$

$$\therefore \quad E_{J_o} = - CkT + E_o \ . \qquad (5.3)$$

This then explains the strong linear temperature dependence of J_o observed by Anderson. According to this theory the curved region of the E versus J characteristic corresponds to the region where $E_J < E_o$, and thermal activation is assisting the motion. Indeed, from equation (5.2), the velocity of flux motion in this region can be expressed by

$$V = V_p \exp ((E_J - E_o)/kT), \qquad (5.4)$$

where V_p is a constant, being the flux velocity when $E_J = E_o$.

Evidence in favour of flux creep was provided by the experiments of Beasley et al (1969) and Kim et al (1963). Recently, however, the existence of flux creep in Type II materials has been called into question and indeed the experiments of Osborne and Rose-Innes (1973) seem to indicate that the curvature of the characteristic is not due to flux creep since a precise critical current could always be detected even for extreme sensitivity of the field measurement ($E \sim 2 \times 10^{-10}$ V.cm^{-1}).

The second mechanism suggested to account for the characteristic's curvature is that the pinning force F_p is dependent on the velocity of the flux motion for currents $J \sim J_o$. This has received some experimental support in the work of Farrell et al mentioned above, and Lowell has shown that such behaviour might be expected for an array of interacting fluxons (i.e. the flux lattice of the mixed state) being elastically distorted in flow past a series of pinning sites. The situation is, of course, somewhat different in the intermediate state where no strongly interacting flux structure exists. Lowell's work in the above paper on the motion of an isolated fluxon is then applicable (Lowell (private communication)) and

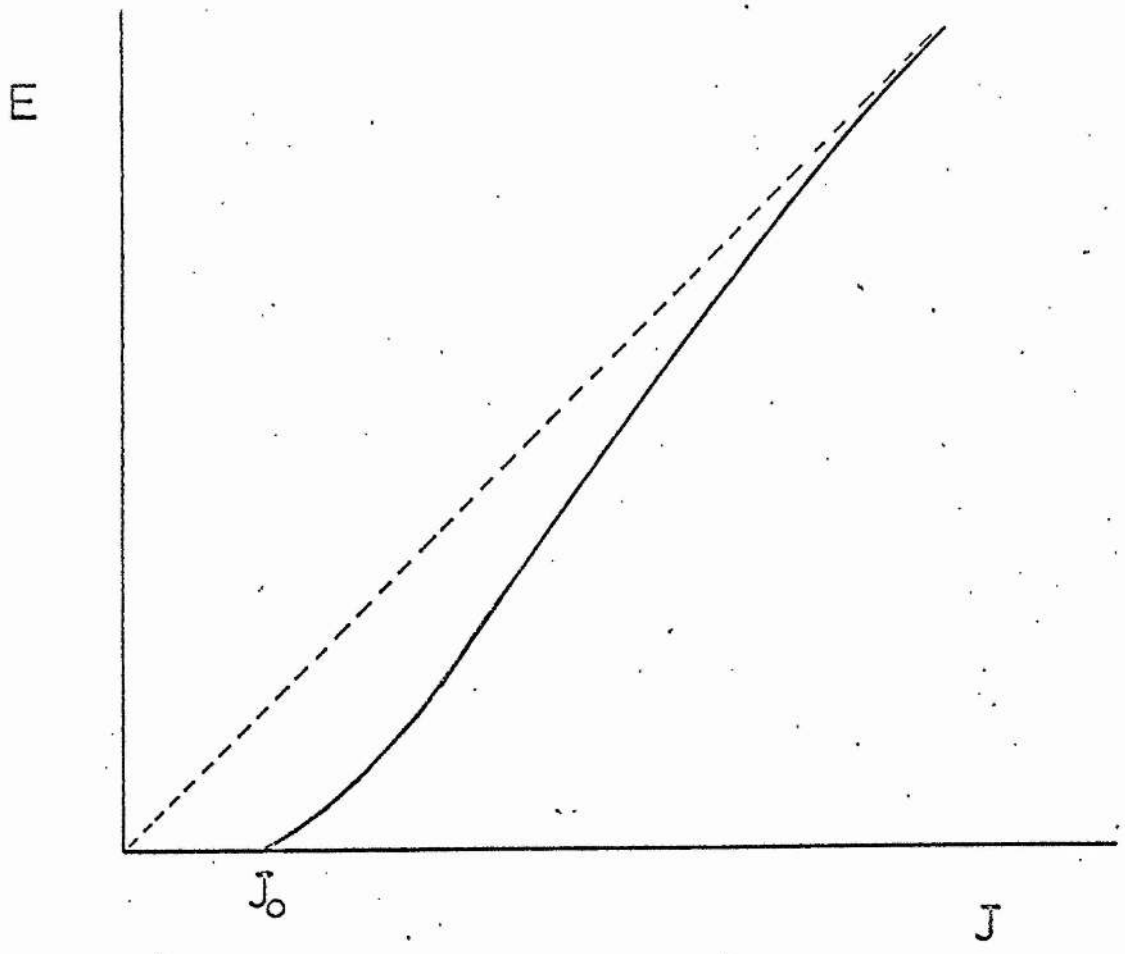

Fig. 5.3 Flow Characteristic for the Intermediate State based on Lowell's work.

a characteristic of the form illustrated schematically in Fig. 5.3 is predicted. It is curved for low $J \sim J_o$ and tends asymptotically to meet a straight line through the origin at high J where the frictional force vanishes. In the presence of such a velocity-dependent pinning force the slope of a measured flux velocity versus current characteristic would not correspond to that predicted by the general theory of Chapter IV.

The third mechanism suggested to account for the curvature of the characteristic is that non-uniformity in the purity or surface conditions of the sample would lead to a variation of critical current along its length. The resultant voltage measured across the whole length would then exhibit curvature in the current region where flux flow had commenced in some parts of the sample but not in others. This explanation might seem less likely in very pure Type I samples whose surfaces had been carefully prepared.

It should be pointed out that only the thermally activated creep mechanism accounts explicitly for the strong temperature dependence of the critical current J_o.

No final decision upon which of these mechanisms is responsible for the curvature of the characteristic has yet been reached in Type I or Type II materials. A direct visual observation of the flux motion as in this work would be expected to help in distinguishing between them since the character of motion predicted by each is slightly different near the point of flow commencement. In the case of thermally activated creep the observed motion would be expected to be 'jittery' and intermittent; if the pinning force were velocity dependent it should be smooth; if the effect were caused by inhomogeneities the motion should commence in different parts of the sample at different currents and the characteristic observed for flow over a small part of the sample should be linear.

The only instance in which the slope of the linear part of the

characteristic would be expected to differ from that predicted by the general theory of Andreev and Dzikhaev would be if the pinning force were to be velocity dependent. Hence, an observation of the detailed nature of the motion in the curved region and the slope of the characteristic in the linear region can be expected to yield useful information on the way in which flux interacts with pinning sites whilst it is in motion.

h = 0.8

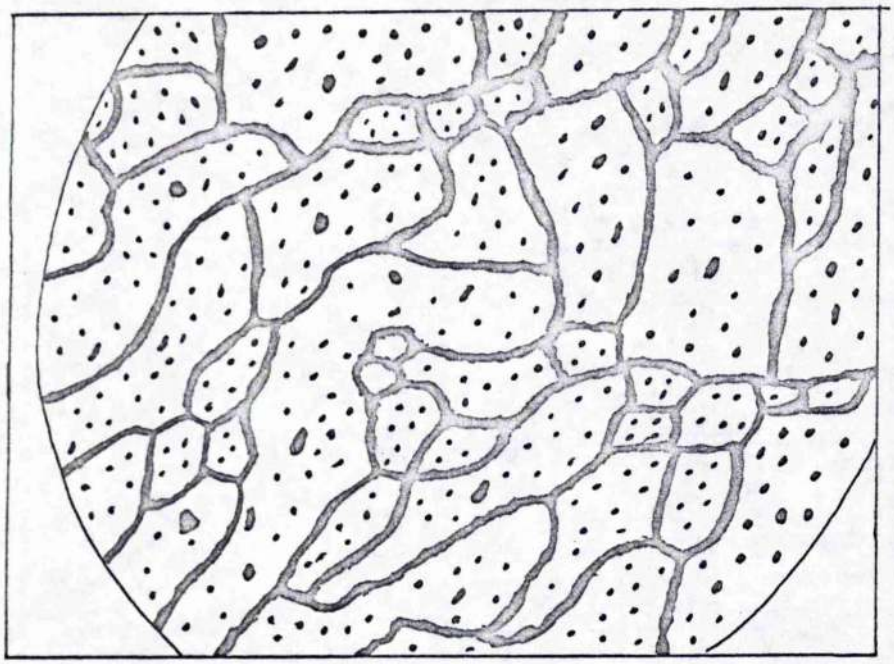

100μm

(a)

h = 0.95

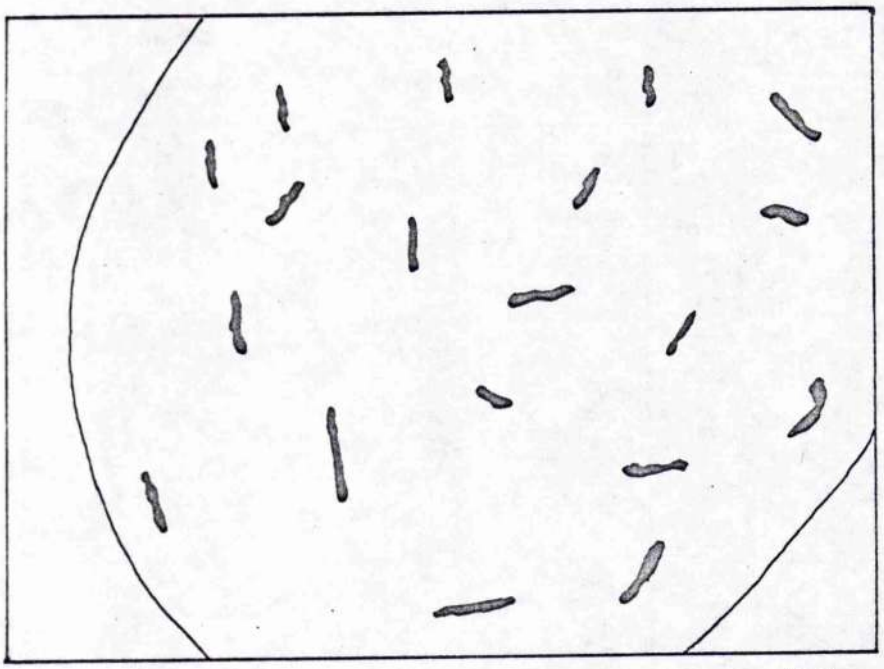

(b)

Fig 6.1 Intermediate state in Pure Pb, T = 1.3K .
(Taken from photographs)

CHAPTER VI - EXPERIMENTAL RESULTS FOR CURRENT INDUCED MOTION

6.1 Introduction

The current induced flux flow observed in the present work in pure Pb showed the same general features as those described by Solomon and Harris (1970, 1971). These, and the different features seen in Sn and In, are described in Section two below.

The comparison of the observed flux flow velocities with those predicted by the theory of Andreev and Dzhikaev is described in Section three, allowance having been made for the effects of pinning.

The nature of the motion at currents close to the critical current J_o is described in Section four, and the reasons for the curvature of the flux velocity versus current characteristic in this region are examined in detail.

6.2 General features of the flux motion

The present observations are in agreement with the conclusion of Solomon and Harris (1971) that any naturally occurring intermediate state topology is unstable with respect to transverse motion in the presence of an electric current. However, it was observed that, due to the presence of pinning, a large variation existed in the size of current necessary to produce continuous motion of different intermediate state structures. As stated in Chapter IV this current is generally called the critical current J_o. Small local movements were observed for currents less than J_o but the discussion of this phenomenon is left to Section three.

The photographs of Fig. 2.8 showed the nature of structures seen for the reduced applied fields $h = 0.4$ and 0.6 in pure Pb and Fig. 6.1 shows the flux structures for $h = 0.8$ and 0.95. Fig. 6.2(a) shows how the observed critical current varied with reduced applied field.

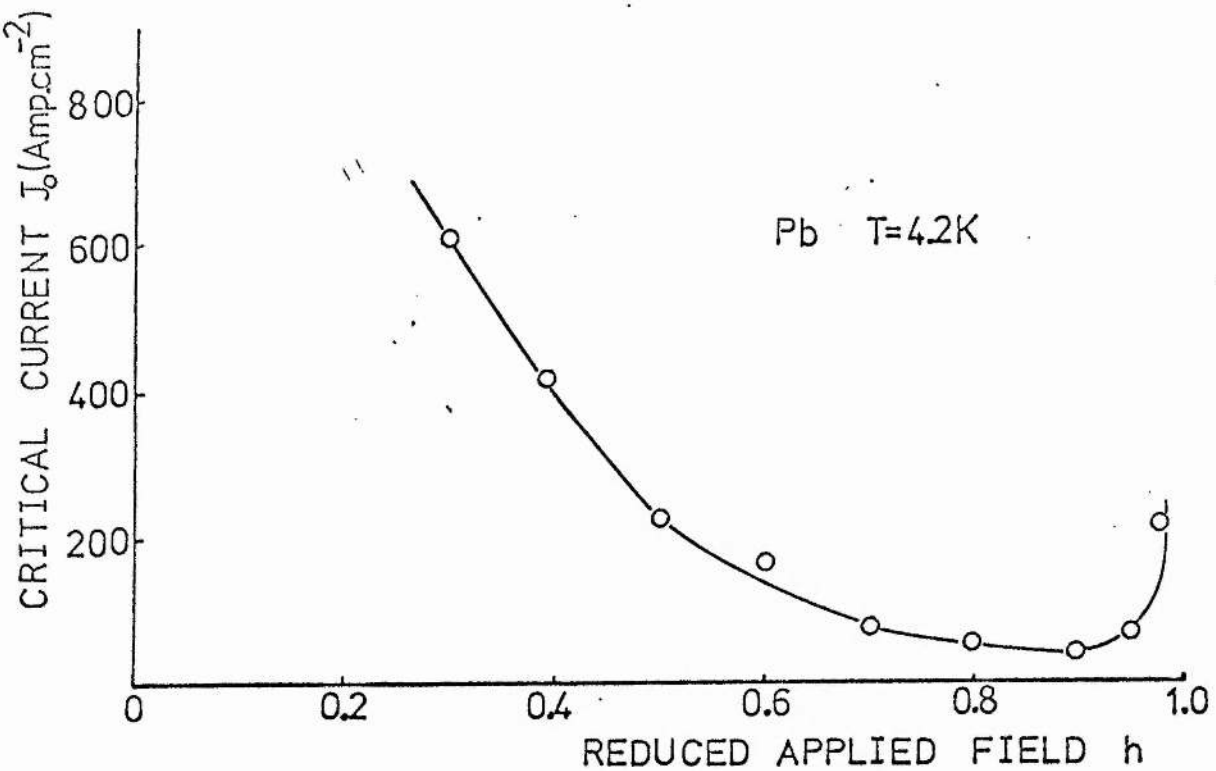

Fig. 6.2a The Variation of the Critical Current J_o for different Intermediate State Topologies (Reduced Applied Field h) for Pb at T = 4.2K.

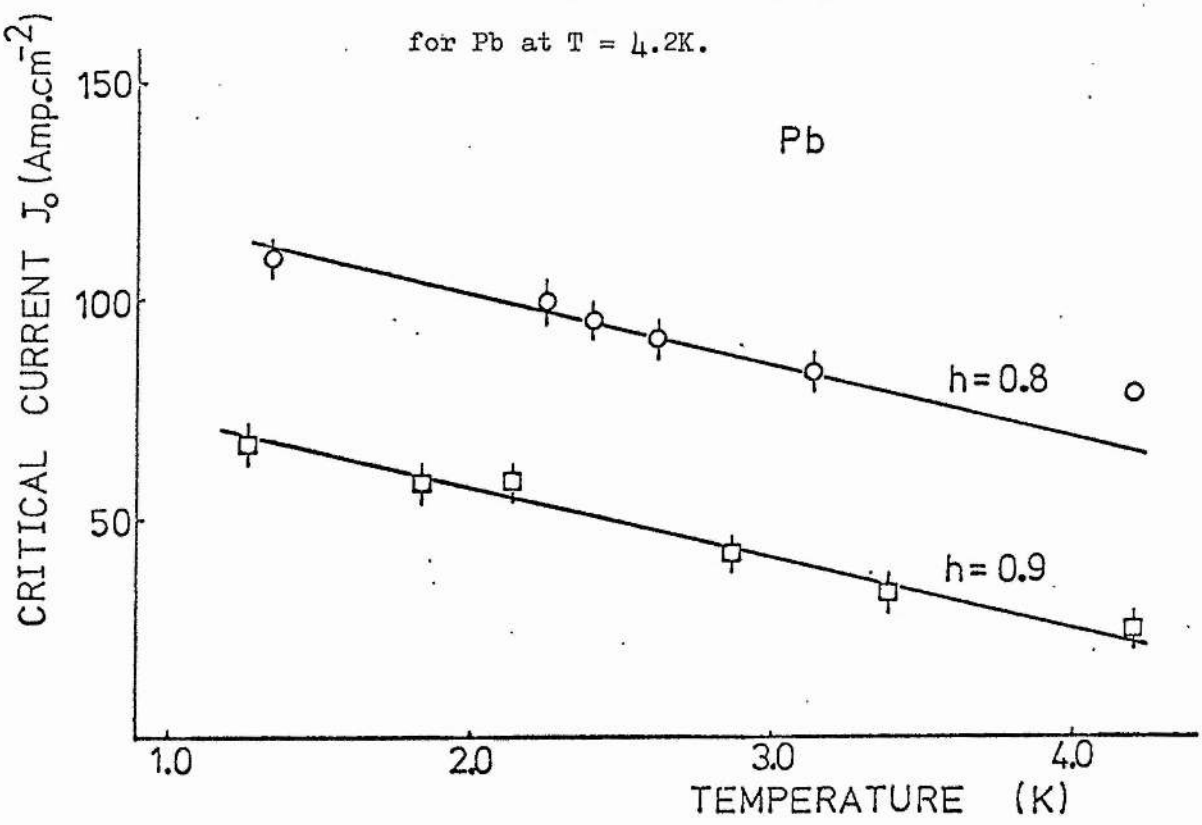

Fig. 6.2b The Variation of Critical Current J_o as a function of temperature in Pb for h = 0.8 and h = 0.9.

This behaviour may be understood qualitatively in terms of the ability of different flux structures to get past pinning sites obstructing their path. It is reasonable to assume that, given a uniform distribution of pinning sites, the critical current for a particular flux structure will be proportional to the surface area of the flux structure normal to the direction of flow (Solomon and Harris (1971)). For h = 0.4 the complex corrugated normal regions present a large surface area normal to the direction of flux flow, are easily caught on the pinning sites and hence J_o is large. As can be seen in the photographs the normal regions expand as h is increased until the pattern takes the form of an array of simply connected superconducting domains. The motion of these superconducting domains will be more easily induced due to their small surface area normal to the flow direction. This feature explains the fall in critical current as h is increased from 0.4 to 0.8. With further increase of the field h, the critical current rises again because the ends of the small thin superconducting 'squiggles' seen in this region (Fig. 6.1(b)), are very easily caught on pinning sites. It is possible, in fact, to observe this process as it happens; the 'squiggles' try to move on application of the driving current but their ends become caught and the current must be increased considerably to overcome the pinning and produce continuous motion.

A quantitative explanation of the variation of critical current J_o with applied field h would demand a knowledge of the pinning interaction and a means of dealing with the complex shape of the flux structures. Since the pinning interaction is unknown this was not attempted. It is proposed, however, that the variation of J_o with h could be explained solely in terms of the geometry of the flux structures.

Fig. 6.2(b) shows how the observed critical current was found to vary with temperature T for two reduced applied fields h = 0.8 and h = 0.9 in Pb.

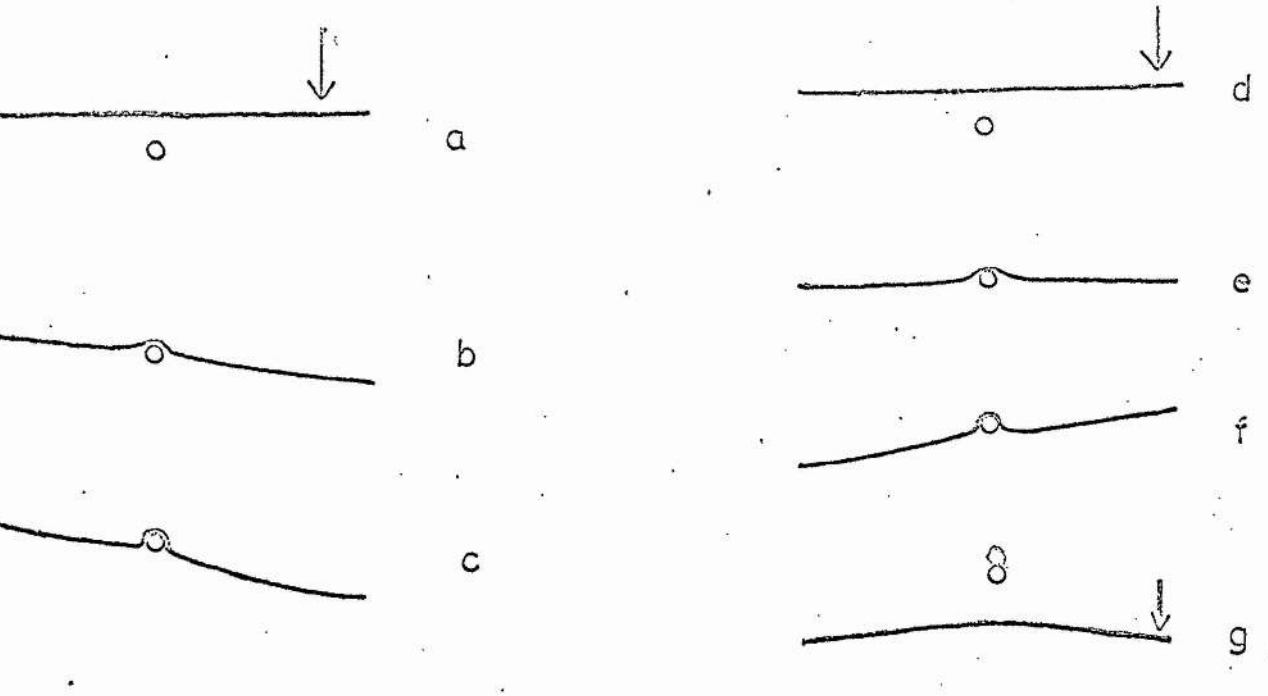

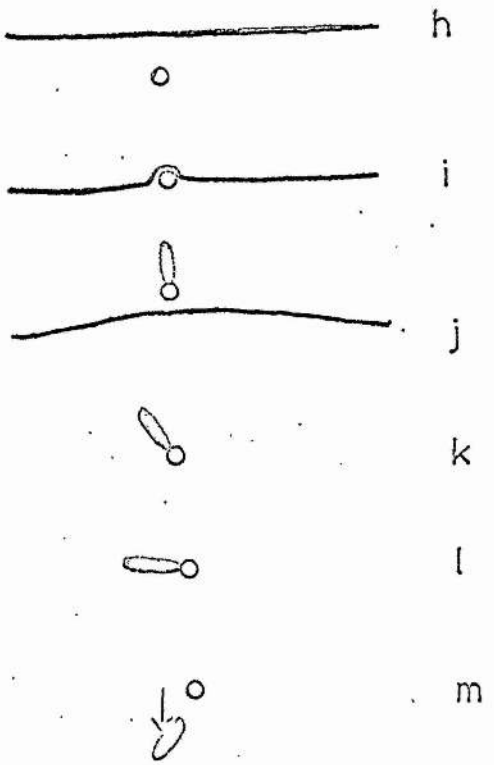

Fig. 6.3 Interaction with a pinning site in In, T = 1.3K, h = 0.9.

This effect may either be due to a temperature dependence of the pinning energy or the thermal activation process discussed in Chapter V assisting the flux over the pinning barriers. This will be discussed more fully in Section four.

One experiment was performed in which the magneto-optic EuS:EuF_2 film was evaporated directly onto the surface of a Pb sample which had been carefully etched to reveal its crystallite boundaries and had been only lightly coated with aluminium. In this way the interaction of the moving flux with the crystallite boundaries or any surface imperfections could be studied. It was observed that only occasionally was a moving domain trapped by a crystallite boundary although a deflection in its direction of motion occurred fairly frequently. These deflections were of a very short duration but it could be seen that they were generally along the crystallite boundary as might be expected. Similar behaviour was observed when a moving domain encountered a particle of dirt impressed in the sample surface. In this case it was deflected around the particle before continuing its motion as before.

An extremely interesting mode of interaction with a pinning site was observed during one experiment with an indium sample. For high applied fields ($h \sim 0.9$) flow of long superconducting laminae perpendicular to their length could be achieved. The sequential diagrams of Fig. 6.3 show how these laminae were seen to interact with a pinning site (of unknown nature) which seemed to have a resolvable size (about 10 μm in diameter).

As one would expect, the exact nature of the interaction depended strongly on the driving electric current, the domain being able to be trapped for low J. Fig. 6.3(a) to 6.3(c) shows the flow for $J = 44$ Amp.cm^{-2}. The laminae could be trapped in either the position b or c.

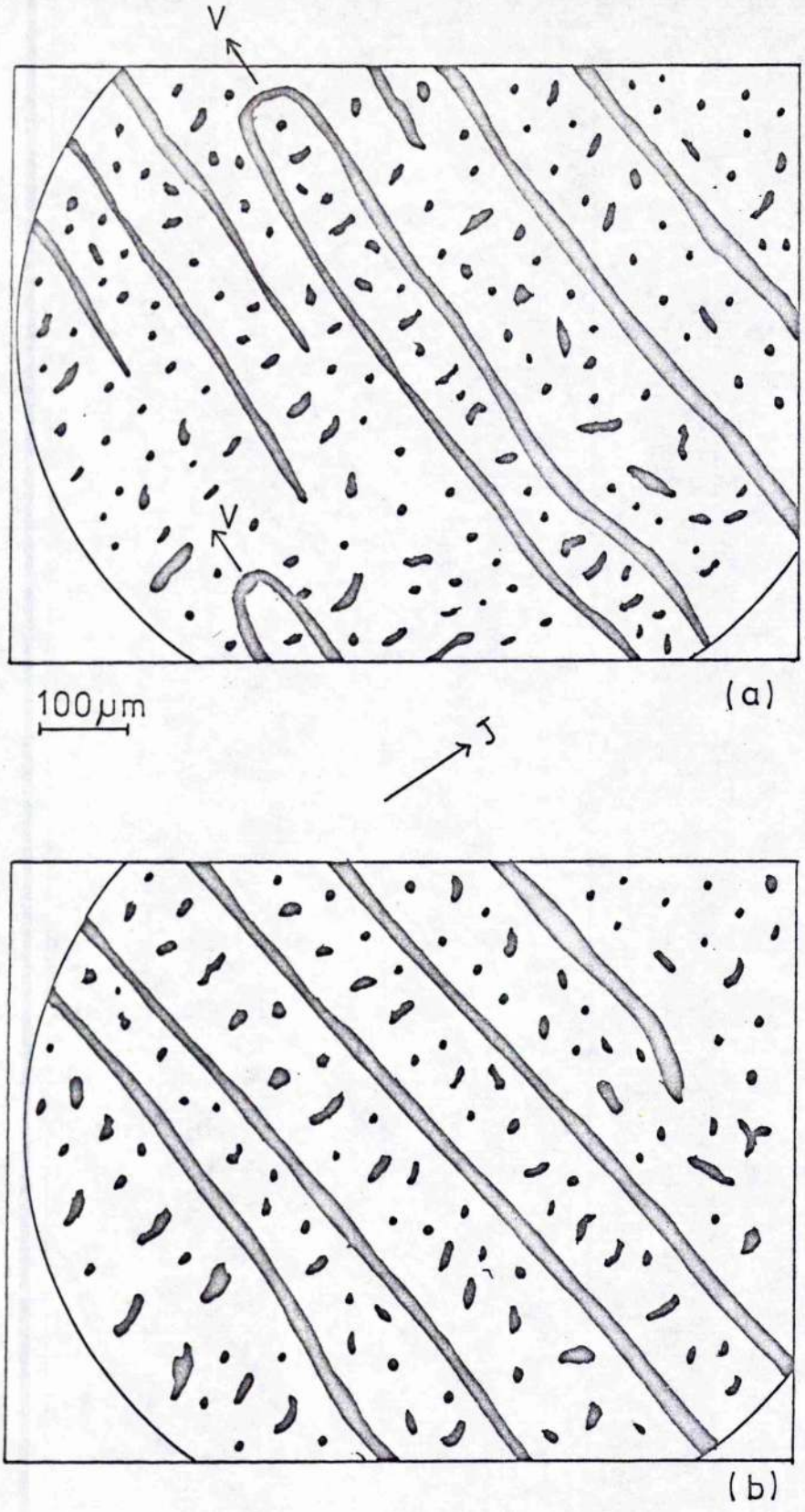

Fig 6.4 Intermediate state flow patterns in pure Pb
h = 0.8 , T = 1.3K
(Taken from photographs)

For a slightly higher J = 55 Amp.cm^{-2} the laminae managed to escape from the pinning site as shown in Fig. 6.3(d) to 6.3(g). Between the stages (e) and (f) the superconducting domain appeared to 'wet' the outside of the pinning site and stretch right round it. Suddenly the laminae would snap and break free, very quickly joining back up and straightening out to continue on its way but leaving a small circular superconducting domain trapped behind the pinning site as shown in (g).

For a much higher J = 110 Amp.cm^{-2} the process was very similar except that it occurred much more quickly and the trapped domain was larger and elongated in the direction of flow as shown in Fig. 6.3(h) to (m). After the superconducting laminae had escaped the small domain usually swung slowly round the pinning site until eventually it flowed away on its own.

The superconducting domain was never observed to travel <u>through</u> the pinning site - a break had to occur before the motion could continue. This pinning may have been caused by a non-superconducting particle impressed in the sample surface as for the above example in Pb, but the exact nature of the particle was not discovered.

A large majority of the flux flow data was taken in the region of $0.7 \lesssim h \lesssim 0.9$. The type of motion studied is illustrated in the sequential diagrams of Fig. 6.4 for the case of h = 0.8 in Pb. The structure before application of the driving electric current was shown in the diagram of Fig. 6.1; the shape of flowing domains is shown in Fig. 6.4(a), arrows indicating the direction of motion. This motion continues until a set of thin superconducting and thick normal laminae are set-up (Fig. 6.4(b)). These are arranged perpendicular to the current and hence all apparent motion ceases. At this and lower applied fields branching points exist between the laminae but the current necessary to induce their motion was found higher than that to produce the above type of motion. At high applied fields ($h > 0.9$) the laminae are, in general, not formed and the

'squiggles' of superconducting material move indefinitely.

These features of the current induced flow no doubt explain the results of early workers, not using a direct method of observation, which suggested that flux motion ceased for $0.6 \leqslant h \leqslant 0.8$. It may also explain the failure of Meissner (1970) to detect flux motion below $h = 0.9$. One appreciates here the advantage of the direct observation of the exact character of the motion using the magneto-optic technique.

The motion in Sn and In exhibited the same general features except that branching points were very seldom seen, the higher surface energy in these materials precluding their formation.

In the case of In, the high conductivity of the material used produced very noticeably slow drift into and out of the sample when the applied field was changed. A long time was required to attain an equilibrium state before making measurements of current induced flow.

It was found interesting to observe the flow onto and off the edge of the sample. The superconducting domains whose shape is shown in the photograph of Fig. 6.4(a) were observed to 'burst' just before reaching the edge, the central region quickly contracting up to join the laminae on either side. However, this was the only case in which a significant distortion was observed, the usual situation being simply a smooth continual flow onto or off the samples with only minor rearrangements occurring. The observed flow was always directed normally to the sample edge i.e. normal to the direction of the current flow.

Flux precession effects (Haenssler and Rinderer (1965)) were not observed in the present work except to a slight extent in In. In view of this, and the above observation of the flow direction to a good approximation the influence of the Hall effect may be neglected.

6.3 Domain velocity versus current characteristics

The velocity of motion of the various types of intermediate state structures was measured as a function of driving current by timing their transit between the edges of the Leitz graticule on the microscope eyepiece. A Hewlett-Packard 5233L counter was used as a clock. No correction for reaction time was required since the moving domain could be seen before crossing the graticule boundary. In general, about five measurements of the transit time were taken for each set of experimental conditions (i.e. current J, field h, temperature T) the magnetic field being cycled to above H_c and down again between measurements. In this manner it was found possible to measure the transit time to within $\pm$ 0.2 seconds. The distance over which the domains were timed was 1020 $\pm$ 5 μm and hence velocities up to about 500 $\mu m.sec^{-1}$ could be measured before the uncertainty in their values reached 10%. The exact H_c corresponding to the temperature of measurement was obtained for Pb from Decker et al (1958), and for Sn and In from Maxwell and Lutes (1954).

The power supply that supplied the electric driving current was programmed by means of switched resistors so that individual current values could be quickly selected.

The structures observed did not correspond to any of the simple types discussed by Andreev and Dzhikaev in their general theory. However, most of the data was collected for small superconducting domains (shaped as shown in Fig. 6.4(a)) moving through a normal medium, which suggests comparison with their result for superconducting filaments moving in a normal medium

$$V_y = \frac{c}{\sigma H_c} J_x \ . \qquad (4.17)$$

It should, in any case, be noted that their theory yields an identical result for the case of normal filaments moving in a superconducting medium or a random layered structure.

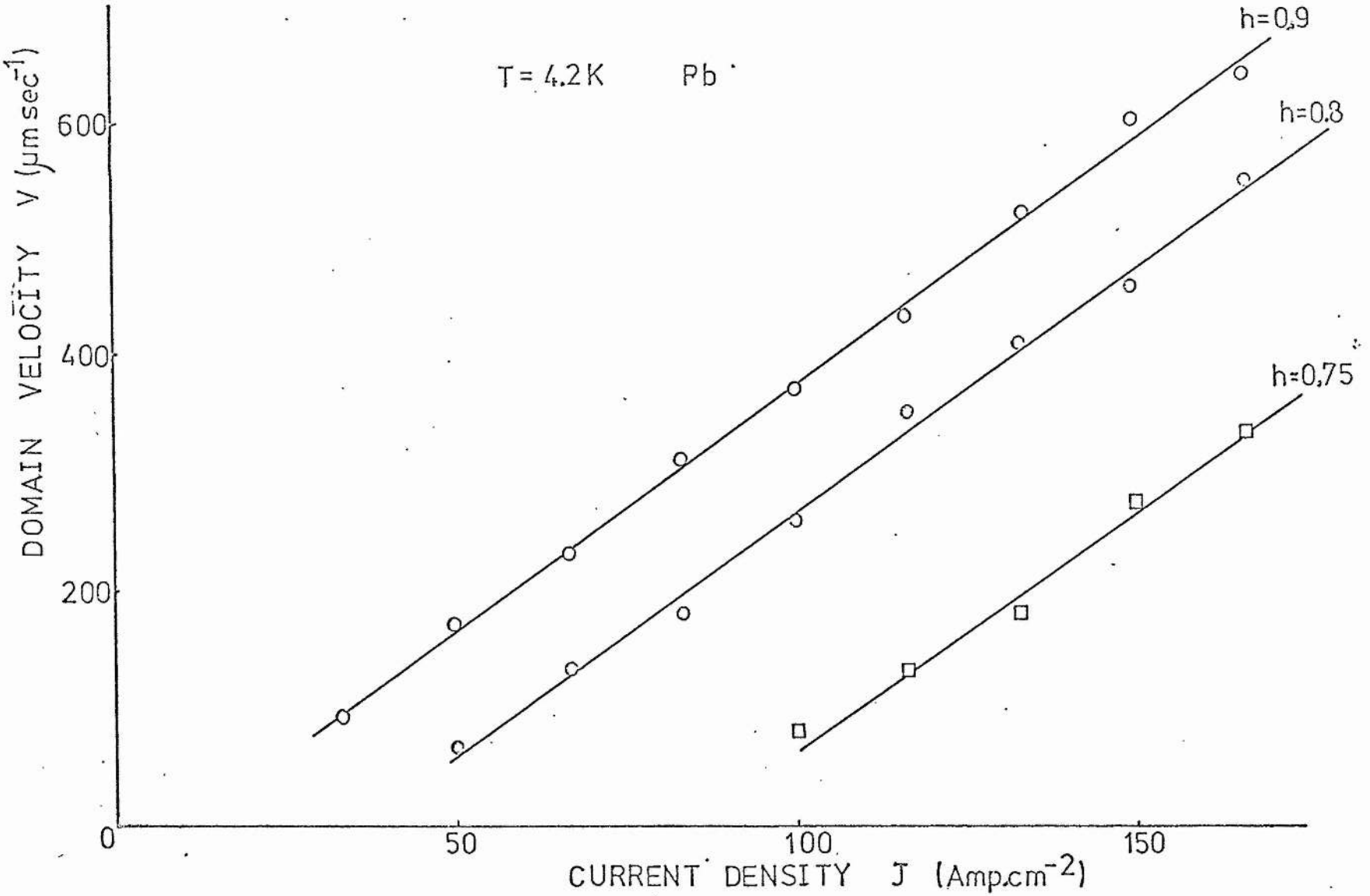

Fig 6.5 Domain velocity versus current characteristics for Pb at constant temperature T = 4.2K with h = 0.9, 0.8, 0.75.

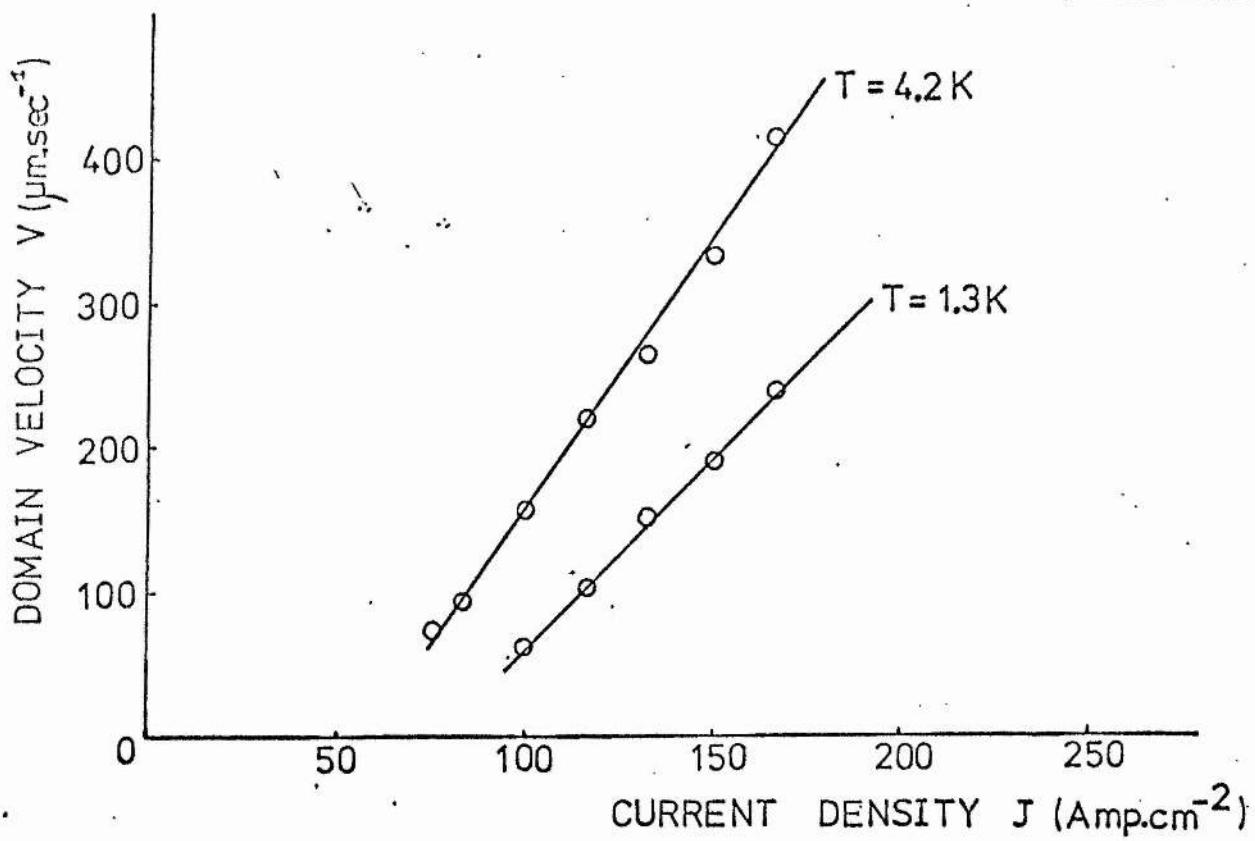

Fig 6.6 Flow characteristics for Pb, h = 0.8 .

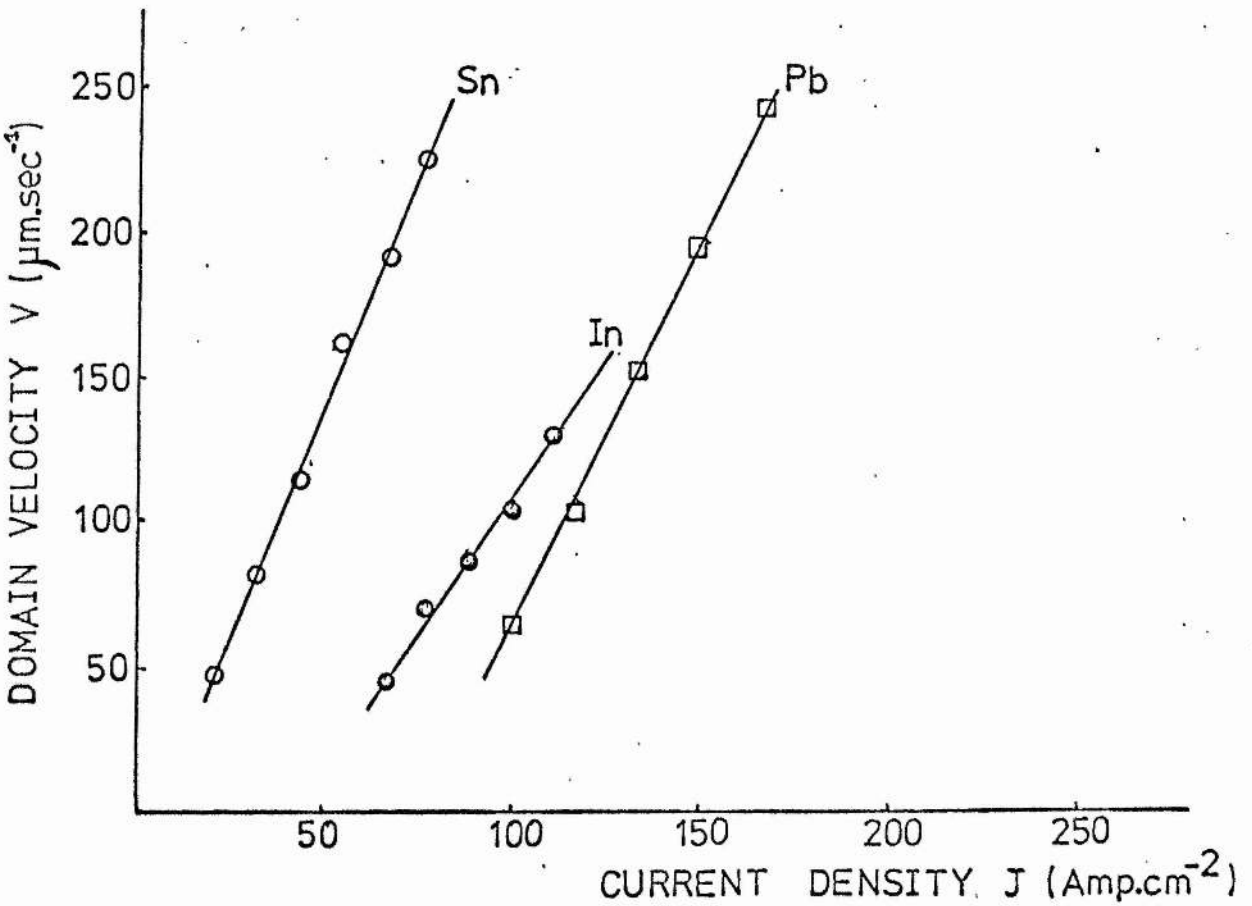

Fig 6.7 Flow characteristics for Sn, Pb, and In, h = 0.8, T = 1.3K

The above equation predicts that a linear domain velocity versus current characteristic will be obtained and that the slope should (a) be unchanged for differing reduced applied field h at constant temperature T, (b) decrease for decreasing temperature due to the rise of the critical field H_c and (c) depend on the particular material under investigation due to the conductivity σ.

Experiments were performed to test all these predictions. Fig. 6.5 shows domain velocity versus current characteristics for various reduced fields taken at constant temperature T = 4.2K for 6-9's Pb. The prediction (a) above is confirmed, no significant change in the slope occurring as h is decreased. This figure also indicates how the critical current (defined by extrapolation of the characteristic to meet the abscissa) depends on the reduced applied field as discussed earlier.

Fig. 6.6 shows domain velocity versus current characteristics for two temperatures T = 4.2K and T = 1.3K for constant reduced applied field for 6-9's Pb. The prediction (b) above is confirmed, the slope decreasing as the temperature falls.

Fig. 6.7 shows domain velocity versus current characteristics for Pb, Sn and In at a temperature of T = 1.3K and reduced field h = 0.8. We see that the slope is different for the three different materials as expected.

These comparisons have only indicated that the predictions of the theory are qualitatively obeyed. A quantitative comparison with the theory demands some method of including or eliminating the effect of pinning on the data. As already stated it is not possible in view of ignorance of the pinning interaction to calculate the critical current J_o. However, it is noticeable that the measured characteristics have proved to have a linear nature and this suggests the extension of the theory by including the critical current as follows

$$V = \frac{c}{\sigma H_c} (J - J_o). \qquad (6.1)$$

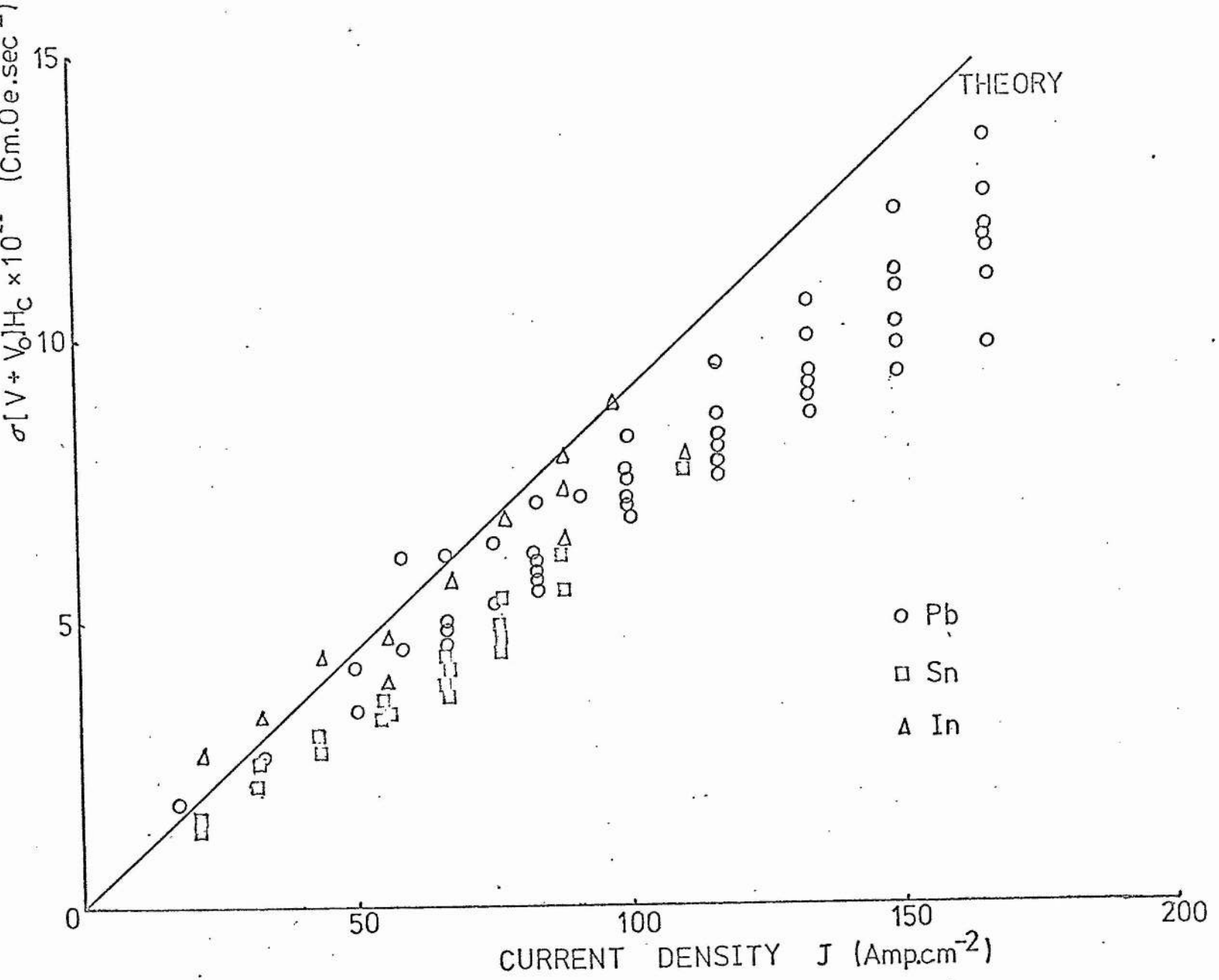

Fig 6.8 Collected flux flow data from Pb, Sn and In.

(Notice that the subscripts y and x on the velocity and current respectively have been dropped).

Further, we may write

$$V = \frac{c}{\sigma H_c} J - V_o \,, \tag{6.2}$$

where we have defined a critical velocity

$$V = \frac{c}{\sigma H_c} J_o \,. \tag{6.3}$$

The critical velocity V_o will be a constant for a particular sample, reduced field h, and temperature T and may be extracted from the experimental characteristics being the intercept on the velocity axis. It is important to note that the above description assumes the pinning force to be velocity <u>independent</u> i.e. V_o does not depend on the current J.

We may write equation (6.2) as

$$\sigma H_c (V + V_o) = cJ. \tag{6.4}$$

This equation predicts that all of the experimental data for different samples, reduced fields, and temperatures may be plotted on one graph of $\sigma H_c (V + V_o)$ versus J, through use of the measured conductivity values and literature data on H_c.

Fig. 6.8 shows the collected experimental data plotted on such a graph. As can be seen although there is some scatter the data from three different Pb samples at temperatures from 4.2K to 1.2K and reduced fields from 0.5 to 0.9, one Sn sample at temperatures from 2.7K to 1.3K and reduced fields 0.6 to 0.8 and one In sample at a temperature of 1.2K and reduced fields of 0.6 to 0.8 all fall just below the theoretical line. The size of the scatter is as expected since the uncertainty in determining the quantity $\sigma H_c (V + V_o)$ is typically about 20% principally due to the extrapolation involved in finding the critical velocity V_o, and the error in the conductivity measurements.

The deviation of the observed slope from the theoretical one (~ 19%)

Fig 6.9 Flux flow characteristics for Pb, T = 1.3K, h = 0.8

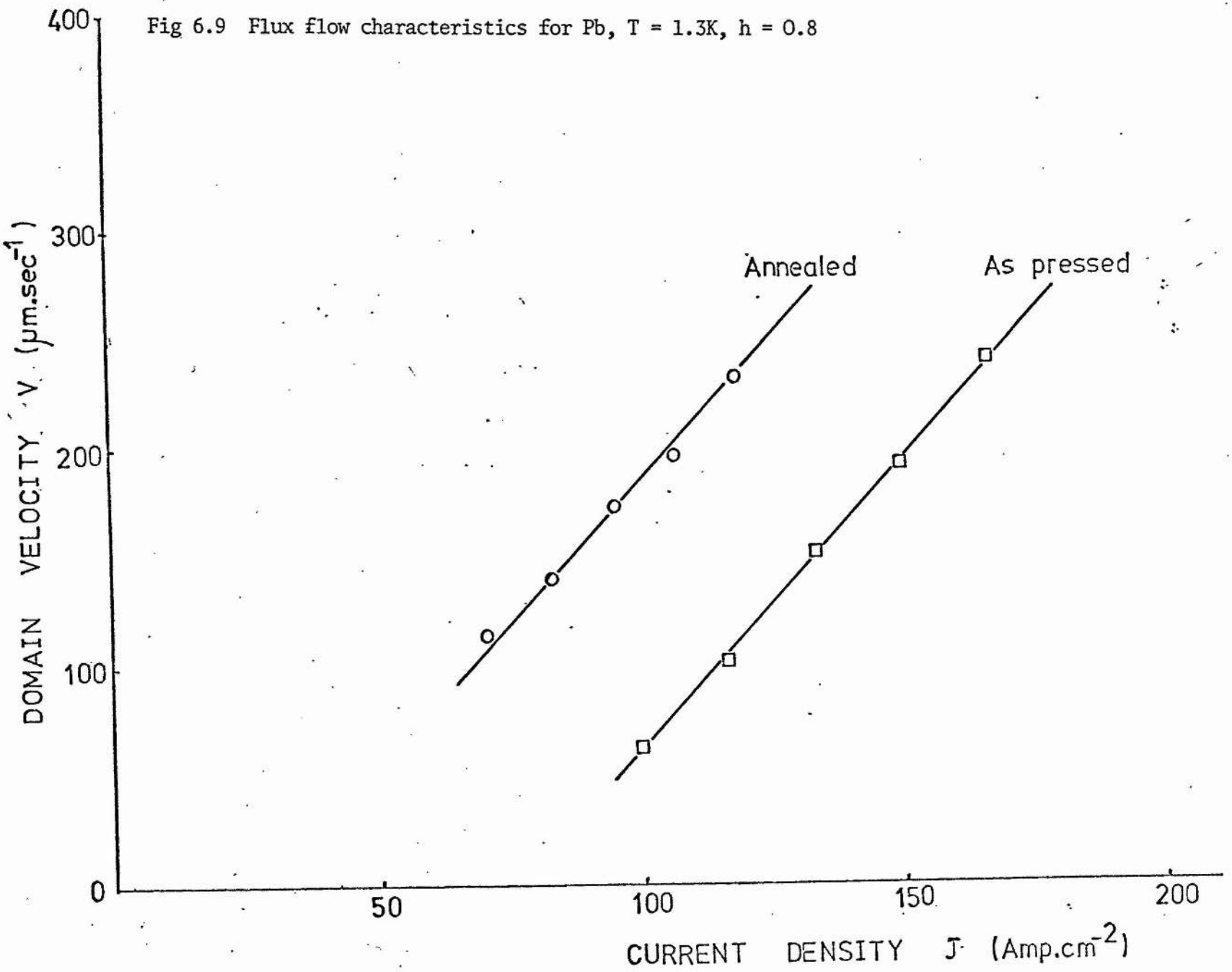

may reasonably be explained by the fact that the conductivity values were determined experimentally for extruded wires and hence because of contamination or induced crystalline defects would always tend to be lower than the value appropriate to the bulk material. The values of bulk mean free path assumed, to allow correction for size effects, may have been too low leading to the same effect. Clearly it would be desirable to develop a means of measuring the conductivity of the slab samples themselves.

One should notice that the deviation does not decrease for high velocities as would be expected if it were due instead to a velocity dependence of the pinning force.

In view of these facts the fit of the experimental data to the theory may be considered reasonably good. This leads to two conclusions: (a) the theory of current induced motion as given by Andreev and Dzhikaev is in reasonable agreement with the experimental data when allowance is made for the effect of pinning, and (b) the present data is consistent with the presence of a velocity independent pinning force.

Further evidence in favour of this second conclusion was provided by an experiment in which two Pb samples were cut out of the same batch of metal, one (Pb 1) being used as pressed and the other (Pb 5) being annealed at 260°C in a vacuum of less than 10^{-5} torr for 48 hours. The annealing process would be expected to reduce the pinning and hence the magnitude of the critical velocity V_o obtained in a measured domain velocity versus current characteristic. However, if the pinning force is velocity independent the annealing should not alter the slope of the characteristic. (The effective conductivity should not be changed by the annealing (Van den Berg (1948))).

Fig. 6.9 shows the results of this experiment for a temperature of 1.3K and reduced field of 0.8. The critical velocity V_o has been reduced markedly from 200 ± 15 $\mu m.sec^{-1}$ to 75 ± 10 $\mu m.sec^{-1}$ but no measurable change has occurred in the slope of the characteristic.

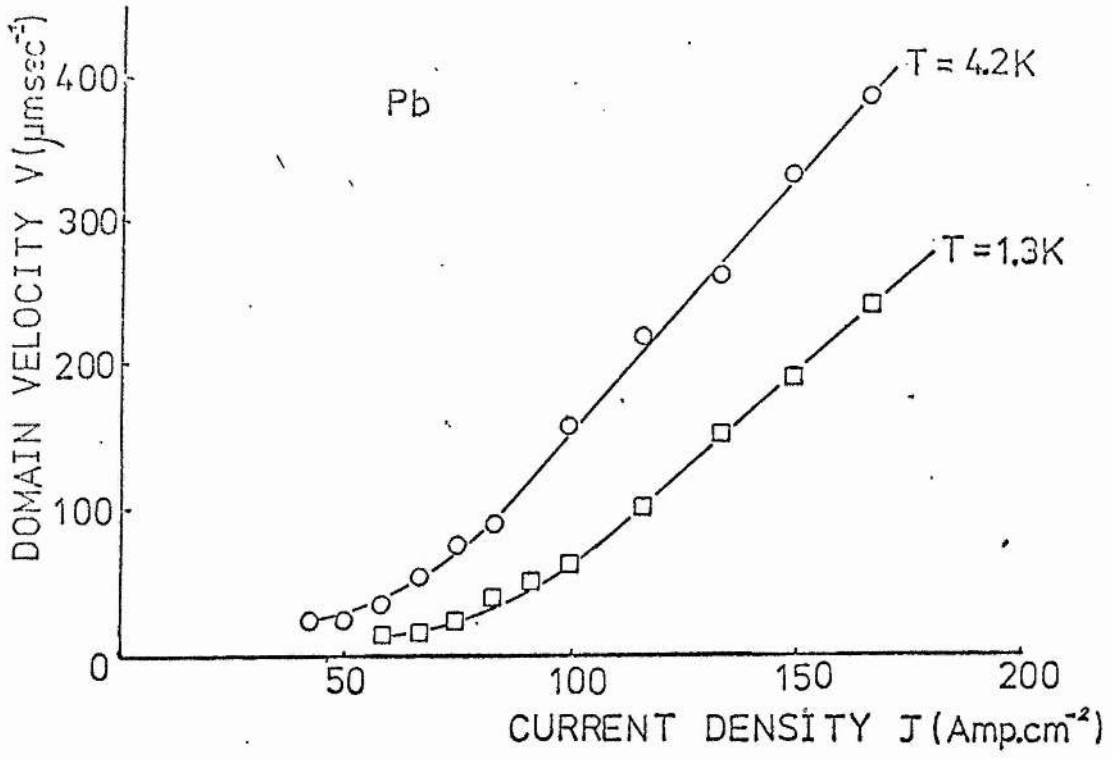

Fig. 6.10 Flow Characteristics in Pb, h = 0.8.

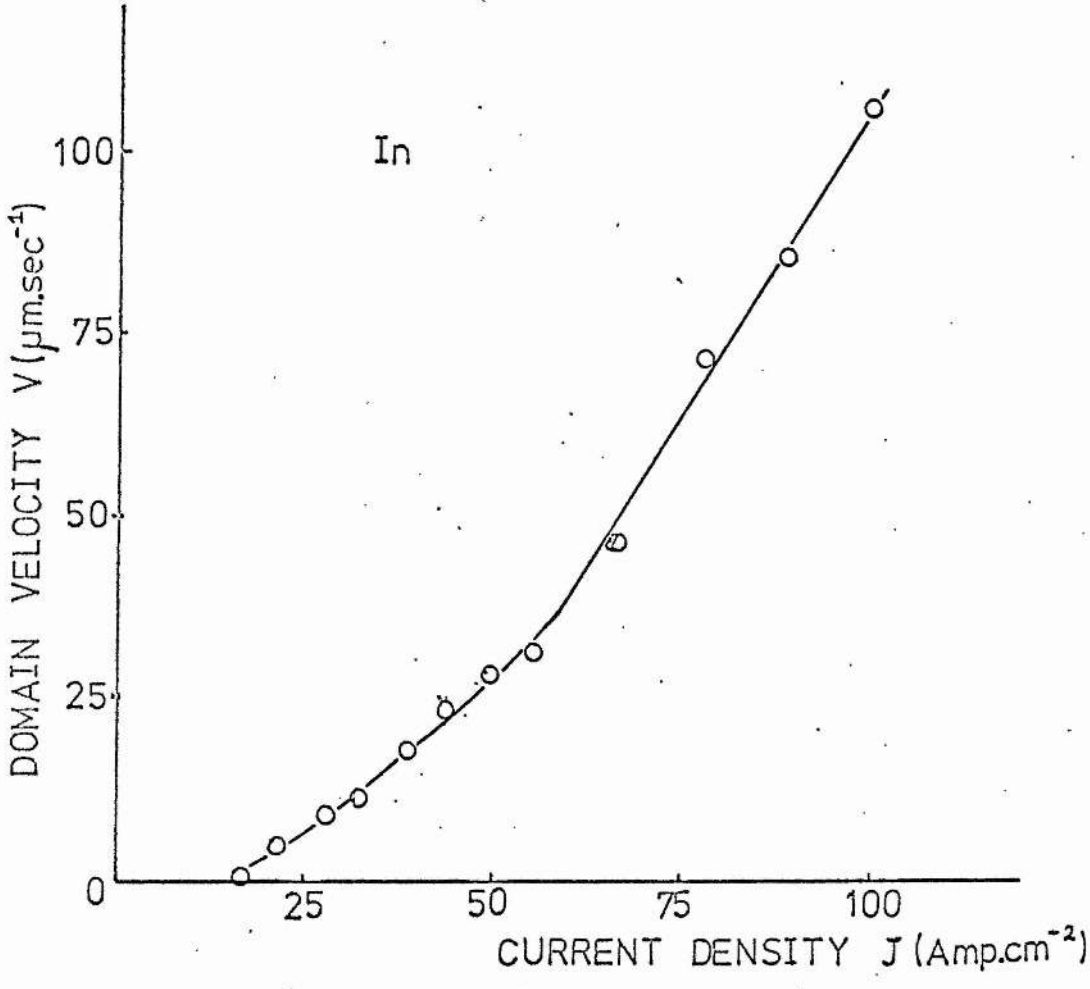

Fig. 6.11 Flow Characteristic in In, h = 0.8, T = 1.3K.

6.4 Nature of the motion near $J = J_o$

The discussion of the previous section was limited to a treatment of the linear part of the flow characteristic found when J was not too close to J_o. Careful measurements for currents nearer J_o revealed a non-linear region as found in earlier work on Type I superconductors using indirect methods of observation (e.g. Takayama et al (1971)).

Fig. 6.10 shows characteristics taken in Pb for two temperatures 4.2K and 1.3K at constant reduced field h = 0.8 showing the curved region near J_o. The curves show that domain motion still takes place for currents J, less than the critical value J_o obtained by extrapolation back to the abscissa. However, one must be careful to distinguish between the nature of the motion in this region and that observed in the linear part of the characteristic. In the $J < J_o$ region the domain displacements tended to be local and the motion tended to be intermittent, the direction of the motion sometimes being deflected in a zig-zag fashion about the perpendicular to the driving current, due presumably to encounters with pinning sites. These deflections occurred mostly in the upper part of the curved region. As can be seen, this type of motion occurred over a fairly wide band of current values (in the above case at T= 4.2K , 50 Amp.cm$^{-2} \leqslant J \leqslant$ 80 Amp.cm^{-2}). Velocity measurements for currents less than 50 Amp.cm^{-2} were not found to be possible due to the displacements being extremely infrequent and of short duration. It was also noticeable that the characteristic flattened off at a higher velocity for the higher temperature.

Fig. 6.11 shows a characteristic obtained at T = 1.3K with h = 0.8 for an In sample again showing a curved region near J_o. In this case, however, the characteristic does not flatten out so much and no motion at all could be observed for $J \leqslant 17$ Amp.cm^{-2}.

As discussed in Chapter V previous workers (in Type II superconductors mainly) have suggested that the curved part of the observed characteristics is

caused by one or other of the following processes:

(i) a thermally activated creep mechanism,

(ii) inhomogeneities in the sample smearing out the precise critical current value,

(iii) a velocity dependent pinning force.

A comparison with the experimental data with a view to deciding which of these processes was, in fact, responsible for the curvature observed in the present work was performed.

(i) Thermally activated creep mechanism

If this mechanism was responsible for the curvature then the equation derived from Anderson's theory

$$V = V_p \exp\left(\frac{E_J - E_o}{kT}\right),$$

should describe the exact shape of the curve at low $J \sim J_o$. The constant V_p is a velocity related to the natural frequency of vibration of the flux and hence one expects it to be constant for a constant reduced field (i.e. shape of domain) and temperature T (not too close to T_c). Its value can be found by noticing that $V = V_p$ for $E_J = E_o$ in the above equation, hence the velocity is V_p at the point where the curved region of the characteristic ends and the linear region begins.

However, in Fig. 6.10 it can be seen that the value of V_p is different for the two temperatures. In fact,

$$T = 4.2K \qquad V_p = 100 \pm 5\ \mu m.sec^{-1}$$

$$T = 1.3K \qquad V_p = 60 \pm 5\ \mu m.sec^{-1}$$

Let us rewrite the above equation as follows

$$\ln(V/V_p) = \frac{E_J}{kT} - \frac{E_o}{kT}$$

$$\text{i.e.} \qquad T\ln(V/V_p) = \frac{E_J}{k} - \frac{E_o}{k} \qquad (6.5)$$

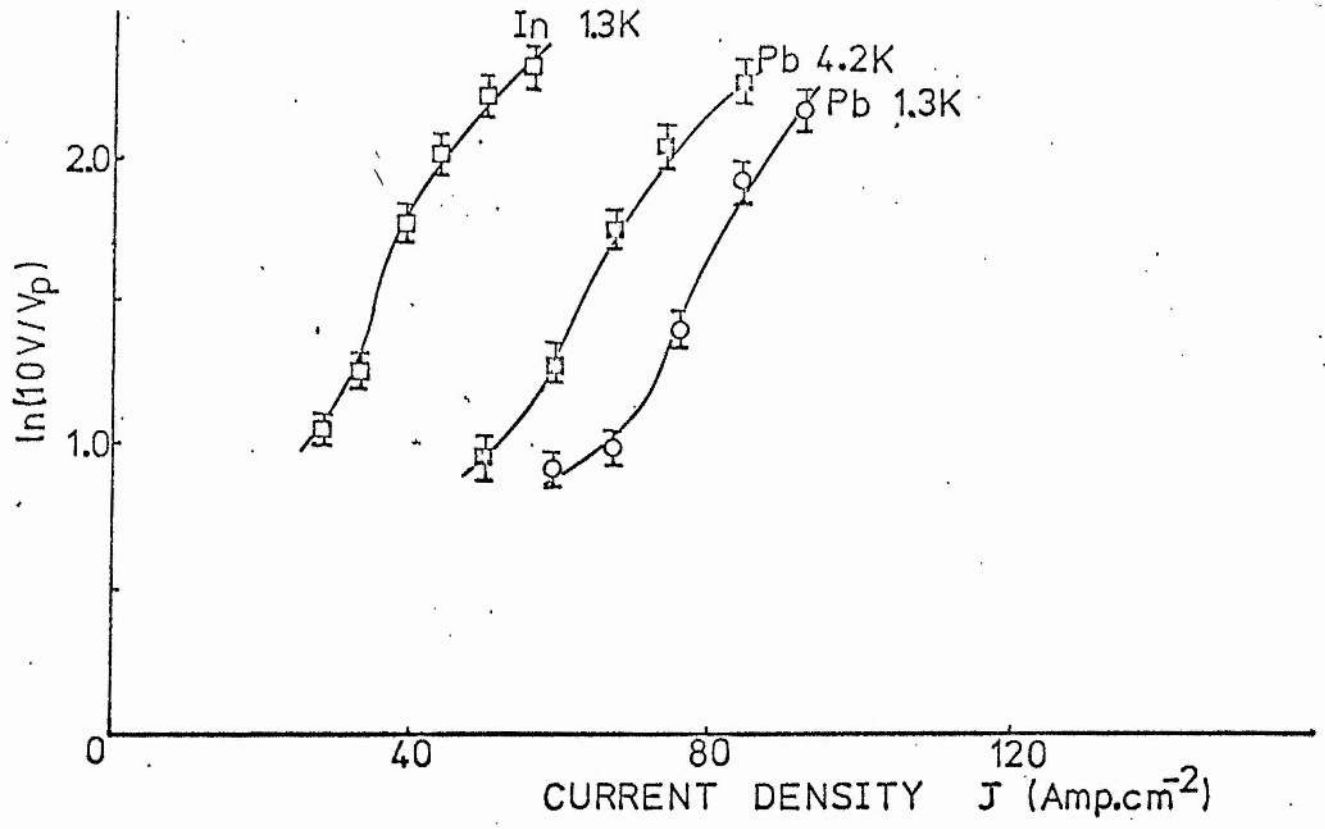

Fig 6.12a $\ell n(10V/V_p)$ Against Current Density J For Pb At 4.2K And 1.3K And For In At 1.3K, Both With h = 0.8.

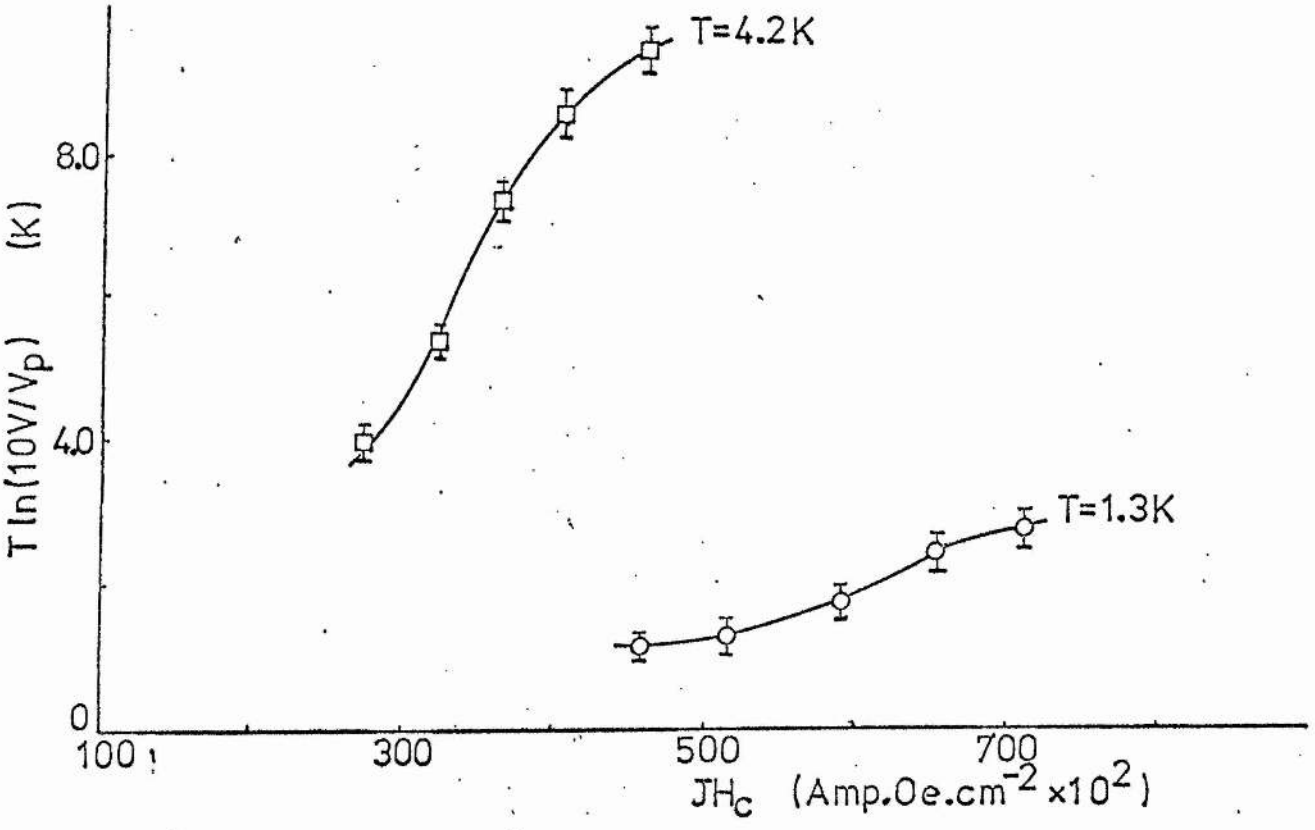

Fig 6.12b $T\ \ell n(10V/V_p)$ Against JH_c For Pb At 4.2K and 1.3K with h = 0.8.

We take $E_J \propto JH_c$ i.e. $E_J = aJH_c$, where a is a constant. Substituting this result in the above equation we obtain

$$T\ln(V/V_p) = \frac{a}{k} JH_c - \frac{E_o}{k} \qquad (6.5(a))$$

This equation predicts that, for constant temperature T, a plot of $\ln(V/V_p)$ versus J should give a straight line and that data from different temperatures should fall on one straight line graph of $T\ln(V/V_p)$ versus JH_c with intercept giving the pinning energy E_o/k.

Fig. 6.12(a) shows the experimental data for Pb at temperatures of 4.2K and 1.3K, and for In at a temperature of 1.3K plotted on a graph of $\ln(V/V_p)$ versus J. In none of these cases is a good straight line obtained within the experimental error.

Fig. 6.12(b) shows the experimental data for Pb at temperatures of 4.2K and 1.3K plotted on a graph of $T\ln(V/V_p)$ versus JH_c. Two very separate curves are obtained in extreme contradiction of the prediction of the above equation.

To summarise, although the critical current is found to rise almost linearly with falling temperature (Fig. 6.2(b)) suggesting the presence of thermal activation, the exact form of the curved region of the flux flow characteristic at low $J \sim J_o$ does not agree with the predictions of Anderson's flux creep theory. One might have expected this result since it is difficult to visualize such relatively large areas of flux domain being thermally activated over pinning barriers to an appreciable extent.

(ii) Inhomogeneities smearing out the precise critical current value

In the case of the critical current varying at different points of the sample one should observe a motion commencing preferentially in the parts of the sample with a low J_o at currents $J \sim J_o$. This type of behaviour was observed.

In this case, the characteristic would exhibit curvature since, although the velocities in the linear region would be determined by some average J_o,

at low J the motion observed and velocity measured would be over regions with low J_o and hence would be higher than expected. The exact shape of the curved region would to some extent vary each time it was measured since the observation of motion over slightly different regions (with varying J_o values) would produce differing velocity values. However, this reasoning would only be valid if the critical current variations occurred over distances small compared with the microscope field of view since the measured characteristics (Fig. 6.10 and 6.11) were generally taken without moving the area of the sample examined.

To examine the spatial variation of the critical current a different method of velocity measurement was developed in which the domain velocity could be measured over small time intervals and hence small areas of the sample.

Suhl (1965) has calculated the effective inertial mass of a fluxoid according to the time-dependent form of the Ginzburg-Landau theory proposed by Stephen and Suhl (1964). His results may be used to give an upper limit for the inertial mass or, more usefully the relaxation time, of the domains observed in the present work. This upper limit for the relaxation time turns out to be $\sim 10^{-16}$ seconds, hence clearly inertial effects may be neglected and we may consider the domains as stopping and starting their motion instantaneously upon application or removal of the driving current.

If the current is applied as a pulse of known duration and magnitude then a measurement of the distance travelled by the domain in this time will yield the velocity. Equally, if a series of current pulses of equal length and magnitude are applied to the domain, its position being noted after each pulse, then the variation in distance travelled during successive pulses will reflect the variation in velocity and hence critical current across the sample.

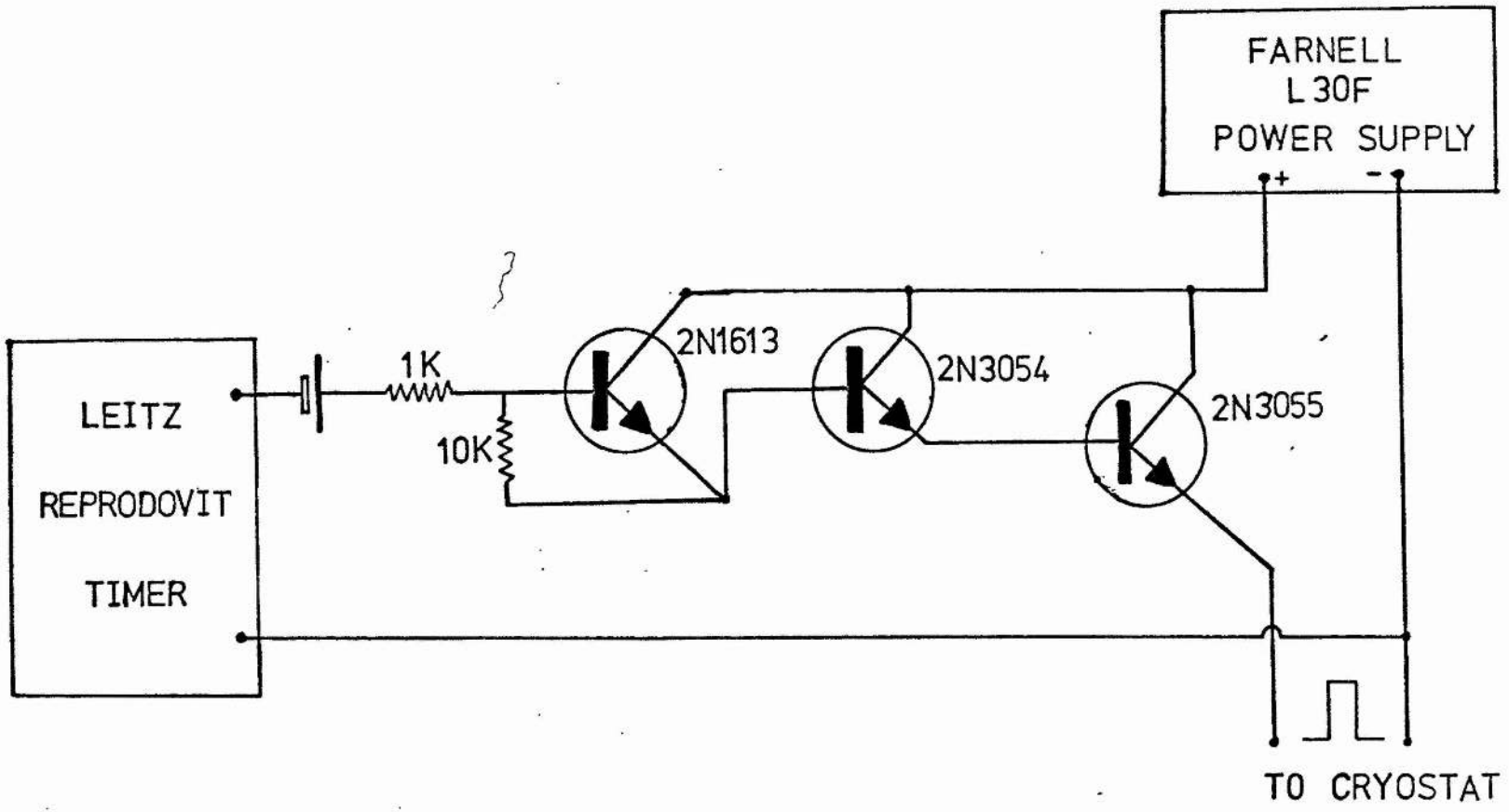

Fig. 6.13 Circuit For The Production Of High Current Pulses

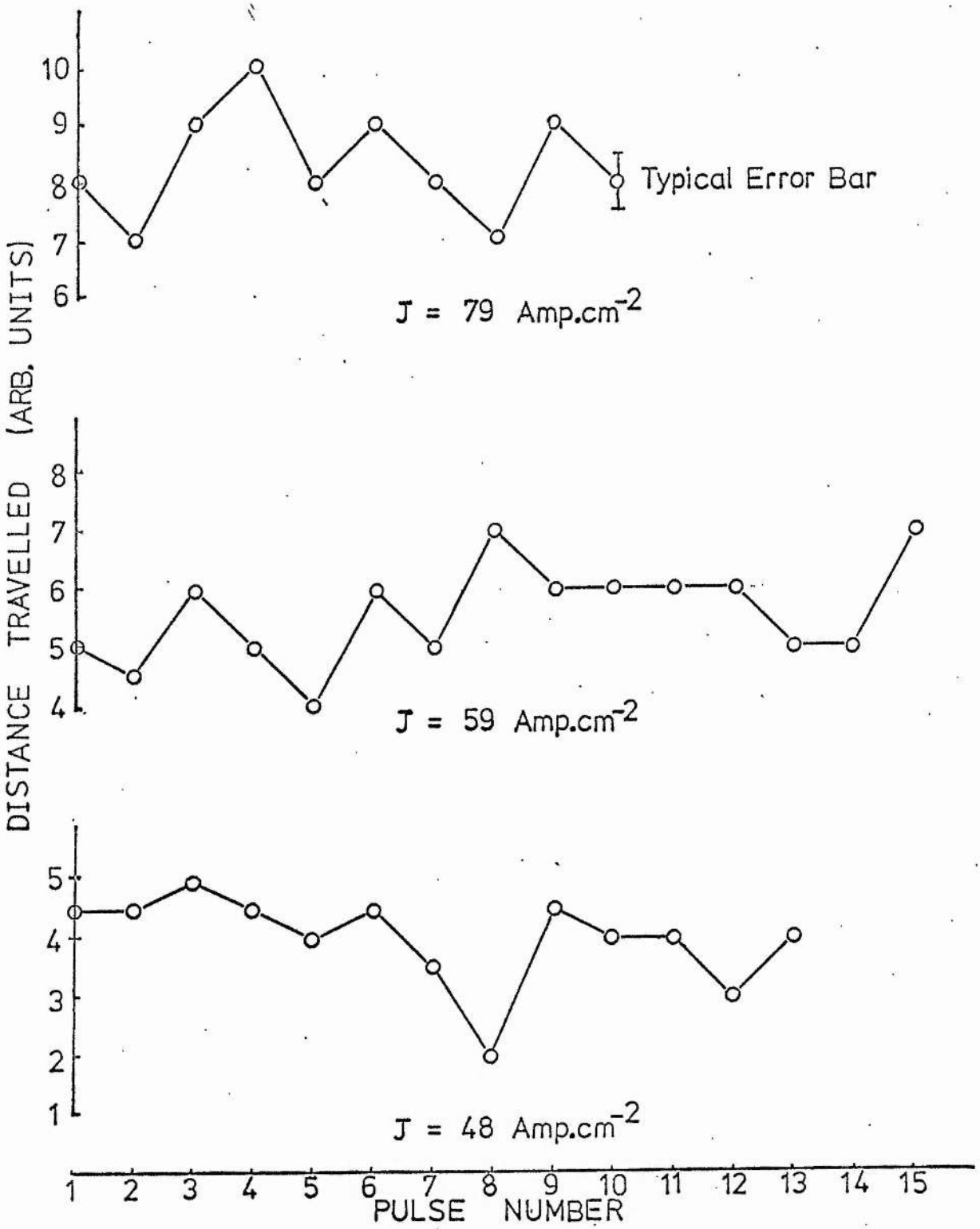

Fig. 6.14 Distance Travelled By A Domain Subjected To 0.5 Second Current Pulses Of Various Magnitudes, Pb, h = 0.8, T = 1.3K.

Fig. 6.13 shows the electronic circuit used to produce the required current pulses. A Leitz Reprodovit photographic timer connected to a 6V battery was used to switch on and off a 2N3055 transistor via a pair of transistor drivers. The current from the Farnell L30F power supply was hence converted to a pulse which proved upon examination (with a Hewlett-Packard oscilloscope) to have a length constant to within 2% and magnitude constant to within 1%. The rise and fall times of the pulse were found negligible compared with the lengths of the pulses used (generally 0.5 seconds).

Fig. 6.14 shows the observed variation in distance travelled for a domain subjected to successive 0.5 second pulses of various magnitudes at h = 0.8 and T = 1.3K in pure Pb. The distances were measured using a micrometer scale in the Reichert Wein eyepiece. The three sets of data were taken from flow over different parts of the sample and it can be seen that in all cases appreciable variations in the distance travelled and hence the local critical current values occur.

It has been previously established (Section three) that the linear part of the flow characteristic may be described by the equations

$$V = \frac{c}{\sigma H_c} (J - J_o) \qquad J \geqslant J_o$$

$$V = 0 \qquad J < J_o$$

where J_o is the critical current obtained by extrapolation of the linear region to intersect the abscissa. Let us now take the J_o above to be average, $\overline{J}_o$, of a critical current distribution over the sample caused by variations in, say, surface conditions or metallurgical state. That is, we now describe the linear region by

$$V = \frac{ch}{\sigma H_c} (J - \overline{J}_o) \qquad J \geqslant \overline{J}_o$$

$$V = 0 \qquad J < \overline{J}_o \qquad (6.6)$$

Further, let us assume that the distribution of critical current

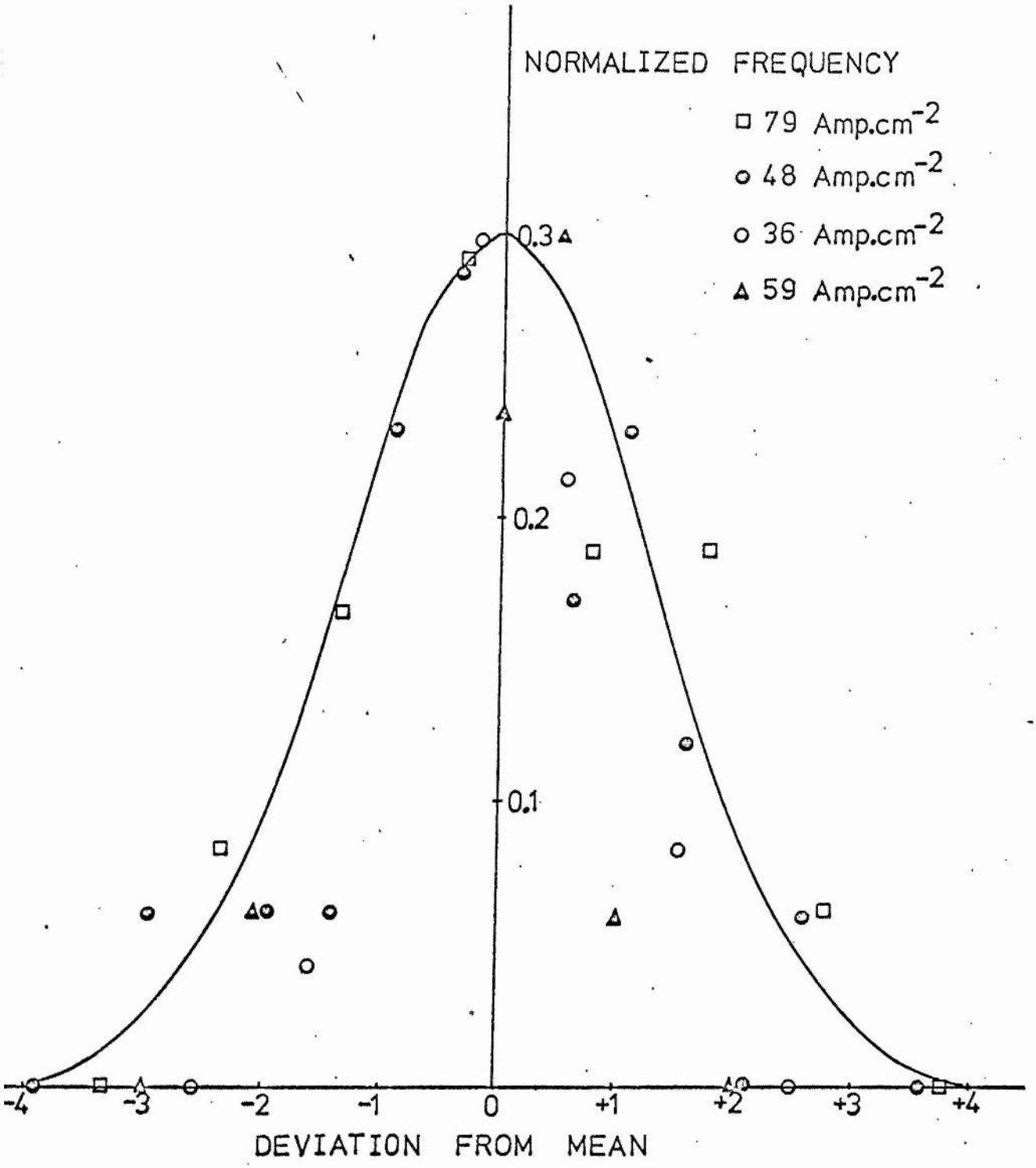

Fig. 6.15 The Distribution Of Distances Travelled By A Domain Subjected To 0.5 Second Current Pulses Of Various Magnitudes, Pb, h = 0.8, T = 1.3K.

values over the microscope's field of view may be represented by a distribution function $Z(J_o)$ of Gaussian form

$$Z(J_o) = \frac{1}{S\sqrt{2\pi}} \exp\left(-(J_o - \bar{J}_o)^2/2S^2\right) \quad , \qquad (6.7)$$

where S is the standard deviation of the normalised curve.

The available experimental data is in reasonable agreement with the representation of the critical current distribution by a Gaussian form, as shown in the frequency distribution of distances travelled by a domain subjected to successive 0.5 second current pulses of various magnitudes (in Pb, h = 0.8 at T = 1.3K) given in Fig. 6.15. This data was constructed from results like those of Fig. 6.14 by normalization of the frequency distributions, the curve shown being a Gaussian normalised in the same manner. The agreement is most satisfactory for the data taken in the case of J = 79 Amp.cm^{-2} (represented by □) where 51 observations were made. In the case of the other J values less observations were taken and the agreement is less satisfactory, as might be expected.

Now, if there is a distribution of critical current values of this nature then, when the applied driving current J begins to fall below the upper tail of the distribution the effective average critical current will become less than $\bar{J}_o$. No motion will be observed in regions with critical currents above J and the motion seen in other parts of the sample will be governed by this new effective average critical current value. Let us write

$$(\bar{J}_o)_{eff} = \bar{J}_o - \delta(J), \qquad (6.8)$$

$\delta(J)$ expressing the amount by which the effective average critical current differs from $\bar{J}_o$ and depending on the driving electric current J. Clearly, $\delta(J)$ may be considered zero for J values above the beginning of the critical current distribution where the observed flow will be the linear type discussed earlier and described by equation (6.6), but $\delta(J)$

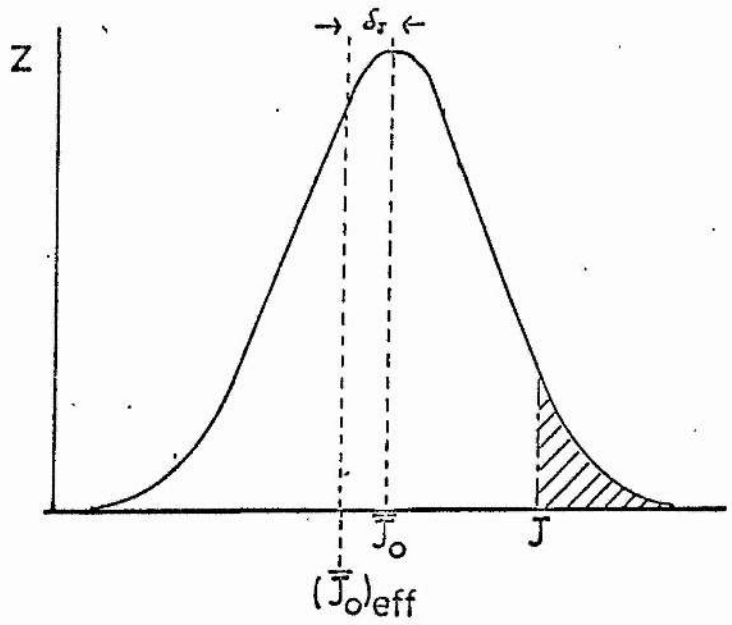

Fig 6.16 The Critical Current Distribution.
δ_J Measures The Shift In Average When The Distribution Is Terminated At J, The Shaded Area Being Neglected.

will become non-zero when J encroaches on the critical current distribution and the observed characteristic will become non-linear.

Let us attempt to describe the curved region by substituting the effective average critical current $(\bar{J}_o)_{eff}$ in place of the average $\bar{J}_o$ in equation (6.6)

$$\text{i.e. } V_{curved} = \frac{c}{\sigma H_c} \left(J - (\bar{J}_o)_{eff}\right)$$

and using (6.8)
$$V_{curved} = \frac{c}{\sigma H_c} \left(J - \bar{J}_o\right) + \frac{c}{\sigma H_c} \delta(J). \qquad (6.9)$$

This equation will be valid for $J < \bar{J}_o$ as long as $\delta(J)$ is large enough to stop V_{curved} becoming negative. Clearly, there may exist some J_{limit} defined by

$$J_{limit} - \bar{J}_o = \delta(J_{limit}),$$

below which this is not possible and we must take

$$V = 0 \quad J < J_{limit}.$$

The correction term $\delta(J)$ may be calculated using the assumption that there is a Gaussian distribution of critical current values. Fig. 6.16 shows the proposed distribution and indicates the meaning of $\delta(J)$. We calculate the effective mean when only part of the distribution up to a value J is considered.

$$\text{Effective mean } (\bar{J}_o)_{eff} = \frac{\frac{1}{S\sqrt{2\pi}} \int_{-\infty}^{J} \exp\left(-\frac{(J-\bar{J}_o)^2}{2S^2}\right) J dJ}{\frac{1}{S\sqrt{2\pi}} \int_{-\infty}^{J} \exp\left(-\frac{(J-\bar{J}_o)^2}{2S^2}\right) dJ}.$$

The lower limit of the integration should strictly be zero since we consider only positive values of J but the use of $-\infty$ will lead to negligible error in the description of the curved region as long as $\bar{J}_o > 3S$.

$$\text{i.e., } (\bar{J}_o)_{eff} = \frac{\frac{1}{S\sqrt{2\pi}}\int_{-\infty}^{J}\exp(-\frac{(J-\bar{J}_o)^2}{2S^2})(J-\bar{J}_o)dJ + \frac{1}{S\sqrt{2\pi}}\int_{-\infty}^{J}\exp(-\frac{(J-\bar{J}_o)^2}{2S^2})J_o dJ}{\frac{1}{S\sqrt{2\pi}}\int_{-\infty}^{J}\exp(-\frac{(J-\bar{J}_o)^2}{2S^2})dJ} .$$

The first integral in the numerator may be simply integrated by a change of variable, and the other integral has been given by Abramowitz and Stegun (1964). The result obtained is

$$(\bar{J}_o)_{eff} = \frac{-\frac{S}{\sqrt{2\pi}}\exp(-\frac{(J-\bar{J}_o)^2}{2S^2}) + \frac{\bar{J}_o}{2}(1+\text{erf}(\frac{(J-\bar{J}_o)}{S\sqrt{2}}))}{\frac{1}{2}(1+\text{erf}(\frac{(J-\bar{J}_o)}{S\sqrt{2}}))} .$$

$$\text{i.e., } (\bar{J}_o)_{eff} = \bar{J}_o - \frac{2S}{\sqrt{2\pi}} \cdot \frac{\exp(-\frac{(J-\bar{J}_o)^2}{2S^2})}{(1+\text{erf}(\frac{(J-\bar{J}_o)}{S\sqrt{2}}))} . \qquad (6.11)$$

Comparing this result with equation (6.8) we obtain

$$\delta(J) = \frac{2S}{\sqrt{2\pi}} \cdot \frac{\exp(-\frac{(J-\bar{J}_o)^2}{2S^2})}{(1+\text{erf}(\frac{(J-\bar{J}_o)}{S\sqrt{2}}))} . \qquad (6.12)$$

This result may be directly compared with the experimental data for Pb with h = 0.8 contained in Fig. 6.10. To accomplish this we note that from equation (6.9)

$$V_{curved} - \frac{c}{\sigma H_c}(J-\bar{J}_o) = \frac{c}{\sigma H_c}\delta(J) .$$

Let us call the velocity given by the left hand side of this equation V_δ

$$\text{i.e.} \qquad V_\delta = V_{curved} - \frac{c}{\sigma H_c}(J-\bar{J}_o) . \qquad (6.13)$$

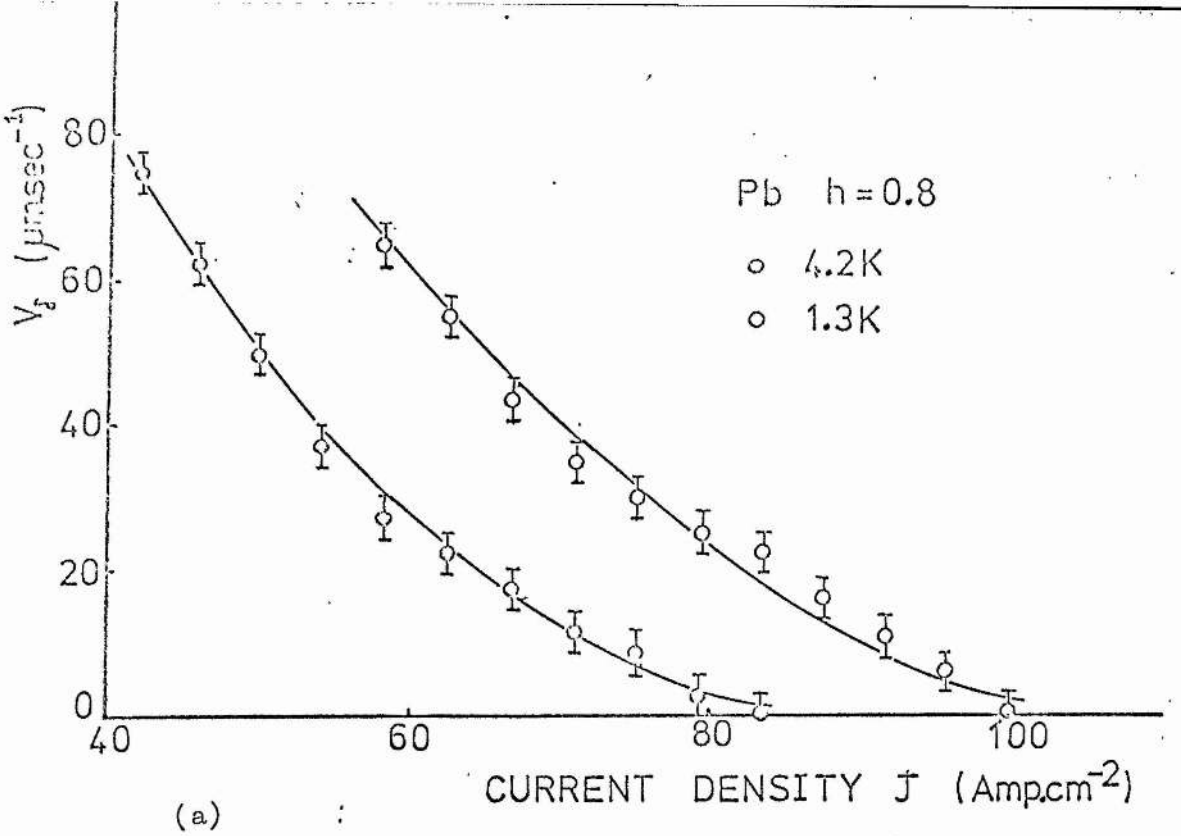

(a)

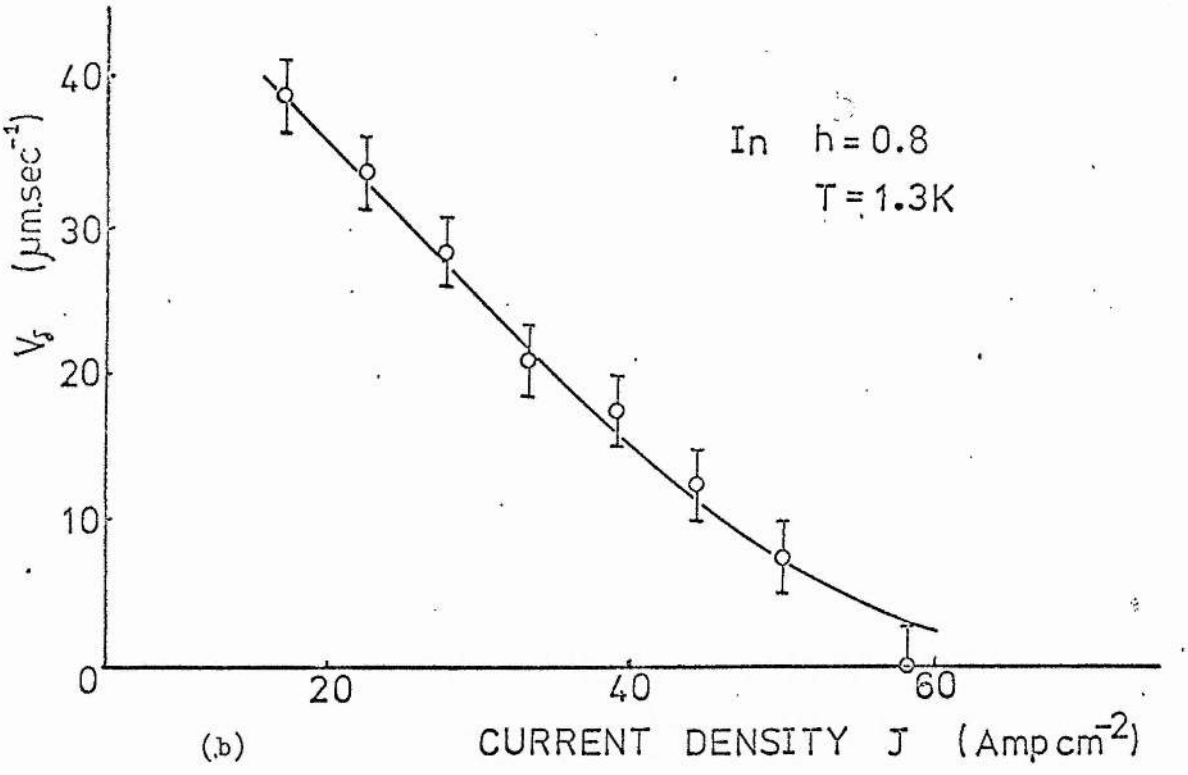

(b)

Fig 6.17a and b Experimental data for V_f (see text) plotted against J, with theoretical curves calculated assuming a Gaussian disribution of critical current values.

V_δ may be extracted from the experimental data by measurement of the difference between the experimentally determined velocity and the corresponding value on the extrapolated linear part of the characteristic. The theory we have developed gives

$$V = \frac{c}{\sigma H_c} \delta(J) \qquad (6.14)$$

where $\delta(J)$ is given by equation (6.12).

Now, in section three (Fig. 6.8) it was found that the calculated slope $(\frac{c}{\sigma H_c})$ was always too low, probably due to an error in the values of the conductivity. Therefore, let us take the slope $(\frac{c}{\sigma H_c})$ in equation (6.14) to be that of the linear part of the <u>experimental</u> characteristics. In this way we shall compare only the predictions of the present model with the data, avoiding any difficulties over the conductivity values.

Fig. 6.17(a) shows the experimental data for the two temperatures T = 4.2K and T = 1.3K in Pb (h = 0.8) together with theoretical curves fitted to the points using a least squares method. Fig. 6.17(b) shows similar data for T = 1.3K in In (h = 0.8) with a similar theoretical curve.

In all cases the phenomenological model, which assumed a Gaussian distribution of critical current values, gives a good fit to the data. The only adjustable parameter is S, the standard deviation of the critical current distribution. For <u>both</u> temperatures in Pb, S = 12.8 Amp.cm^{-2} and for the one temperature examined in In, S = 15.1 Amp.cm^{-2}.

The slight tendency of the experimental points to rise above the theoretical curve at high J in Pb (particularly at T = 1.3K) can be understood if one recalls the type of motion observed during measurements in this region of J values. The flowing domains were

often seen to be deflected round pinning sites in the course of their motion. In this case the velocity measured would be lower than that predicted by the model which takes no account of such deflections. If the measured velocity were too low then V_δ would be too high, as observed. As J falls this discrepancy would disappear since the domains were no longer observed to be deflected round the pinning sites but rather were trapped by them. Hence, the velocity would only be measured between such pinning sites and would correspond to that predicted by the theory. Such behaviour was not observed in In during the measurement of the data of Fig. 6.17(b).

(iii) A velocity dependent pinning force

As discussed in Chapter V, the work of Lowell (1970) suggested that in Type I superconductors the pinning force may be velocity dependent due to the loosely interacting nature of the intermediate state, and may vanish for large J. The experimental data discussed so far has not supported the presence of a velocity dependent pinning force but it was decided to extend the measurements to higher velocities (and currents) in order to confirm this conclusion.

As mentioned earlier, the error in measuring the transit time of a moving domain (by visual means) was $\pm$ 0.2 seconds which limited the accuracy in determining velocities above 500 $\mu m.sec^{-1}$. Consequently, an alternative method of measurement had to be used to enable velocities greater than this to be measured. The pulse technique described previously was extended to allow currents of up to 20 amps to be used by the substitution of a Farnell H60/50 power supply for the usual Farnell L30F supply and the addition of a further 2N3055 transistor in parallel with the first in the switching circuit. The pulse shape was not significantly degraded at these high current values. The distance travelled by a domain upon application of

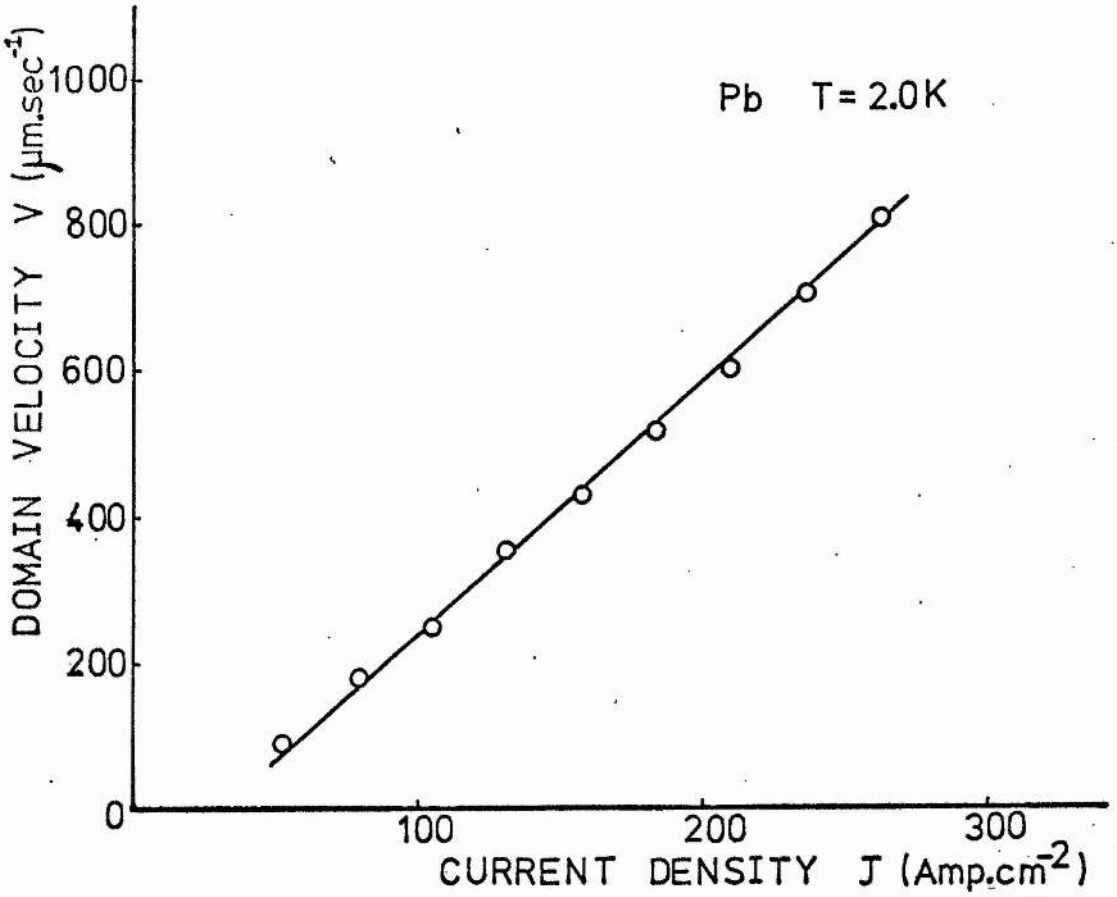

Fig 6.18 Flow Characteristic For Pb, h = 0.8,
T = 2.0K Extended To Higher Velocities.

0.5 second pulses was measured as described before and hence the velocity calculated.

Fig. 6.18 shows a characteristic obtained using this method for pure Pb at 2.0K with h = 0.8. As can be seen, for velocities up to the highest used (800 $\mu m.sec^{-1}$) no change in slope and hence no evidence for the existence of a velocity dependent pinning force can be detected.

6.5 Conclusions

A quantitative study of the variation of flux flow velocity as a function of driving electric current has been made in the Type I superconductors, lead, tin and indium for various reduced applied fields h and temperatures T.

The observed characteristics have been found to exhibit two distinct regions.

Firstly, a linear region where the measured velocity was found to agree reasonably well with that calculated from the general theory of Andreev and Dzhikaev, when allowance was made for the effects of pinning by the introduction of a velocity independent pinning force. Exact agreement was not obtained, but this was probably due to the fact that the conductivity values were measured for extruded wires rather than for the same slab samples as were used in the flux flow experiments.

Secondly, at low values of J, a curved region of the characteristic was seen where the motion was observed to commence preferentially in certain parts of the sample. The velocity in this region was found to agree, within the experimental error, with a phenomenological model which was developed based on the presence of a Gaussian distribution of critical current values throughout the samples due presumably to metallurgical changes causing variations in the pinning

strength. Separate experiments were performed to examine directly the variation of critical current values throughout the sample. These were found to be appreciable and their distribution was approximately of Gaussian form although much more data would be required to confirm this positively.

Lastly, two alternative mechanisms that might have explained the curved part of the characteristic were examined viz., the presence of thermal activation or a velocity dependent pinning force. The experimental data was found to be in disagreement with the theory of the first of these and provided no evidence for the existence of the second.

CHAPTER VII - EXPERIMENTAL RESULTS FOR TEMPERATURE GRADIENT INDUCED MOTION

7.1 Introduction

The experimental observation of pure thermally induced motion is very difficult. There is agreement between theory (Kim and Stephen (1969)) and experiment (Otter and Solomon (1967)) that unit thermal gradient ($1K.cm^{-1}$) across a superconducting sample in the intermediate state gives rise to a force on the flux domains equivalent to that produced by an electric current of 5 $Amp.cm^{-2}$. Since the lowest value of critical current observed in the experiments of the last chapter was 17 $Amp.cm^{-2}$ for $h = 0.9$ in Pb, one can see that no pure thermally activated motion can be expected to be produced until the thermal gradient at least exceeds $\sim 3K.cm^{-1}$.

It is instructive to calculate the heat current density produced by this thermal gradient in the geometry of samples used. For Pb we may take an average thermal conductivity value of 3 $W.K^{-1}.cm^{-1}$ (De Haas and Rademakers (1940)) and hence for the sample Pb3

$$Q = \frac{3 \times 3}{\text{Length}} \quad W.cm^{-2}$$

$$\sim 6.0\ W.cm^{-2}$$

It was found very difficult to reduce the thermal resistance between the sample and the copper post to which its 'cold' end was attached to an extent sufficient to preclude the entire sample heating up considerably when heat currents of the above order were passed through it.

For these reasons no observations of pure thermally induced motion were accomplished below $T \sim 5.8K$ and investigations were only possible over a restricted range of reduced field values ($0.7 \leqslant h \leqslant 0.8$). Consequently, a thorough comparison of the observed motion with that predicted by the theory of Andreev and Dzhikaev did not prove possible. Experiments were only performed using Pb.

7.2 The observation of pure thermally induced motion

The method of measurement of the domain velocity under conditions of thermally induced flow was exactly the same as that described in the previous chapter for the case of current induced flow. The procedure required for setting up the flow was, however, more complex. The usual sequence of events was as follows.

The bath temperature was reduced to as low a value as possible ($T \sim 1.3K$) in order to have the sample at the lowest possible temperature before application of the heat current. With no heat current applied, the sample temperature generally fell to around 1.8K. The difference between this and the bath temperature was presumably caused by the radiation falling on the sample from the window system and not from a heat leak through the electrical leads since the temperature measured by the resistors was always consistent with the value calculated from an observation of the magnetic field necessary to drive the sample completely normal. Having attained this sample temperature, heat was applied to the 'hot' end of the sample by passing a current through the heater resistor. An equilibrium heat flow through the sample with constant temperatures indicated by the resistors R_h and R_c was generally attained in about 60 seconds. The magnetic field was then reduced fairly slowly to the value desired, appropriate to the average temperature of the sample.

The motion of the domains could then be observed and their transit across the graticule timed. As indicated above, the critical field in the region of the sample under observation could be determined optically as a check on the temperature obtained from the resistors R_h and R_c.

Due to the design of the sample mount the heat generated in the heater resistor was assumed to all flow through the sample to the bath. Hence, a measurement of the current flowing through the heater together with its resistance (corrected for the resistance of the thin leads) was taken to

yield the heat current through the sample to an accuracy of ~ 5%.

In agreement with the arguments presented in the introduction and the results of Laeng and Rinderer (1973) no motion was seen until the heat current Q became greater than $4 W.cm^{-2}$. Motion could only be induced for high values of h, and in particular, the flux 'star' structures seen at low h were not seen to move. All of the observed motion was directed on average perpendicular to the heat current direction in disagreement with the theory of Andreev and Dzhikaev but in agreement with that of Rothen (1972) and with the results of Laeng and Rinderer. The direction of the motion was established by comparison with the direction of the motion induced by passing an electric current through the sample in the same direction as the heat current. The precise direction of motion was found to vary on occasion by as much as 10° on either side of the perpendicular to the heat current.

Fig. 7.1 shows typical experimental results for the domain velocity V versus heat current Q at h = 0.7 in Pb. As can be seen velocities in the range up to 250 $\mu m.sec^{-1}$ were observed for the heat currents used. The comparison of this raw data with the theoretical predictions is not directly possible since the average temperature of the sample is increasing slowly as the heat current rises. We wish to compare the observed velocity with that predicted by the theory of Rothen

$$V_{th} = - \frac{c \alpha_N}{H_c \kappa_n} Q, \qquad (4.20)$$

and also verify that it is considerably greater than that predicted by the theory of Andreev and Dzhikaev

$$V_\kappa = - \frac{c^2 L}{\sigma T H_c^2} \cdot \frac{x_s}{x_n} \cdot \frac{\kappa_n - \kappa_s}{\kappa_n + \kappa_s} \frac{\partial T}{\partial x} \qquad (4.18)$$

(using the expression appropriate to the flow of superconducting domains in a normal medium, as before), so as to confirm that the thermoelectric effect in the normal phase dominates the motion at high temperatures, as suggested by Laeng and Rinderer.

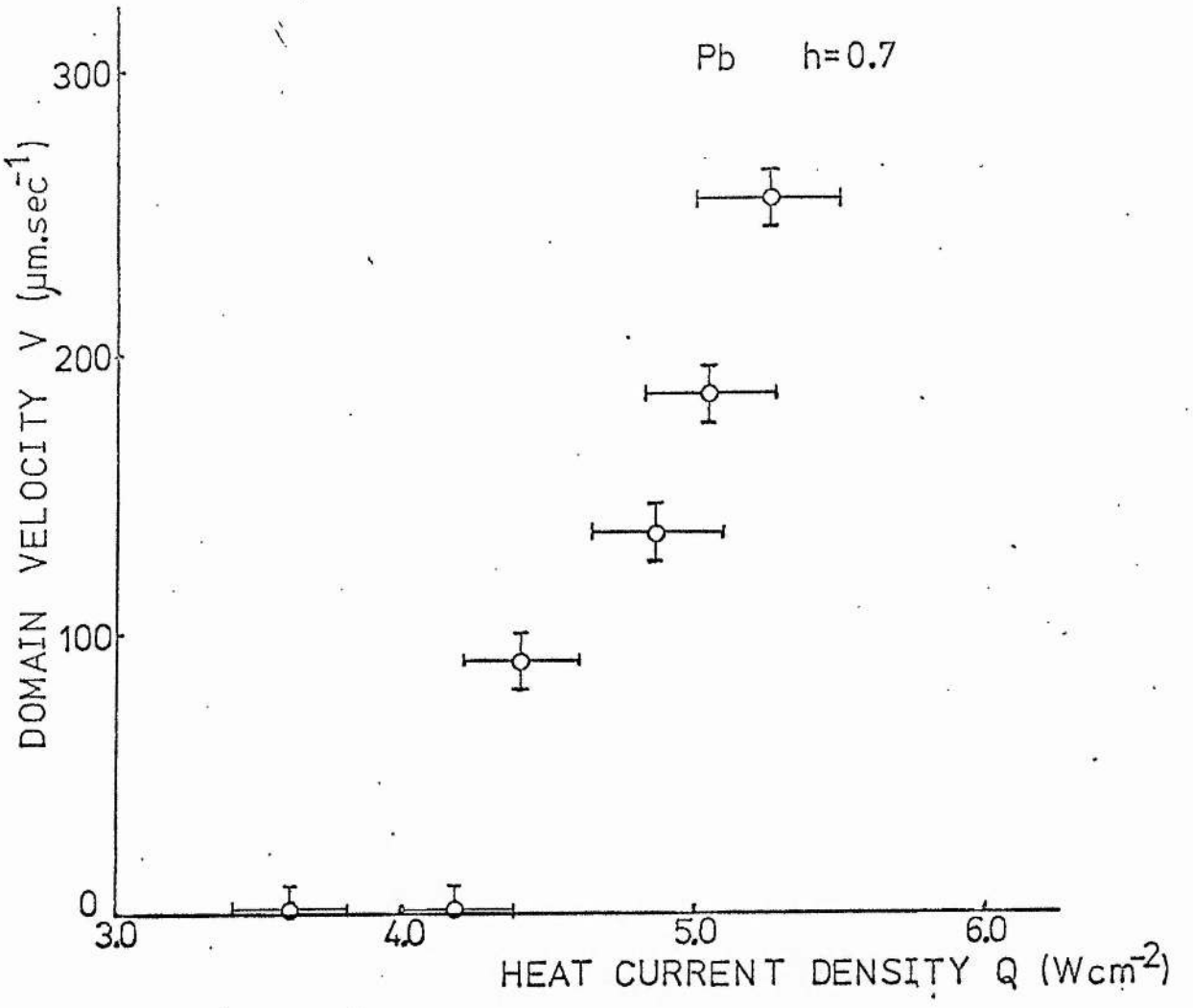

Fig. 7.1 Typical Data For Domain Velocity V Versus Heat Current Density Q In Pb At h = 0.7. (Lowest Points Displaced Slightly From Axis For Clarity).

To allow for the effects of pinning let us, by analogy with the treatment used to describe the current induced motion, rewrite the above equations as follows

$$V_{th} = - \frac{c\alpha_N}{H_c \kappa_n} (Q - Q_o) , \qquad (7.1)$$

and

$$V_\kappa = - \frac{c^2 L}{\sigma T H_c^2} \cdot \frac{x_s}{x_n} \cdot \frac{\kappa_n - \kappa_s}{\kappa_n + \kappa_s} \left(\frac{\partial T}{\partial x} - \left(\frac{\partial T}{\partial x}\right)_0\right). \qquad (7.2)$$

where Q_o and $\left(\frac{\partial T}{\partial x}\right)_0$ are a critical heat current and critical temperature gradient respectively.

Equation (7.1) can be written

$$\frac{V_{th} H_c \kappa_n}{\alpha_N} = - c(Q - Q_o). \qquad (7.3)$$

The experimental data may then be compared with the theory by plotting values of $\frac{V H_c \kappa_n}{\alpha_N}$, calculated using literature data for H_c, κ_n and α_N, against $Q - Q_o$.

The extraction of κ_n from the literature is slightly unsatisfactory since like the electrical conductivity σ it depends on the purity of the material employed. It was, however, found impossible, due to lack of time, to perform separate experiments to measure its value for the samples used. The values used were taken from De Haas and Rademakers (1940).

Steele (1951) has given the thermoelectric power of normal lead as

$$\alpha_N = (2.29 \times 10^{-8}) T \quad \text{Volts.K}^{-1} .$$

The value appropriate to the average temperature of the sample may hence be calculated.

The choice of a value for Q_o, the critical heat current is subject to considerable uncertainty. The graphs of domain velocity versus heat current density obtained (such as Fig. 7.1) were not taken at constant temperature and consequently a straight line which could be extrapolated

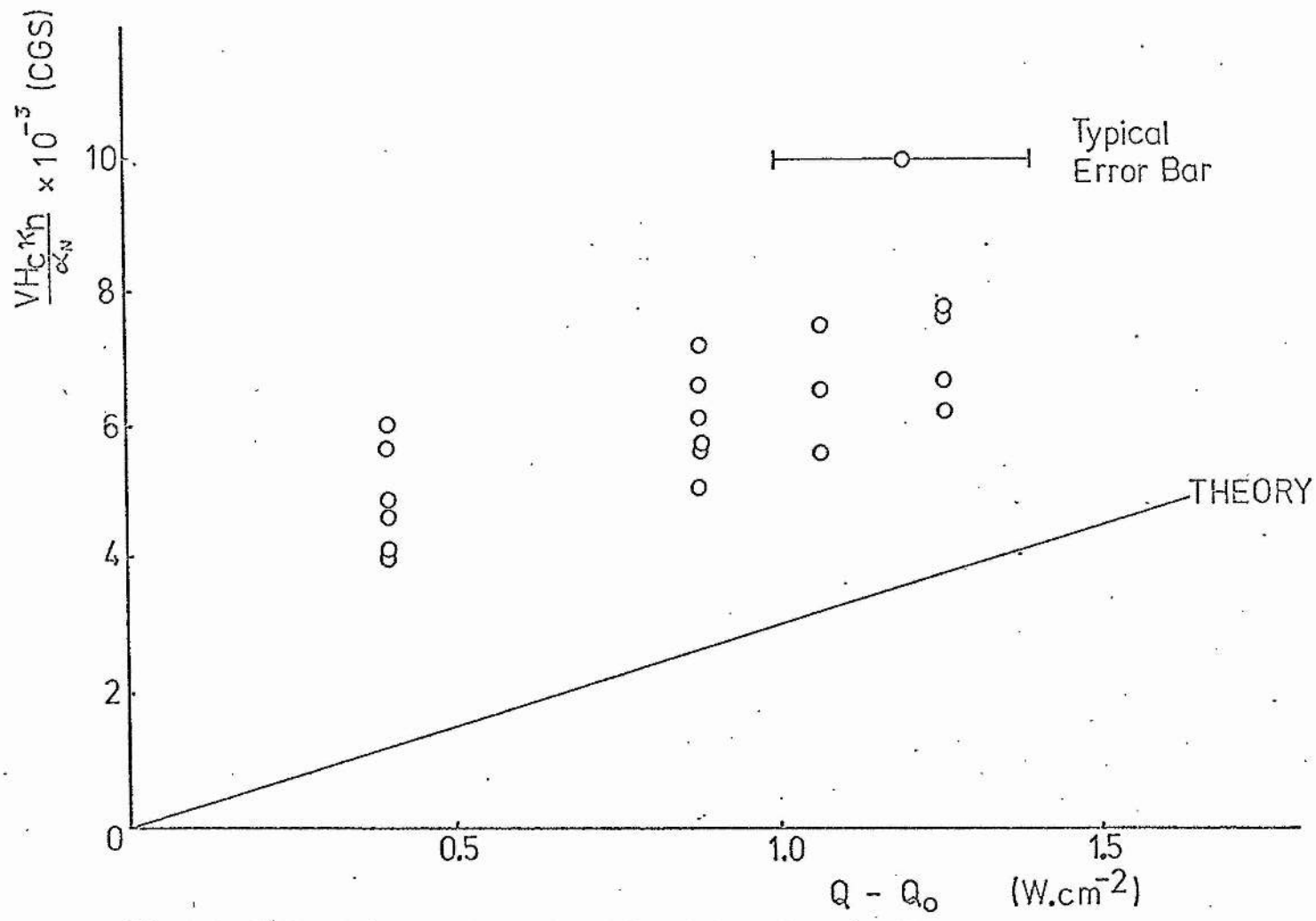

Fig 7.2 Collected pure thermally induced flow data for Pb.

to meet the abscissa was not expected nor obtained. In the case of the data of Fig. 7.1 the value of Q_o chosen was 4.0 ± 0.2 W.cm^{-2} and since $Q - Q_o$ was never greater than 1.26 W.cm^{-2} this leads to a large uncertainty in its value. It should also be pointed out that variations in Q_o over the temperature range of measurement (5.8→6.6K) were neglected and were found small over the small range of reduced applied fields investigated.

Fig. 7.2 shows the collected experimental data plotted in the above manner. It can be seen that the experimental points fall considerably above the theoretical line, even allowing for the large uncertainties in the data. There are three possible reasons for this result:-

(i) the value of Q_o used may have been too high since a line fitted to the experimental data would not pass through the origin.

(ii) Steele showed that the value of α_N increased strongly with increasing purity of the material and since the purity used by him was only 99.98%, his value may be too low. One would expect this to give too large values of $\frac{VH_c\kappa_n}{\alpha_N}$.

(iii) the values of κ_n may be in error as discussed before.

Of these, (i) would seem the most likely, since a line fitted to the experimental data would be almost parallel to the theoretical line. Clearly, it would be interesting to measure α_N and κ_n for the actual material used in order to make more definite comparisons possible.

It remains to calculate the velocity predicted by the result of Andreev and Dzhikaev

$$V_\kappa = -\frac{c^2 L}{\sigma T H_c^2} \cdot \frac{x_s}{x_n} \cdot \frac{\kappa_n - \kappa_s}{\kappa_n + \kappa_s} \left(\frac{\partial T}{\partial x} - \left(\frac{\partial T}{\partial x}\right)_0\right) .$$

In view of the experimental fact that the motion occurred perpendicular to the direction of the heat flow we expect this velocity, which is

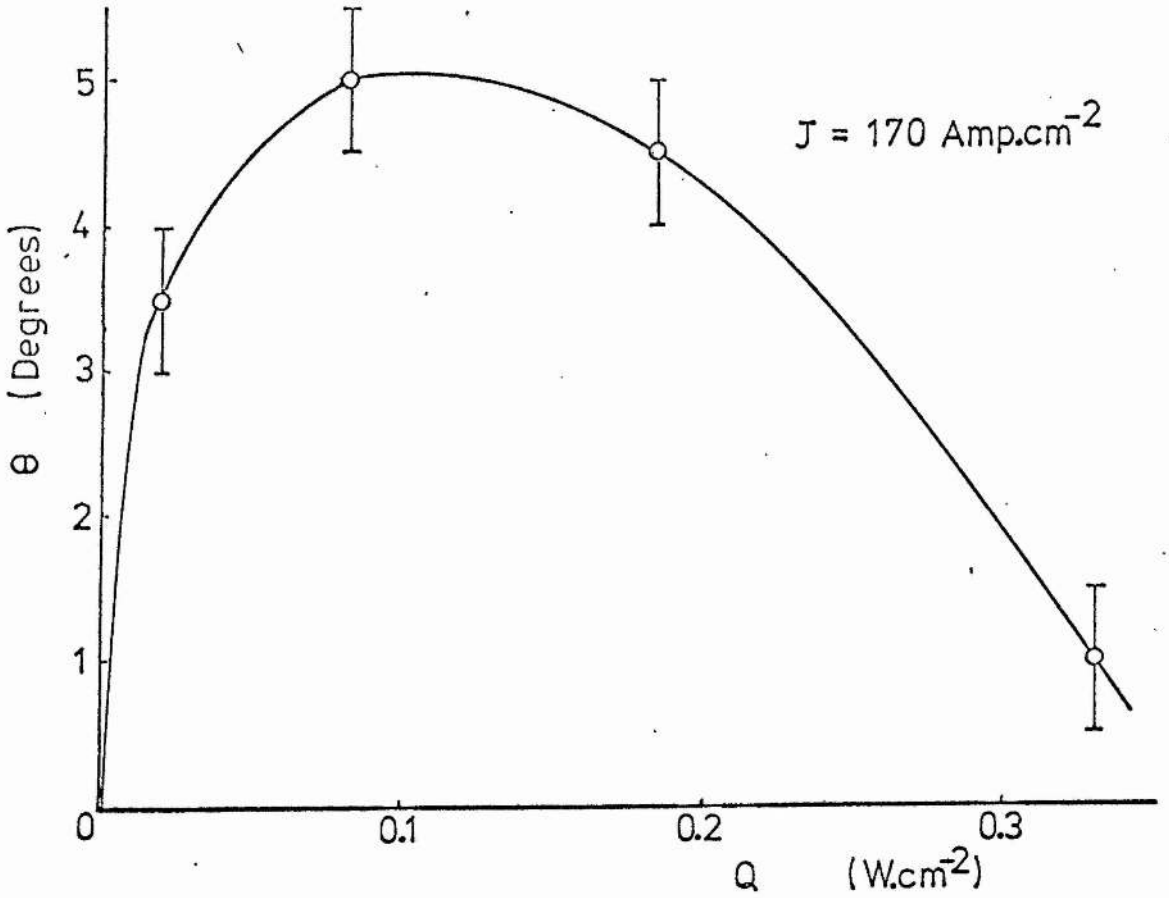

Fig. 7.3 The angle θ (see next figure) versus heat current Q, Pb, J = 171 Amp.cm^{-2}, h = 0.8.

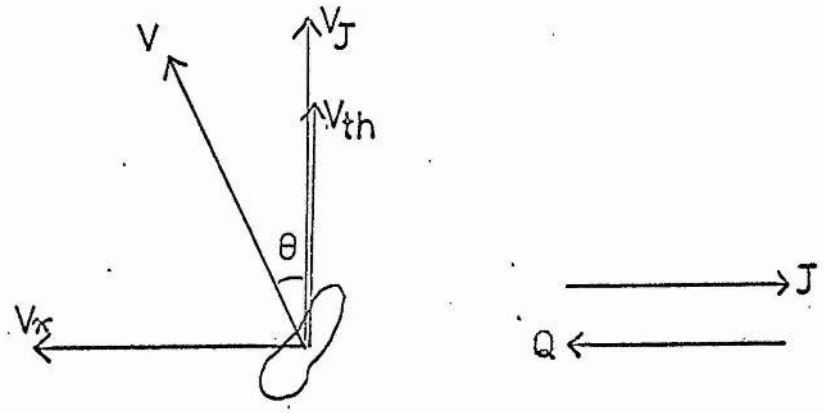

Fig. 7.4 The components of domain velocity in the presence of an electric current J and heat current Q.

directed in the same direction as the heat flow, to be negligibly small compared with the experimentally observed values. For T = 5.8K, h ≈ 0.7 with Q = 4.4W.cm^{-2} ($\frac{\partial T}{\partial x}$ = 2.2K.cm^{-1}) and Q_o = 4.0 ± 0.2W.cm^{-2} ($(\frac{\partial T}{\partial x})_o$ = 2.0K.cm^{-1}) the velocity observed was V = 93 μm.sec^{-1}. The above equation yields upon substitution of these values together with the latent heat data of Dolecek (1954), the thermal conductivity values of De Haas and Rademakers and the measured conductivity at 4.2K (which will be too high) the result

$$V_\kappa = 50 \text{ μm.sec}^{-1},$$

as a lower limit for the velocity. Hence, the velocity predicted by the theory of Andreev and Dzhikaev is not negligible compared with the experimental value. This result is difficult to understand.

7.3 The observation of current assisted motion

As described in section two, due to the thermal contact difficulties pure thermally induced motion was only observed for temperatures above 5.8K. In an attempt to extend the measurements to lower temperatures, experiments were performed in which the flux motion was assisted by passing an electric current in the same direction as the heat current.

Unfortunately, the presence of the two competing thermal driving forces makes the analysis of data obtained from such an experiment quite difficult. Qualitatively, we expect that for increasing temperature and thermal gradient the angle θ (the amount which the direction of motion changes from that of the pure current induced motion when a thermal gradient is applied) will not increase monotonically. For low temperatures the mechanism of Andreev and Dzhikaev should dominate and θ will increase as Q increases since the thermally induced flow will be at right angles to the direction of the current induced flow, but for high temperatures the thermoelectric mechanism will dominate (as found in the previous section) and hence θ will decrease again. These ideas are supported by the raw experimental data shown in Fig. 7.3. Here θ is plotted against Q the heat current density for constant J = 171 Amp.cm^{-2}, with the average temperature of the sample increasing as Q increases.

Fig 7.5 Cotangent of the angle θ (see text) versus current density J, Pb, h = 0.8 with thermal gradient as shown.

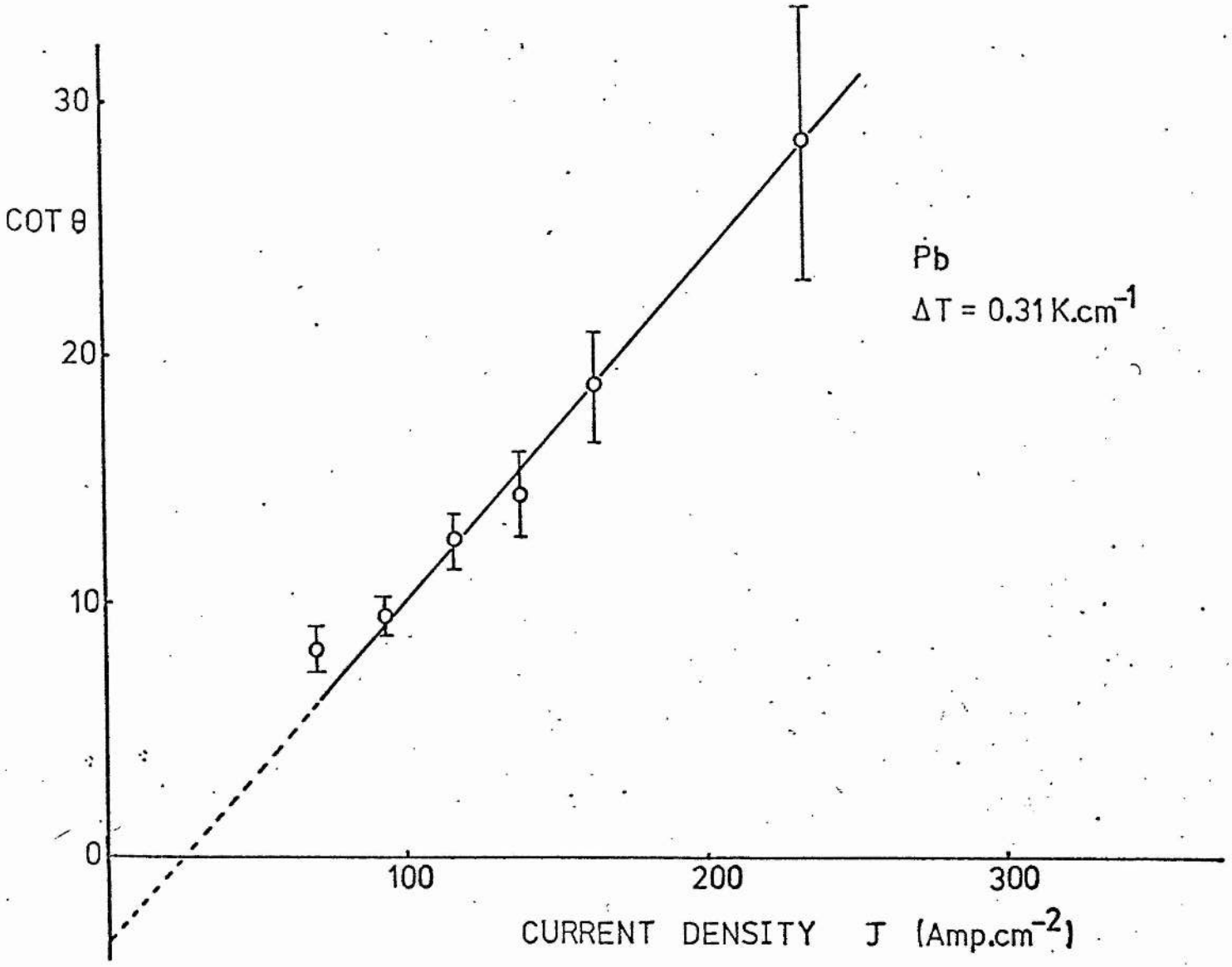

The angle θ was measured with a specially constructed goniometer. A pointer was attached to an X5 eyepiece with crosshairs which rotated inside a plastic protractor. Angles could be measured with this device to $\pm 0.5^{\circ}$, the measurement being aided by the fact that all the data was taken in that reduced field region where a laminar set-up was produced, arranged along the direction of flow.

Quantitative results can be obtained by considering the velocity components and resultant velocity of a domain subject to electric current J and heat current Q (Fig. 7.4). V_J is the velocity component due to the current J, V_{th} the component due to the thermoelectric mechanism and V_κ the component due to the mechanism of Andreev and Dzhikaev. The resultant velocity will be at an angle θ to V_J and V_{th}. Clearly

$$\frac{V_\kappa}{V_J + V_{th}} = \tan \theta \ , \qquad (7.4)$$

and we have established in Chapter VI that V_J may be expressed as

$$V_J = k_T (J - J_o) \ ,$$

where the constants k_T and J_o may be extracted from the current induced flow data as long as measurements are restricted to the linear flow region. Hence

$$\frac{k_T}{V_\kappa} J + \left(\frac{V_{th}}{V_\kappa} - \frac{k_T J_o}{V_\kappa}\right) = \cot \theta \ . \qquad (7.5)$$

If measurements of θ are made at constant heat current Q as a function of J, a plot of cot θ versus J should yield a straight line whose gradient will yield V_κ and whose intercept should then yield V_{th}.

The result of a typical experiment is shown in Fig. 7.5. A good straight line is obtained within the experimental error. Clearly in this case $V_{th} < k_T J_o$ and hence a negative intercept is obtained. Several sets of data like this were obtained giving values of V_κ and V_{th} as a function of temperature and heat current or thermal gradient.

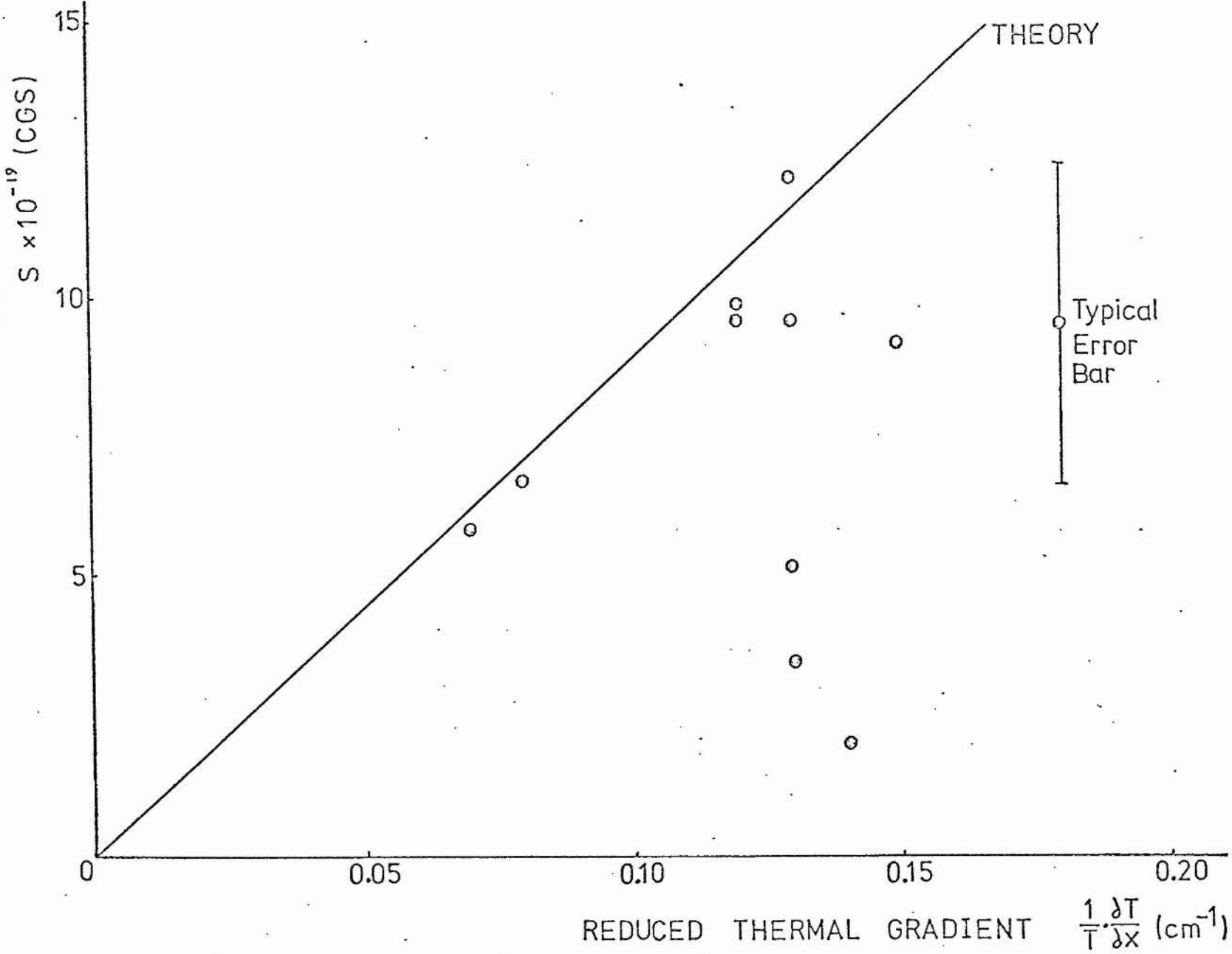

Fig 7.6 The function S (see text) versus reduced thermal gradient for Pb, h = 0.8.

Although reasonable values were obtained for V_κ this method of analysis gives large errors in the values of V_{th} since the intercept is always small. However, in the lower part of the temperature range ($T \leqslant 3.0K$) the values of V_{th} were all scattered about zero, and between 3.0K and 4.2K they began to rise slightly attaining a maximum of about 150 $\mu m.sec^{-1}$. Measurements above 4.2K with this technique are not possible since no current induced flow data could be taken at these temperatures.

We may compare the data obtained for V_κ with the theory (equation 4.18) by plotting the function

$$S = \frac{\sigma H_c^2 V_\kappa \; x_n(\kappa_n + \kappa_s)}{L \; x_s \; (\kappa_n - \kappa_s)} \; ,$$

against $1/T(\partial T/\partial x)$, the reduced thermal gradient. The theory of Andreev and Dzhikaev predicts that a straight line be obtained with gradient c^2. Fig. 7.6 shows the collected experimental data plotted on such a graph. A large scatter is obtained but six out of the eleven points include the theoretical value within their error bars. No systematic deviation with respect to temperature was found to exist.

7.4 Conclusions

Clearly, much work remains to be done to clarify the nature of thermally induced flux flow in Type I superconductors. The data obtained in the present work in Pb has confirmed the suggestion of Laeng and Rinderer (1973) that there exist two driving forces on the flux - one acting in the same direction as the heat flow and another acting perpendicular to it. The second of these was found to dominate at high temperatures.

However, the magnitude of the velocity of the perpendicular motion was found not to agree with the theory due to Rothen, being higher than predicted. This may have been due to the uncertainties involved in

extraction of values for the thermoelectric power and thermal conductivity from the literature or to the experimental difficulty of determining the critical heat current.

At low temperatures the data obtained for the velocity of the parallel motion was in quite reasonable agreement with the theory due to Andreev and Dzhikaev, but at high temperatures, although the theory predicted it to be still observable, experimentally it was found negligible.

Progress in these measurements could be achieved by improving the thermal contact to the bath so as to allow unassisted motion to be observed over the whole liquid helium temperature range. A redesign of the sample mount should allow the thermal conductivity in the normal and superconducting states to be measured quite easily but a separate experiment would have to be designed to measure the thermoelectric power of the normal lead.

It should be pointed out that the nature of the flow is such that precise measurements of its direction are, in general, not possible. In the case of the current assisted motion, the direction of flow could be measured fairly accurately ($\pm$ 0.5°) because the laminar state produced by a high driving force ($J \sim 170$ Amp.cm^{-2}) was found well defined in the reduced field range $0.7 \lesssim h \lesssim 0.9$. As discussed earlier, no thermal driving force of this magnitude can be produced and hence the pure unassisted flow does not have a well defined direction.

CHAPTER VIII - SUMMARY

8.1 Discussion of results

The purpose of the research was to measure and compare flux flow velocities in the intermediate state with the general theory of Andreev and Dzhikaev for the cases of electric current induced and heat current induced motion.

To accomplish this, a metal dewar with optical access for a polarized light microscope was specially designed and built so as to resolve the details of the stationary and moving intermediate state with a resolution of ~ 5 μm employing the Faraday effect in thin films of EuS:EuF_2. This direct observation of the character of the flux motion was found extremely useful in clarifying the motions observed for various applied fields. Some interesting interactions of the moving flux with pinning sites such as crystallite boundaries and particles of dirt were also observed.

In the case of the current induced motion two distinct regions in the flux velocity versus current characteristics were seen.

Firstly, a linear region where the observed velocity for the three materials Pb, Sn and In was found to agree reasonably well with the predictions of Andreev and Dzhikaev's theory when allowance was made for the effects of pinning by the introduction of a velocity independent pinning force. Exact agreement was not obtained because the electrical conductivity values required had to be measured with thin extruded wires instead of the slab samples used in the flux flow experiments.

Secondly, for currents close to the critical current J_o, a curved region was seen in agreement with earlier work using other methods of observation. In view of the uncertainty that exists as to the cause of this curvature this region was studied in some detail. A phenomenological model, based on the presence of a Gaussian distribution

of critical current values throughout the sample, was developed and was found to account satisfactorily for the observed curvature. The presence of such a distribution was confirmed by means of an experiment in which a domain was subjected to a pulsed driving current, the distance travelled during each pulse being measured. The variations in distance travelled were found appreciable reflecting the variations in critical current. The observed curvature was found in disagreement with the theory of thermal activation and no evidence could be found for the presence of a velocity dependent pinning force.

In the case of the thermally induced motion such satisfactory comparisons with the theory did not prove possible. Due to thermal contact difficulties no observations of pure thermally induced motion were possible below ~ 5.8K and all motion below this temperature was assisted with an electric current. It was found, however, that in agreement with the recent suggestion of Laeng and Rinderer there exist two mechanisms driving the flux, one acting parallel to the heat flow (that treated by Andreev and Dzhikaev) and another acting perpendicular to it.

At high temperatures the second of these was found to dominate, the observed motion being perpendicular to the heat flow. The magnitude of the velocity in this region did not, however, agree with that predicted by the recent theory of Rothen although this may have been due to the experimental difficulty of determining the critical heat current or to the extraction of other quantities from the literature. It should be noted that the theory of Andreev and Dzhikaev did not predict a negligible velocity parallel to the heat flow at these temperatures, again in disagreement with the experimental data.

At low temperatures ($\leqslant$ 3.0K) the parallel motion was found to dominate and its magnitude agreed quite reasonably with the prediction of the theory. Measurements of the velocity of the perpendicular

motion at these temperatures were subject to considerable uncertainty but below T = 3.0K they were scattered about zero rising as the temperature was increased.

8.2 Suggestions for further work

The high resolution magneto-optic method is an extremely elegant one and many further experiments could be performed with its aid. Those that are suggested by the present work will now be discussed.

The interaction of moving flux with pinning sites of a known nature could be observed by means of evaporating the EuS:EuF_2 films directly onto the samples. It should be possible, for example, to deal mathematically with the pinning caused by a non superconducting particle impressed in the sample surface.

The agreement between the measured flow velocities in the case of the linear part of the current induced flow characteristic and the theoretical predictions was not exact. This was probably due to the doubt attached to the conductivity measurements and it would be desirable to perform these on slab samples.

The phenomenological model developed to deal with the curved part of the characteristic could be further improved with the aid of more extensive experiments on the shape of the critical current distribution.

Clearly, a lot of questions are left unanswered concerning the thermally induced flow. The present data has shown that two mechanisms require to be investigated and the first step would be to improve the thermal contact to the sample to allow pure thermally induced motion to be observed over a wider temperature range. The use of single crystal samples with less pinning might also be an advantage.

Finally, there exist Type II alloys (e.g. NbMo) where the fluxon diameter in the mixed state is around 1 μm. With some modification

the magneto optic method could achieve this resolution. The study of flux flow in Type II materials would then prove possible and a host more interesting experiments become feasible.

REFERENCES

1(a) Books on superconductivity

De Gennes P G (1966), Superconductivity of Metals and Alloys, Benjamin New York.

Lynton E A (1962), Superconductivity, Methuen London.

Parks R D (Editor) (1969), Superconductivity, Marcel Dekker New York.

1(b) Book on mathematical methods

Jaeger L G (1966), Cartesian Tensors in Engineering Science Pergamon Oxford.

REFERENCES

2. Original Papers

Abramowitz M and Stegun I A (1964), Handbook of Mathematical Functions AMS 55, NBS Washington.

Abrikosov A A (1957), Sov Phys JETP 5 1174.

Alers P B (1956), Phys Rev 105 104.

Alers P B (1959), Phys Rev 116 1483.

Allen J F and Lerski R A (1972 a), Proc 13th Int Conf Low Temp Physics, Boulder USA. (to be published).

Allen J F and Lerski R A (1972 b), Unpublished.

Anderson P W (1962), Phys Rev Lett 9 309.

Anderson P W and Kim Y B (1964), Rev Mod Phys 36 39.

Andreev A F and Dzhikaev Y K (1971), Sov Phys JETP 33 163.

Andrew E R (1948), Proc Roy Soc A194 80 and 98.

Baird D C (1964), Can J Phys 42 1682.

Baird D C (1965), Can J Phys 43 971.

Balashova B M and Sharvin Y V (1956), Sov Phys JETP 4 54 (1957).

Baixeras J and Fournet G (1967), J Phys Chem Sol 28 1541.

Bardeen J, Cooper L N and Schrieffer J R (1957), Phys Rev 108 1175.

Beasley M R, Labusch R and Webb W W (1969), Phys Rev 181 682.

Blatt F J, Burmester A and Lardy B (1967), Phys Rev 155 11.

Brailsford F (1966), Physical Principles of Magnetism, D Van Norstrand London.

Brandt B L and Parks R D (1967), Phys Rev Letters 18 43.

Chandrasekhar S, Farrell D E and Huang S (1967), Phys Rev Letters 18 43.

Clem J R (1968), Phys Rev 176 531.

Cody G D and Miller R E (1968 a), Phys Rev 173 481.

Cody G D and Miller R E (1968 b), Phys Rev 173 494.

Cooper L N (1956), Phys Rev 104 1189.

Decker D L, Mapother D E and Shaw R W (1958), Phys Rev 112 1888.

De Haas W J, Voogd J and Jonker J M (1934), Physica 1 281.

De Haas W J and Rademakers A (1940), Physica 7 992.

De Sorbo W (1960), Phys Rev Letters 4 406.

De Sorbo W and Newhouse V L (1962), J App Physics 33 1004.

De Sorbo W and Healy W A (1964), Cryogenics 4 257.

De Sorbo W (1965), Phil Mag 11 853.

Dew-Hughes D (1971), Rept Prog Physics 34 821.

Dolecek R L (1954), Phys Rev 94 540.

Enz V, Fast J F, Van Houten S and Smit J (1962), Philips Res Repts 17 451.

Essmann U, Bodmer A and Träuble H (1972), Phys Stat Sol 13A 471.

Faber T E (1958), Proc Roy Soc A248 460.

Farrell D E, Dinewitz I and Chandrasekhar B S (1966), Phys Rev Lett 16 91.

Fiory A T and Serin B (1966), Phys Rev Letters 16 308.

Fröhlich H (1950), Phys Rev 79 845.

Ginzburg V L and Landau L D (1950), JETP USSR 20 1064.

Gorter C J and Casimir H B G (1934 a), Physica 1 306.

Gorter C J and Casimir H B G (1934 b), Phys Z 35 963.

Gorter C J (1957), Physica 23 45.

Gorter C J and Potters M L (1958), Physica 24 169.

Gupta A K and Farrell D E (1973) Phys Rev 7B 3037.

Haenssler F and Rinderer L (1965), Phys Letters 16 29.

Hendry A W (1966), Photoelastic Analysis, Pergamon Press London.

Huebener R P, Kampwirth R T and Rowe V A (1970 a), Rev Sci Instr 41 722.

Huebener R P, Rowe V A and Kampwirth R T (1970 b), J Appl Phys 41 2963.

Huebener R P, Kampwirth R T and Rowe V A (1971), Solid State Comm 9 1183.

Huebener R P, Kampwirth R T and Rowe V A (1972 a), Cryogenics 12 100.

Huebener R P, Kampwirth R T and Farrell D E (1972 b), Phys Letters 41A 105.

Jones R G, Rhoderick E H and Rose-Innes A C (1967), Phys Letters 24A 318.

Kamerlingh Onnes H (1911), Leiden Comm 122b,124c.

Kamerlingh Onnes H (1913), Leiden Comm Supl 34.

Kim Y B and Stephen M J (1969), Superconductivity 2 1107, Dekker New York.

King R J and Talim S P (1970), J Phys E4 93.

Kirchner H (1968 a) Phys Letters 26A 651.

Kirchner H (1968 b) Proc 11th Int Conf on Low Temp Phys, St. Andrews Scotland.

Kirchner H (1969), Phys Letters 30A 437.

Kirchner H and Kiendl A (1972), Phys Letters 39A 293.

Kramer E J (1970), J Appl Phys 41 621.

Kuper C G (1951), Phil Mag 42 961.

Laeng P, Haenssler F and Rinderer L (1971), J Low Temp Physics 4 533.

Laeng P and Rinderer L (1972), Cryogenics 12 315.

Laeng P and Rinderer L (1973), Helv Phys Acta 46 8.

Landau L D (1937), JETP USSR 7 371.

Landau L D (1943), JETP USSR 13 377.

Landau L D and Lifshitz E M (1960), Electrodynamics of Continuous Media, Pergamon Press London.

Lifshitz E M and Sharvin Y V (1951), Doklady Akad Nauk USSR 79 783.

London F and London H (1935 a), Proc Roy Soc A149 71.

London F and London H (1935 b), Physica 2 341.

London F (1936), Physica 3 450.

London H (1935), Proc Roy Soc A152 650.

Lowell J, Muñoz J S and Sousa J (1967), Phys Letters 24A 376.

Lowell J (1970), J Phys C 3 712.

Martin L C (1966), The Theory of the Microscope, Blackie London.

Maxwell E and Lutes O S (1954), Phys Rev 95 333.

Meissner W and Ochsenfeld R (1933), Naturwiss 21 787.

Meissner H (1970), J Low Temp Physics 2 267.

Mendelssohn K and Moore J R (1935), Proc Roy Soc A151 334.

Meshkovsky A and Shalnikov A (1947), J Phys USSR 11 1.

Newhouse V L (1964), Applied Superconductivity p106, Wiley New York.

Olafsson R (1971), Ph.D Thesis, University of St.Andrews.

Olsen J L (1962), Electron Transport in Metals, Interscience New York.

Osborne K E and Rose-Innes A C (1973), Phil Mag 27 683.

Otter F A and Solomon P R (1967), Phys Rev 164 608.

Panofsky W K H and Phillips M (1962), Classical Electricity and Magnetism, Addison-Wesley Massachusetts.

Peierls R (1936), Proc Roy Soc A155 613.

Pippard A B (1950), Proc Roy Soc A203 210.

Pippard A B (1951), Proc Camb Phil Soc 47 617.

Pippard A B (1953), Proc Roy Soc A216 547.

Quinn III D J and Ittner III W B (1962), J Appl Phys 33 748.

Radebaugh R and Keesom P H (1966 a), Phys Rev 149 209.

Radebaugh R and Keesom P H (1966 b), Phys Rev 149 217.

Rothen F (1972), Phys Letters 42A 291.

Sarma N V and Moon J R (1967), Phil Mag 16 433.

Schawlow A L and Devlin G E (1958), Phys Rev 110 1011.

Schawlow A L, Devlin G E and Hulm J K (1959), Phys Rev 116 626.

Sharvin Y V (1965), Sov Phys JETP Letters 2 183.

Solomon P R (1969), Phys Rev 179 475.

Solomon P R and Harris R E (1971), Phys Rev 3B 2969.

Solomon P R (1971), Colloque Franco Allemand Sur La Supraconductivite Aussois (Unpublished).

Steele M C (1951), Phys Rev 81 262.

Stephen M J and Suhl H (1964), Phys Rev Letters 13 797.

Stromberg T F and Swenson C A (1962), Phys Rev Lett 9 370.

Suhl H (1965), Phys Rev Letters 14 226.

Suits J C and Argyle B E (1965), J Appl Phys 36 1251.

Takayama T, Ogushi T and Shibuya Y (1971), J Phys Soc Japan 30 1083.

Träuble H and Essmann U (1966 a), J Sci Instr 43 344.

Träuble H and Essmann U (1966 b), Phys Stat Sol 18 813.

Van Den Berg G J (1948), Physica 14 111.

Van Gurp P J (1969), Phys Rev 178 650.

Wilson A H (1953), The Theory of Metals, Cambridge University Press.